DECLARATION UNDER 37 C.F.R. 1.132
U.S. Appln. No. 10/774,378

IN THE UNITED STATES PATENTS AND TRADEMARK OFFICE

In re the application of   Docket No: Q79834

Hideaki TADA, *et al.*

Application No. 10/774,378   Group Art Unit: 1872

Filed: February 10, 2004   Examiner: O'Hara, B. Eileen

For: Novel polypeptides, DNAs encoding the same and use thereof

DECLARATION UNDER 37 C.F.R. §1.132

Commissioner for Patents
P.O. Box 1450
Alexandria, VA 22313-1450

Sir:

I, Tsutomu AKIYAMA, declare the followings.

1. I reside at 1-12-7, Jyounan-cho, Takatsuki-city, Osaka 569-0056, JAPAN.

2. In March 1995, I graduated from Osaka University, Faculty of Pharmaceutical sciences. In March 1997, I was awarded a Master degree of Pharmaceutical from Osaka University. Since April 1997, I have been employed by Ono Pharmaceutical Co., Ltd. and have been engaged in the study of Pharmacology, Molecular-biochemistry and Brain Science at the Research Institute of the company.

3. I make this Declaration in the support of that OAF065 possesses the following functions:

    I)   the clone can improve the abnormal neurite extension;

    II) the clone can normalize the proliferation of astrocytes; and

    III) the clone can normalize the increase of the expression of inflammatory cytokines in astrocytoma/glioblastoma.

4. The following experiments were conducted by me or under my immediate supervisor.

- 1 -

Experiment 1

Experiment of neurite outgrowth using dorsal root ganglion (DRG)
cells

<Method>

Dorsal root ganglion cells were prepared from four-week old
rat using the 2-well culture slides coated with
Poly-D-Lysine/Laminin, followed by adding rat Nogo-A protein
alone or in combination with rat Nogo-A and human OAF065
protein to the cells. One-day after the seeding, cells were
fixed by adding paraformaldehyde. Detection of neurites was
performed by fluorescence staining with beta-III tubulin
antibody. Each of Nogo-A and OAF065 used in the present
Experiments are follows:

Nogo-A: Fragment protein-Fc fusion; R&D Systems catalogue no.
1548-TR
OAF065: soluble TROY-Fc fusion; R&D Systems catalogue no.
3515-NG

<Result>

Inhibition of neurite outgrowth of DRG neurons by Nogo-A protein was
observed. Effect of Nogo-A was suppressed by adding OAF065 protein.
Neurite outgrowth of DRG neurons was not effected by treatment with
OAF065 alone(data not shown).

Fig. 1 Effect of Nogo-A or combination of Nogo-A and OAF065 on neurite outgrowth in DRG cells
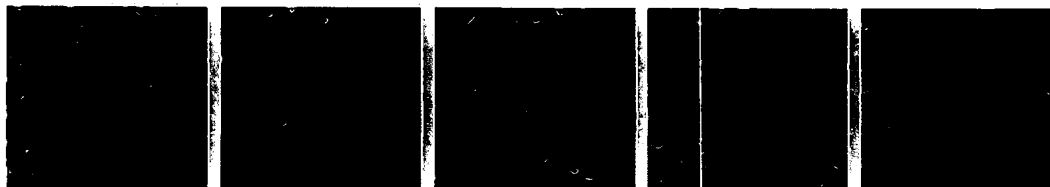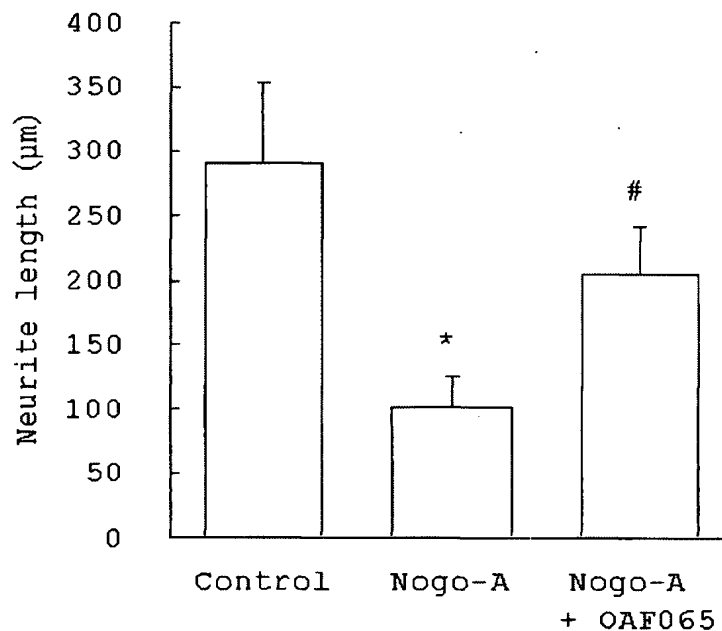

Control
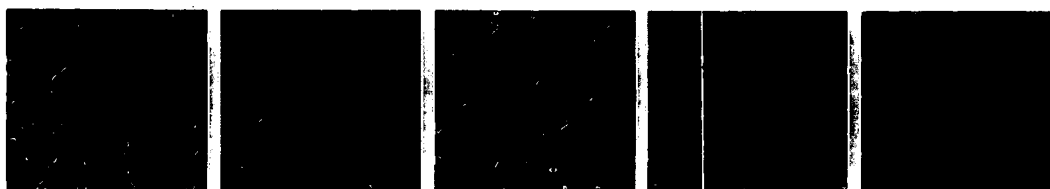
Nogo-A treated

OAF065 and Nogo-A treated

Green fluorescent were observed with beta III tubulin antibody immuno-staining.

Fig. 2 Effects of Nogo-A or Nogo-A and OAF065 on neurite outgrowth in DRG cells

*p<0.05 vs. Control, #p<0.05 vs. Nogo-A (t-test)

Experiment 2

Experiment of cell proliferation in rat cultured astrocytes.

<Method>

Primary astrocytes were derived from newborn rat cortex. Cells were seeded on 96 well plates. After one day, cells were treated with Nogo-A or the combination of Nogo-A and OAF065 proteins. Cells were counted one day after the treatment.

<Result>

Proliferation of astrocytes was promoted by a one-day treatment with Nogo-A protein. Activity of Nogo-A protein was inhibited by treatment with OAF065 protein. Proliferation of astrocytes was not effected

by treatment with OAF065 alone.

Table 1 Effects of OAF065, Nogo-A on the proliferation of astrocytes

Treatment	cell numbers (%)		
Control	100	±	2.5	
OAF065	100	±	1.9	
Nogo-A	124	±	2.7	***
Nogo-A + OAF065	99	±	3.4	###

***$p < 0.001$ vs. Control, ###$p < 0.001$ vs. Nogo-A (t-test)

Experiment 3

Experiment of inflammatory cytokine expressions in human
astrocytoma/glioblastoma U373MG cells
<Method>
Human astrocytoma/glioblastoma U373MG cells were treated with OAF065
or Nogo-A protein alone or in combination with them. Twenty-four
hours after treatments, total RNA was prepared. Each Cytokine mRNA
expression level was measured by RT-PCR method.

<Result>
Treatment with Nogo-A protein increased expression of inflammatory
cytokines in U373MG cells. Addition of OAF065 protein to the system
and expression of inflammatory cytokines were suppressed.

Table 2 Effects of OAF065 or combination of Nogo-A and OAF065 on expression of cytokines in U373MG cells

	OAF065	Nogo-A	Nogo-A + OAF065
IL-α	0.9	3.7	0.8
IL-1β	0.9	2.1	0.9
IL-4	0.6	1.8	0.5
IL-8	0.9	1.5	0.8
IL-12p35	0.9	2.1	0.9
IL-15	0.8	2.3	1.1

Each value was shown in the ratio when the control was assumed to be one.

    5. As set forth above in greater detail, the clone OAF065 of the present application possesses the following functions:

        I)   improvement activity of the abnormal neurite extension;

        II)   normalization activity of the abnormal proliferation of astrocytes; and

        III) normalization activity of the increase of the expression of inflammatory cytokines in astrocytoma/glioblastoma.

Therefore, I believe that the invention of the present application is supported by the experiments.

I declare that all statements made herein of my own knowledge are true and correct and that all statements made on information and belief are believed to be true; and further, that these statements were made with the knowledge that willful false statements and the like so made are punishable by fine or imprisonment, or both, under the Section 1001 of Title 18 of the United States Code, and that such willful false statements may jeopardized the validity of the application or any patent issuing thereon.

Respectfully submitted,

May 23, 2007
Date:

Tsutomu AKIYAMA

Development/Plasticity/Repair

Nogo-A Inhibits Neurite Outgrowth and Cell Spreading with Three Discrete Regions

Thomas Oertle,[1]* Marjan E. van der Haar,[1]* Christine E. Bandtlow,[2] Anna Robeva,[3] Patricia Burfeind,[3] Armin Buss,[1] Andrea B. Huber,[1] Marjo Simonen,[1] Lisa Schnell,[1] Christian Brösamle,[1] Klemens Kaupmann,[4] Rüdiger Vallon,[3] and Martin E. Schwab[1]

[1]Brain Research Institute, University of Zurich, and Department of Biology, Swiss Federal Institute of Technology, CH-8057 Zurich, Switzerland, [2]Institute of Medical Chemistry and Biochemistry, Leopold-Franzens-University of Innsbruck, A-6020 Innsbruck, Austria, [3]Novartis Institute for Biomedical Research, Functional Genomics, Novartis Pharmaceuticals Corporation, Summit, New Jersey 07901, and [4]Novartis Pharma AG, Nervous System Research, CH-4002 Basel, Switzerland

Nogo-A is a potent neurite growth inhibitor *in vitro* and plays a role both in the restriction of axonal regeneration after injury and in structural plasticity in the CNS of higher vertebrates. The regions that mediate inhibition and the topology of the molecule in the plasma membrane have to be defined. Here we demonstrate the presence of three different active sites: (1) an N-terminal region involved in the inhibition of fibroblast spreading, (2) a stretch encoded by the Nogo-A-specific exon that restricts neurite outgrowth and cell spreading and induces growth cone collapse, and (3) a C-terminal region (Nogo-66) with growth cone collapsing function. We show that Nogo-A-specific active fragments bind to the cell surface of responsive cells and to rat brain cortical membranes, suggesting the existence of specific binding partners or receptors. Several antibodies against different epitopes on the Nogo-A-specific part of the protein as well as antisera against the 66 aa loop in the C-terminus stain the cell surface of living cultured oligodendrocytes. Nogo-A is also labeled by nonmembrane-permeable biotin derivatives applied to living oligodendrocyte cultures. Immunofluorescent staining of intracellular, endoplasmic reticulum-associated Nogo-A in cells after selective permeabilization of the plasma membrane reveals that the epitopes of Nogo-A, shown to be accessible at the cell surface, are exposed to the cytoplasm. This suggests that Nogo-A could have a second membrane topology. The two proposed topological variants may have different intracellular as well as extracellular functions.

Key words: Nogo; reticulon; inhibitory regions; active sites; membrane topology; neurite outgrowth

Introduction

Regenerative nerve fiber growth and structural plasticity are limited in the adult mammalian CNS, in part because of the presence of neurite growth inhibitory constituents (Schwab and Bartholdi, 1996; Behar et al., 2000). An important step in elucidating the mechanisms mediating this inhibition was the molecular characterization of *nogo-A*, which encodes an oligodendrocyte-associated neurite growth inhibitor (Spillmann et al., 1998; Chen et al., 2000; GrandPré et al., 2000; Prinjha et al., 2000).

The *nogo* gene gives rise to three major protein products, Nogo-A, -B, and -C, by both alternative splicing and alternative promoter usage (Chen et al., 2000; Oertle et al., 2003b). All Nogo isoforms share a common C-terminus of 188 amino acids, called reticulon-homology domain (RHD; Pfam PF02453) because of its similarity with the Reticulon (RTN) protein family (Roebroek et al., 1994, 1998; Moreira et al., 1999; Oertle et al., 2003c). Outside of this RTN domain, Nogo and the other three RTN genes have no obvious sequence similarities. Two long hydrophobic stretches (35 and 36 aa), which could serve as transmembrane (TM) domains and are probably responsible for the endoplasmic reticulum (ER) association of the proteins, are located in the RHD (van de Velde et al., 1994; Oertle et al., 2003a).

Myelin, oligodendrocytes, rat NI-250/NI-35 (for neurite outgrowth inhibitor of M_r 250 and 35 kDa) as well as purified bovine Nogo-A-ortholog bNI-220 were shown to be inhibitory for fibroblast spreading and neurite outgrowth and to induce growth cone collapse of rat dorsal root ganglion (DRG) and chick retinal ganglion cell (RGC) neurons (Caroni and Schwab, 1988; Bandtlow et al., 1993; Rubin et al., 1995; Loschinger et al., 1997; Spillmann et al., 1998). The identification of the regions of Nogo-A that exert these diverse inhibitory effects *in vitro* and their possible accessi-

bility at the cell surface of oligodendrocytes would help us understand the mechanisms underlying the lack of regeneration in the CNS of higher vertebrates. Moreover, this information is crucial for the identification of Nogo-interacting molecules and for the development of optimal reagents for the neutralization of Nogo proteins. Potent neurite growth inhibitory activity was found in the Nogo-A-specific part of the molecule (Chen et al., 1999; Oertle et al., 2000; Prinjha et al., 2000). However, Nogo-A does not appear to be a conventional type I membrane protein: it does not possess an N-terminal hydrophobic sequence that could serve as a signal peptide such as is common to proteins that are secreted or expressed at the cell surface.

GrandPré et al. (2000) presented evidence that the 66 amino acid residue region (termed Nogo-66) between the two hydrophobic stretches of the RTN domain induces growth cone collapse and is exposed on the surface of nogo-A-transfected cells. The cloning of a glycosyl phosphatidyl inositol (GPI)-anchored receptor (NgR) has been described recently that interacts with the Nogo-66 peptide (Fournier et al., 2001) as well as with the CNS myelin proteins OMgp (oligodendrocyte-myelin glycoprotein) and MAG (myelin-associated glycoprotein), both of which also have neurite growth inhibitory activity (Domeniconi et al., 2002; Liu et al., 2002; Wang et al., 2002a). The observation that Nogo-66 is inhibitory implies that all three Nogo isoforms should exert neurite growth inhibitory properties.

In the present study we provide evidence that three discrete regions of Nogo-A exhibit different inhibitory properties *in vitro*. Binding of Nogo-A-specific fragments to brain cortical membranes and the surface of responsive cells strongly argues for the existence of Nogo-A-specific receptor molecules. Antibody studies are suggestive for the expression of Nogo-A at the cell surface of cultured oligodendrocytes and of 3T3 fibroblasts and would imply that the N-terminal region of Nogo-A as well as the Nogo-66 region can face the extracellular space. A large intracellular pool of Nogo-A is associated with the endoplasmic reticulum (ER) and Golgi complex as revealed by double staining with marker proteins for these two organelles. Selective permeabilization studies suggest that a major part of the intracellular Nogo-A exhibits a second topology in which the N-terminus and Nogo-A-specific part of the molecule are exposed at the cytoplasmic side of membranes.

Materials and Methods

Rat Nogo-A deletion library. Deletion constructs have been made using internal restriction sites, by ExonucleaseIII/Mung Bean Nuclease treatment and by PCR with rat Nogo-A-specific primers on rat Nogo-A, Nogo-B, or Nogo-C as templates (Chen et al., 2000): Nogo-A (aa 1–1163), Nogo-B (aa 1–172 + 976–1163), Nogo-C (Nogo-C N-terminal 11 aa + aa 976–1163), Nogo-66 (aa 1019–1083), rat glutathione S-transferase (GST)-Nogo-66 (aa 1026–1091), NiR-G (aa 1–979), NiR (1–172), NiR-Δ1 (aa 1–31), NiR-Δ2 (aa 59–172), NiR-Δ3 (aa 1–31 + 59–172), EST (aa 762–1163), NiG (aa 174–979), NiG-Δ1 (aa 174–909), NiG-Δ2 (aa 174–865), NiG-Δ3 (aa 172–723), NiG-Δ4 (aa 172–646), NiG-Δ5 (aa 293–647), NiG-Δ6 (aa 763–975), NiG-Δ7 (aa 174–235 + 294–979), NiG-Δ8 (aa 218–653), NiG-Δ9 (aa 172–259 + 646–974), NiG-Δ10 (aa 293–979), NiG-Δ11 (aa 209–268), NiG-Δ12 (aa 198–233), NiG-Δ13 (aa 174–216), NiG-Δ14 (aa 174–260), NiG-Δ15 (aa 174–190 + 493–979), NiG-Δ16 (aa 174–190 + 621–979), NiG-Δ17 (aa 174–190 + 259–979), NiG-Δ18 (aa 174–190 + 263–979), NiG-Δ19 (aa 763–865), NiG-Δ20 (aa 544–725), NiG-Δ21 (aa 812–918), NiG-Δ22 (aa 866–975), NiG-Δ23 (aa 914–975), NiG-Δ24 (aa 544–685), NiG-Δ25 (aa 614–725), NiG-Δ26 (aa 544–613), NiG-Δ27 (aa 581–648), NiG-Δ28 (aa 614–685), NiG-Δ29 (aa 648–725), NiG-Δ30 (aa 682–725), NiG-Δ31 (aa 544–580), NiG-Δ32 (aa 581–613), NiG-Δ33 (aa 614–648), NiG-Δ34 (aa 648–685), NiG-Δ35 (aa 260–556), NiG-Δ36 (aa 260–415). Human

GST-Nogo-66 (aa 1055–1120 of human Nogo-A) has been cloned by PCR on human Nogo-A as a template.

Deletion constructs were cloned into pET28 vector (Novagen), pGEX-6P (Amersham Biosciences) and pET26 vector (Novagen). Human GST-Nogo-66 corresponds to the GST-nogo protein published by GrandPré et al. (2000). Synthetic rat peptide 4 EELVQKYSNSALGHVN-STIKELRRL corresponds to the human peptide 4 (ibid.) with one mismatch. Synthetic Pro/Ser-rich peptide (PSSPPPSSPPPSSPPPS) as well as rat peptide 4 have been produced and HPLC-purified by Primm SA. P472 (NYESIKHEPENPPPYEEA) was synthesized and purified by Research Genetics.

Production of recombinant Nogo-A-deletion library. The bacterial Nogo-A-deletion library was expressed in *Escherichia coli*. Proteins were extracted by repeated sonication in sonication buffer (20 mM Tris, 50 mM NaH$_2$PO$_4$, 100 mM NaCl, pH 8.0) with 0.75 mg/ml Lysozyme, by solubilization with B-Per (Pierce), or with 8 M urea. NiG expressed with pelB-leader was obtained from the periplasmic space according to the Novagen protocol for periplasmic protein purification. Supernatants of pET28 constructs were purified using the Co^{2+}-Talon Metal Affinity Resin (Clontech) in a batch procedure. Urea (8 M) and B-Per solubilized lysates were brought to nondenaturing conditions by increasingly substituting the buffer with sonication buffer during the resin-batch procedure. Proteins were eluted with 250 mM imidazole in sonication buffer on a gravity column (Bio-Rad). NiG was further purified by gel filtration on Superdex 200 (Amersham Biosciences) HiLoad 16/60. Supernatants of pGEX-6P constructs were purified with G-Sepharose column in a batch procedure according to manufacturer's instructions (Amersham Biosciences). Cleavage of GST-Nogo-66 was performed by incubating solubilized GST-Nogo-66 with PreScission protease and subsequent HPLC purification.

Gel electroelution was performed by preparative SDS-PAGE of immobilized metal-affinity chromatography (IMAC)-purified recombinant Nogo and elution with Bio-Rad Electro-Eluter into 50 mM Tris, pH 7.4, 100 mM NaCl, 0.2% (w/v) 3-[(3-cholamidopropyl)dimethylammonio]-1-propanesulfonate (CHAPS) for 1 hr at 250 mA, followed by 30 sec of reversed electrode polarities.

Protein concentrations of chromatography-purified proteins were determined using Pierce Coomassie Stain and BSA as standard protein. Protein concentrations of gel-eluted proteins were estimated on the basis of band intensity of silver-stained gels (Merril et al., 1981) with BSA as a standard.

Production of recombinant Nogo in Chinese hamster ovary cells. A 3119 bp fragment resulting from a partial *Hinc*II digest of rat Nogo-A cDNA, NiR-G, was cloned into pSecTag2 expression vectors (Invitrogen, Groningen, The Netherlands). Transfection of pNiR-G into Chinese hamster ovary (CHO) cells resulted in intracellular, cytoplasmic expression of NiR-G. Stable NiR-G CHO cell lines were selected with 250 μg/ml Zeocin (Invitrogen). Recombinant NiR-G from cell lysate was purified over a Ni^{2+}-NTA column (Qiagen AG, Basel, Switzerland).

Rat NiG-Δ20 and Nogo-66 were cloned into pAPtag5 vector by PCR. Transfection of pNiG-Δ20-AP into CHO cells resulted in NiG-Δ20-AP that was secreted into the culture supernatant. Stable pNiG-Δ20-AP and pNogo-66-AP cell lines were selected with 250 μg/ml Zeocin (Invitrogen). Both cell lines were adapted to serum-free medium (Invitrogen) conditions and grown in a cell-line chamber (Integra). Supernatants were concentrated 10-fold before use, and the concentration of fusion protein was assessed as described elsewhere (Flanagan and Leder, 1990).

Cloning of rat NgR and stable NgR-expressing CHO cell line. Adult rat brain poly-A$^+$-RNA was prepared using the Direct Quick Messenger RNA kit (Talent) according to manufacturer protocol. cDNA was prepared from 250 ng of poly-A$^+$-RNA with Moloney murine leukemia virus reverse transcriptase polymerase and poly-dT primers from Novagen. cDNA (1 μg) was used as a template for a PCR of 35 cycles with 5′-GTTCGGATCCAAGATGAAGAGGGCGTCC-3′ and 5′-GTTCTCGAGTCAGCAGGGCCCAAGCACTG-3′ as forward and reverse primers, respectively. The PCR product was subcloned into the *Bam*HI–*Xho*I sites of pBluescriptII-KS and fully sequenced (Microsynth GmbH, Balgach, Switzerland).

pIgκ−V5-NgR was derived by subcloning rat NgR lacking the signal

peptide into BamHI–XhoI sites of pSecTag2A with primers 5′-GCTCGGATCCACCTGGTGCCTGTGTGTG-3′ and 5′-GTTCTCG-AGTCAGCAGGGCCCAAGCACTG-3′ in frame with the Igκ-leader peptide of the vector and C terminal to an introduced V5-tag (cloned by PCR from pYES2/NT with 5′-CACGAAGCTTGGGTAAGCCTAT-CCCT-3′ and 5′-GTGGATCCGACGTAGAATCGAGACC-3′ into Hin-dIII–BamHI sites of pSecTag2A). A stable pIgκ–V5-NgR CHO cell line was selected with 250 μg/ml Zeocin (Invitrogen).

Radioactive labeling and binding experiments. IMAC-purified NiG-Δ20 was iodinated by ANAWA Trading SA (Wangen, Switzerland) (2030 Ci/mmol) using Lactoperoxidase and purified by reverse-phase HPLC. Membranes from rat brain cortex were prepared as described (Olpe et al., 1990). Binding was performed for 1 hr at room temperature essentially as described (Kaupmann et al., 1997) using 1.5 ml tubes preincubated for 2 hr with 1% (w/v) bovine serum albumin to reduce nonspecific binding. Membrane homogenates in HEPES buffer, pH 7.4 (125 mM NaCl, 5 mM KCl, 0.6 mM MgCl$_2$, 1.8 mM CaCl$_2$, 20 mM HEPES, 6 mM dextrose), containing protease inhibitors (Rôche Diagnostics, Mannheim, Germany) were incubated with 1.3 nM iodinated NiG-Δ20 in the absence or presence of increasing concentrations of unlabeled NiG-Δ20.

Antibodies. Rat and bovine antisera (AS) 472 were produced against the synthetic peptide NYESIKHEPENPPPYEEA (bovine sequence) or the corresponding rat sequence SYDSIKLEPENPPPYEEA (aa 623–640) (Chen et al., 2000) (Research Genetics Huntsville, AL). AS 922 was raised against the peptide RIYKGVIQAIQKSDEGHPFRAYLESEVAISEE-LVQKYSNSALGHV (aa 1055–1099 of human Nogo-A) from the Nogo-66 region, and AS 294 was raised against the C-terminal Nogo-A peptide KDAMAKIQAKIPGLKRKAD (Research Genetics). AS Rosa and AS Bianca were produced by intradermal immunization of prokaryotically produced, IMAC-purified, and gel electroeluted NiR-a and NiR-Δ3. AS Florina and AS Laura were produced similarly by intradermal immunization of NiG. As controls, the corresponding preimmune sera or antisera preincubated with an excess of the corresponding immunogenic peptides were used.

For the monoclonal antibodies, mice (C3H and C57Bl6/J strains) were immunized subcutaneously with the synthetic peptide SYDSIKLEPEN-PPPYEEA, corresponding to rat sequence aa 623–640 for monoclonal antibody (mAb) 11C7, whereas mAbs 11A8, 7B12, and 3D11 were produced against recombinant prokaryotically produced NiR-G. Spleen cells were fused with myeloma cells, and monoclonal lines were selected and subcloned. Supernatants of the obtained clones were screened on ELISA plates coated with the Nogo-A deletion library to localize their epitopes.

Rabbit anti-NgR antisera (AS α–NgR) were raised against three synthetic peptides of human NgR (EQLDLSDNAQLRSVDPA, EVPCS-LPQRLAGRDLKR, and GPRRRPGCSRKNRTRS) and affinity purified by Research Genetics.

Western blot analysis. SDS-PAGE and Western blotting were performed as described previously (Kelleher et al., 1992; Huber et al., 2002); blocking was done with 3% (w/v) Top Block (Juro Supply, Lucerne, Switzerland). Antibodies were diluted as follows: AS 472 1:2000; AS Bianca 1:10,000; AS Florina: 1:20,000; affinity-purified AS 922 1.5 μg/ml; affinity-purified AS 294 0.3 μg/ml; affinity-purified AS α–NgR 0.11 μg/ml; α-BiP 2 μg/ml (Stressgen); mAb α-β-tubulin (Boehringer Mannheim, Mannheim, Germany) 1:200; mAb 9E10 α-myc (Invitrogen) 1:5000; monoclonal hybridoma culture supernatants 1:150. Secondary antibodies were HRP-conjugated goat anti-rabbit (Pierce; 1:20,000) and anti-mouse (1:50,000).

Cell surface biotinylation. Brain oligodendrocyte cultures (van der Haar et al., 1998) were incubated with 2 mg EZ-LINK-Sulfo-NHS-LC-Biotin (0.25 mg/ml) (Pierce) per 75 cm^2 flask for 30 min at 20°C followed by incubation with 8 ml of 10 mM glycine in PBS with Ca^{2+}/Mg^{2+} for 15 min to stop the biotinylation reaction and three washes with PBS. Cells were scraped, lysed in 1 ml lysis buffer [0.05 M NaH$_2$PO$_4$ pH 8.0, 0.15 M NaCl, 0.5% (w/v) CHAPS (Sigma), 2.5 mM iodacetamide, 1 mM phenyl-methylsulfonyl fluoride, 0.1 μg/ml aprotinin, 1 μg/ml leupeptin, 1 μg/ml pepstatin A] and precipitated three times with 100 μl of Dynabeads M-280 streptavidin (Dynal).

Immunocytochemistry. Optic nerve oligodendrocytes were prepared as

described (Schwab and Caroni, 1988). Cultures (3–5 d old) grown on poly-L-lysine-coated coverslips were washed twice with PBS, fixed in 4% (w/v) paraformaldehyde (PFA), 5% (w/v) sucrose in PBS for 15 min at room temperature; cells were permeabilized with 0.1% (v/v) Triton X-100 (Tx-100) in PBS, and nonspecific binding was blocked with 10% (v/v) FCS. Cells were then incubated with affinity-purified AS 472 (1:200) or AS 922 (1:100) hybridoma culture supernatants containing mAb 11A8, mAb 3D11, and mAb 11C7 (all 1:100), anti-MG160 (1:100), and anti-calnexin (1:1000) for confocal microscopy in PBS, 1% FCS, 0.1% (v/v) Tx-100. Selective permeabilization of the plasma membrane was performed as described by De Strooper et al. (1997) with modifications. The cultures were washed twice with 10 mM PIPES buffer, pH 6.8, containing 0.3 M sucrose, 0.1 M KCl, 2.5 mM MgCl$_2$, and 1 mM EDTA (De Strooper et al., 1997), followed by incubation of 50 min at room temperature in PIPES buffer with 12.5 μg/ml digitonin, containing the primary antibodies. Cells were washed with PIPES buffer and fixed and further processed. Secondary antibodies were goat anti-mouse tetramethylrho-damine isothiocyanate (TRITC) and goat anti-rabbit fluorescein-isothiocyanate (FITC) (Jackson ImmunoResearch Laboratories). A mouse monoclonal antibody against the KDEL sequence (α-BiP, 1:100; StressGen Biotechnologies, Victoria, British Columbia, Canada) was used to confirm the selective permeabilization of only the plasma membrane.

For cell surface staining, 2-d-old rat optic nerve cultures were incubated with AS 472 (1:500), AS 922 (1:500), AS Bianca (1:500), or mono-clonal antibodies (undiluted supernatant) in medium for 25 min at room temperature. For CHO/oligodendrocyte co-cultures, 6000 CHO cells per well were added 24 hr before staining procedures. Cultures were washed, fixed with 4% (w/v) PFA and 5% (w/v) sucrose and blocked with 0.1 M
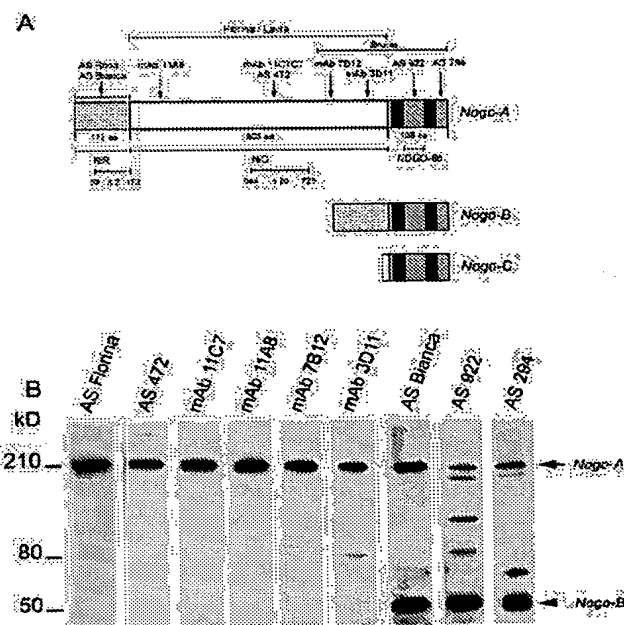
Figure 1. Nogo-A, -B, and –C isoforms, main studied fragments, and antibodies raised against Nogo-A sequence and their specificity on oligodendrocytes. A, Several monoclonal antibodies and polyclonal rabbit antisera (AS) were raised against Nogo-A. AS 472 (Chen et al., 2000) and mAb 11C7 were raised against the same 18 aa peptide. The other three mAbs, 11A8, 7B12, and 3D11, were raised against bacterially expressed NiR-G. AS Bianca was raised against bacterially produced NiR. AS 922 was raised against the Nogo-66 region between the two hydrophobic domains, and AS 294 was raised against the C terminus of Nogo. AS 922 and AS 294 recognize all Nogo isoforms. B, Western blot of lysates of cultured oligodendrocytes. The blot was incubated with different anti-Nogo-A antibodies. All antibodies recognize the 190 kDa Nogo-A band (arrow) and mAb 3D11, AS 922, and AS 294 stain additional bands at 60 and 80 kDa, presumably Nogo-A breakdown products. AS Bianca, AS 294, and AS 922 also recognize Nogo-B at ~55 kDa (arrowhead).

maleic acid with 2% (w/v) blocking reagent (Rôche) for 1 hr. Secondary alkaline phosphatase-conjugated antibodies (Milan Analytica, Lausanne, Switzerland) were used at 1:7500 in 0.1 M maleic acid with 1% (w/v) blocking reagent (1 hr). The cultures were washed twice with maleic acid buffer and once with alkaline phosphatase buffer (0.1 M Tris-HCl, pH 9.5, 0.1 M NaCl, 5 mM $MgCl_2$), and the staining was developed for 3 hr at room temperature with 0.175 mg/ml 5-bromo-4-chloro-3-indolyl-phosphate (Sigma) and 0.338 mg/ml nitroblue tetrazolium (Sigma) in alkaline phosphatase buffer. For surface MAG and intracellular Nogo-A, the staining was developed for 2 hr instead of 3 hr.

The pIgκ—V5-NgR CHO cells were washed, fixed for 15 min at room temperature, and blocked with 10% (v/v) FCS in PBS for 20 min at room temperature. mAb α-V5 (Invitrogen R-960—25) was diluted 1:300 in 1% (v/v) FCS in PBS for 1 hr and washed, and secondary FITC-conjugated anti-mouse antibodies (Jackson ImmunoResearch Laboratories) were used at 1:200 in PBS for 30 min.

Flow cytometry. Flow cytometry and cell sorting were performed on a Cytomation MoFlo high-speed cell sorter (Fort Collins, CO). The flow cytometer was equipped with an argon-ion/UV Enterprise II laser tuned to 488 nm with 130 mW of power. Fluorescein (FITC) fluorescence was collected through a 530/40 nm band-pass filter. For analysis, 3T3 fibroblasts were detached with Cell Dissociation Buffer (Invitrogen) or 0.5% (w/v) trypsin in PBS. The preformed complex used to detect binding of NiR-G to 3T3 fibroblasts was prepared as follows: NiR-G and anti-Myc antibody (9E10; Sigma) were incubated at a 1:1 molar ratio for 30 min at 4°C. Next, FITC-conjugated F(ab)$_2$ goat anti-mouse IgG was added and incubated for an additional 30 min at 4°C. The resulting molar ratio of the trimeric complex was 1:1:0.5. The complex was added to 1 × 10^6 3T3 fibroblasts in a final volume of 100 μl, incubated for 2 hr at 4°C, washed, and analyzed by flow cytometry.

In vitro assays. 3T3 fibroblast spreading assays were performed as described previously (Spillmann et al., 1998).

CHO spreading assays were performed essentially the same way as for 3T3 fibroblasts. Briefly, CHO cells were split 1:2. Twenty-four hours later they were trypsinized in PBS-EDTA for 30 sec, and ~8000 CHO cells were plated onto culture dishes precoated with 5, 1, 0.5, and 0.2 μg per well NiG or Nogo-66. After 30–45 min, the cells were fixed with 4% (w/v) PFA, 5% (w/v) sucrose and then analyzed.

PC12 neurite outgrowth assays were performed as described previously (Rubin et al., 1995).

Neurite outgrowth assays with P7 rat cerebellar granule cells were performed as described by Niederöst et al. (1999).

Retinal ganglion cell stripe assays were performed according to Vielmetter et al. (1990) with modifications (Schmalfeldt et al., 2000). Explants were evaluated after fixation with 4% (w/v) PFA, 0.1% (v/v) glutaraldehyde in PBS for 10 min at room temperature. For immunostainings, fixed explants were blocked for 1 hr at room temperature with RNO-blocking solution [0.5% (w/v) BSA, 0.3% (w/v) Top-Block (Juro Supply), 0.1% (w/v) NaN_3 in PBS], permeabilized for 10 min
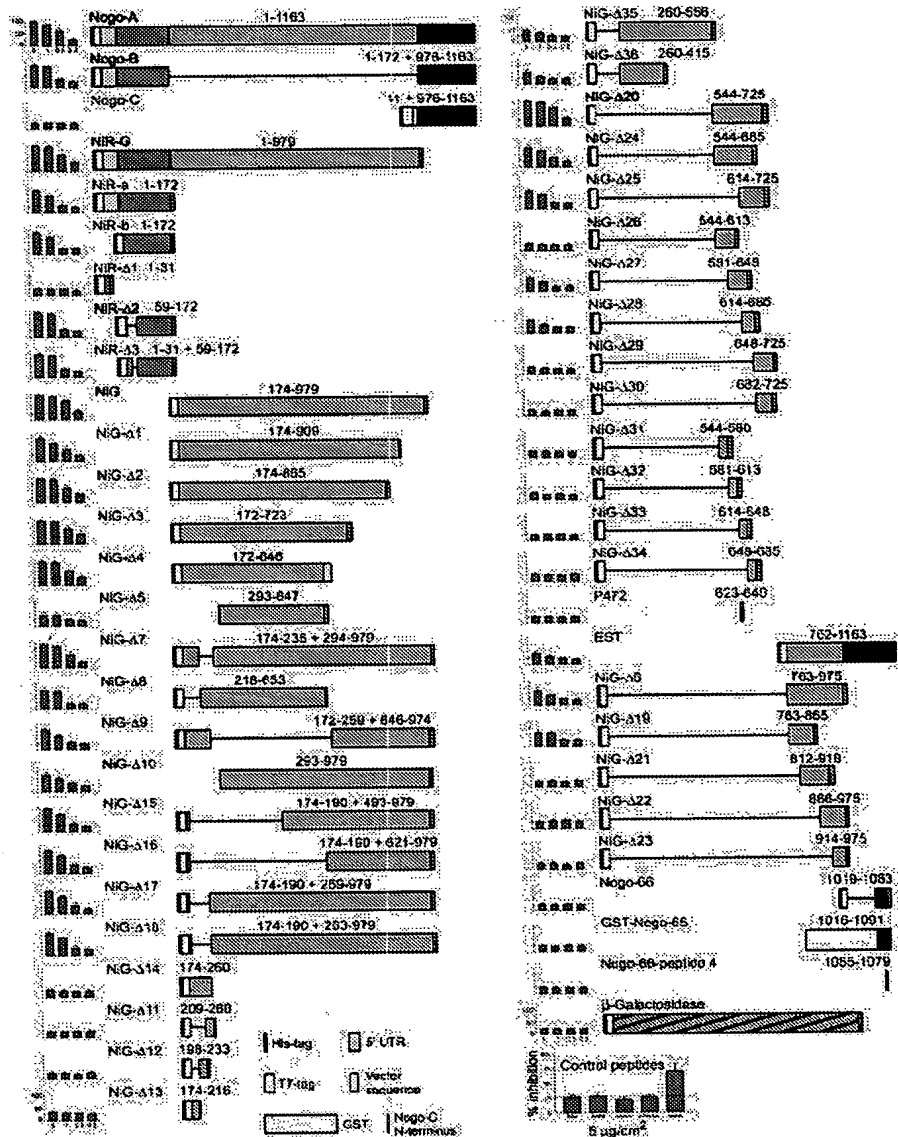
Figure 2. Analysis of the inhibitory properties of various Nogo fragments on 3T3 fibroblast spreading. The main inhibitory activity resides in two regions of the Nogo-A protein. Nogo-A deletion products were tested for their relative inhibitory activity (percentage inhibition) on fibroblast spreading (5 μg/100 μl, 1 μg/100 μl, 0.5 μg/100 μl, and 0.2 μg/100 μl of fragments coated per square centimeter). Mean of spreading on plastic is indicated by the dotted line. For each fragment at least three independent assays with proteins from at least two separate purifications were performed. The fragments that are most inhibitory for fibroblast spreading are highlighted. Control peptides (5 μg/100 μl coated per square centimeter) did not exhibit inhibitory properties except for l-laminin.

with 0.05% (v/v) Tx-100 in RNO-blocking solution, frozen for 1 min at −20°C, and incubated with primary antibodies (AS Bianca for NiR, AS Laura for Nogo-A, NiR-G, NiG, NiG-Δ3, and NiG-Δ20, and Novagen mAb anti-T7 for Nogo-C and β-Gal control protein). After washing with PBS, FITC- and TRITC-conjugated antibodies (Jackson ImmunoResearch Laboratories) were added (1:150) to the explants. The samples were coverslipped in 50% (v/v) glycerol, 25 mM $NaHCO_3$, 40 mM NaCl, 1% (w/v) p-phenylendiamine (Sigma).

Growth cone collapse assays on chick and rat DRG neurons were performed essentially as described previously (Bandtlow et al., 1993; Bandtlow and Löschinger, 1997; Fritsche et al., 1999).

Results

The three main isoforms of Nogo, the most important domains and active sites, and the epitopes of the antibodies and antisera used in this study are summarized in Figure 1.

Two regions in the N-terminal part of Nogo-A are inhibitory for spreading of 3T3 fibroblasts

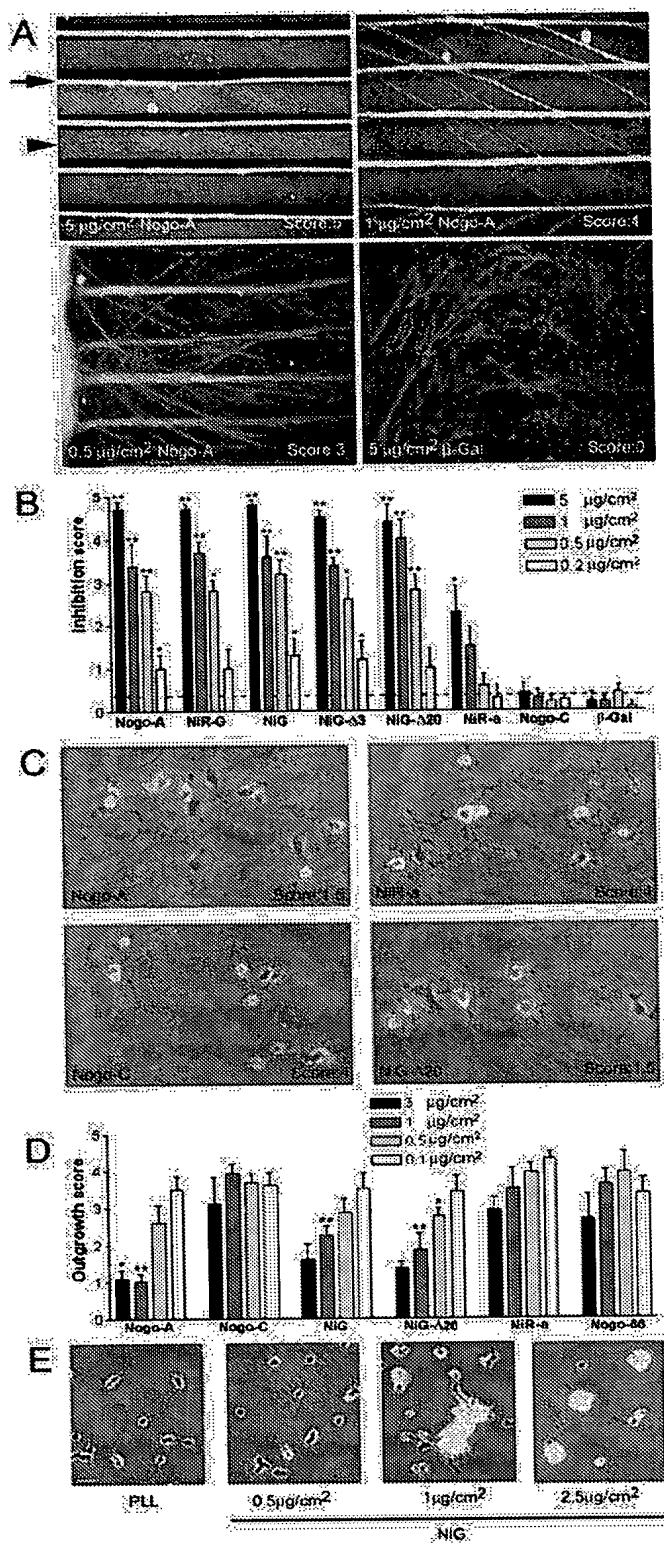To identify the regions of Nogo-A responsible for the inhibition of 3T3 fibroblast spreading, a library of 50 Nogo deletion constructs was made, and recombinant proteins were expressed in bacteria (Fig. 2). The Co^{2+}-affinity chromatography-purified Nogo fragments were coated on tissue-culture dishes. The purified material of some of the recombinant proteins contained lower molecular weight Nogo fragments (Chen et al., 1999), because the Nogo-A cDNA sequence contains internal ribosomal binding sites for *E. coli* and numerous rare codons (our unpublished observations). The purity of fragments was estimated on the basis of silver-stained SDS-PAGE (see Fig. 6D). The comparison between the different deletion constructs is therefore semiquantitative.

The apparent EC_{50} for inhibition of 3T3 fibroblast spreading was ~400–500 ng/100 μl Nogo-A coated overnight per cm^2 of culture dish (~4 pmol/cm^2). Treatment of Nogo-A or its fragments with 8 M urea resulted in a strong reduction of inhibitory activity, indicating that conformation is important.

The analysis of Nogo fragments in the fibroblast spreading assay revealed that at least two stretches of the Nogo-A protein mediate inhibition of the spreading of freshly plated fibroblasts, namely aa 59–172 (NiR-Δ2) and aa 544–725 (NiG-Δ20) (Figs. 2, 3). All of the fragments derived from the Nogo-A-specific region (NiG) displaying inhibitory activity (e.g., NiG-Δ4 and NiG-Δ8) partially overlap with aa 544–725 (NiG-Δ20). Minor inhibitory activity at high protein concentration was seen for the C-terminal part of the Nogo-A-specific region (aa 763–865; NiG-Δ19). At high concentrations, the anti-spreading activity of the Nogo fragments became anti-adhesive. These two effects could be overcome eventually by the cells after longer incubation times, indicating that they were not caused by toxic effects (data not shown). Nogo-C, Nogo-66, and Nogo-66 Peptide 4 [shown to be the inhibitory region of Nogo-66 by GrandPré et al. (2000)] were not inhibitory for fibroblast spreading (Fig. 2).

We found no correlation between the isoelectric point of the protein fragments and their inhibitory character. The high occurrence of proline and serine in the N-terminus of Nogo-A is also

---

←

accompanied by strong axonal fasciculation. Control β-galactosidase/laminin stripes (stained with α-T7 mAb) are permissive substrates for RGC axons. *B*, Inhibition score for RGC outgrowth on different Nogo fragments. Cultures were evaluated by giving a score of 5 for striped neurite outgrowth with no fibers crossing the Nogo containing stripes, 4–2 for striped neurite outgrowth with increasing numbers of crossing fibers, 1 for random outgrowth with tendency to grow in the direction of the stripes, and 0 for complete random neurite outgrowth. The dotted line indicates the mean of all β-galactosidase control experiments. Values are represented as mean $\pm$ SE. The groups have been compared with the scores for Nogo-C at the same coated protein concentration ($*p < 0.05$; $**p < 0.01$; Mann–Whitney U test). *C*, Examples of PC12 neurite outgrowth on different substrates. On Nogo-A and its fragment NiG-Δ20, the number of neurites is reduced and they are shorter compared with cells grown on Nogo-C and NiR. *D*, Quantification of outgrowth of PC12 neurites grown on different Nogo substrates (scores from 0 = no outgrowth to 5 = long, branched neurites). Values are represented as mean $\pm$ SE. The groups have been compared with the scores for Nogo-C at the same coated protein concentration ($*p < 0.05$; $**p < 0.01$; Mann–Whitney U test). *E*, Primary rat cerebellar granule cells were plated on increasing amounts of coated NiG. The inhibition of neurite outgrowth and cell adhesion by NiG is dose dependent.

Figure 3. Analysis of the inhibitory activity of Nogo-A on neurite outgrowth. *A, B*, Nogo-A is an inhibitory substrate for E7–E9 RGC neurite outgrowth in a stripe assay. Stripes of Nogo/laminin (arrowhead) versus laminin-only stripes (arrow) were compared. *A*, The axons (stained with anti-neurofilament mAb) growing from chicken retina explants avoid the Nogo/laminin stripes (stained with AS Laura; arrowhead). This avoidance is concentration dependent and

not responsible for the observed effect because a poly-Pro/Ser peptide is not inhibitory (Fig. 2, Control peptides).

These data show that the anti-spreading activity of Nogo-A on 3T3 fibroblasts resides in two defined stretches located at the N-terminus (aa 59–172) and within the Nogo-A-specific part (aa 544–725; NiG-Δ20) of the protein. Nonspecific physicochemical properties (acidity of the fragments, structural effects attributable to proline and serine residues) are not responsible for this effect. The C-terminal RTN-homology domain including Nogo-66 is not involved in the inhibition of fibroblast spreading.

Several regions of Nogo-A are inhibitory for neurite outgrowth

To determine whether the fragments of Nogo-A that were non-permissive for cell spreading are also inhibitory for neurite outgrowth, we tested a series of bacterially produced Nogo-A fragments as well as eukaryotically produced Nogo-fragment–alkaline phosphatase (Nogo-AP) fusion proteins in different neuronal assays.

In a substrate stripe assay (Vielmetter et al., 1990), we tested whether Nogo stripes are inhibitory for the growing embryonic chicken [embryonic day (E) 7–9] RGC axons. Neurites avoided laminin/Nogo-A-coated stripes, growing on the laminin-only stripes (Fig. 3A), whereas stripes coated with laminin/β-galactosidase were not circumvented. Full-length Nogo-A was strongly nonpermissive for RGC neurites, whereas the N-terminal part of Nogo-A/-B (aa 1–172) had only marginal effects. Nogo-C activity was indistinguishable from the control protein β-galactosidase (Fig. 2A,B). The Nogo-A-specific region NiG-Δ20 (aa 544–725) appears to contain the main inhibitory region for these neurites (Fig. 3B). The growth cones were also seen to stop when entering NiG-Δ20-coated "dead-end" lanes (data not shown). These nonpermissive effects were concentration dependent: increasing numbers of crossing fibers were observed at lower concentrations of Nogo-A or its active fragments (Fig. 3A,B). No obvious difference was detected between nasal and temporal RGC neurites concerning their responsiveness to Nogo-A regions.

A laminin-independent, NGF-responsive clone of PC12 cells (Rubin et al., 1995) was primed with 50 ng/ml NGF for 24 hr and then plated onto dishes coated with bacterially produced Nogo fragments at 0.1–3 μg/cm^2. Neurite outgrowth was scored 1 d later. The Nogo-A-specific region (NiG) and its aa 544–725 fragment (NiG-Δ20) strongly inhibited PC12 neurite outgrowth (Fig. 3C,D). In contrast, the N-terminal fragment (aa 1–172) had only minor activity, detectable only at high protein concentration. Nogo-C and Nogo-66 were inactive.

Substrate-coated NiG (aa 174–979) also acted as a strong neurite growth inhibitor of primary mammalian neurons: neurite outgrowth of postnatal day (P) 7 rat cerebellar granule cells was prevented in a dose-dependent manner, and cells aggregated at higher Nogo substrate concentrations (Fig. 3E).

We further tested the growth cone collapsing activities of the various Nogo constructs. Murine GST-Nogo-66, human GST-Nogo-66, and HPLC-purified Nogo-66 lacking the GST tag induced growth cone collapse of E13–E15 chicken DRG explants as described previously (GrandPré et al., 2000; Fournier et al., 2001). The growth cone collapsing activities of these proteins were relatively low (~50% collapsed at ~1 μM) and varied between preparations, probably because of the poor solubility of these recombinant proteins. Nogo-66 peptide 4 was inactive. In contrast, soluble dimeric Nogo-66-AP was collapse-inducing in a
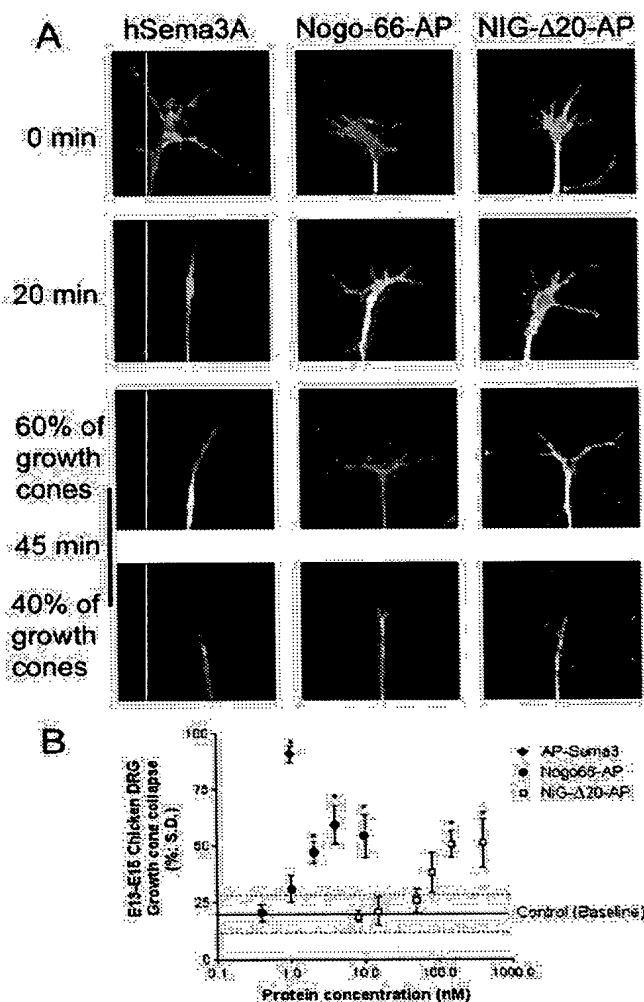
Figure 4. Analysis of the collapsing activity of different Nogo-A fragments on DRG growth cones. *A*, Time course of the growth cone collapse of dissociated rat P6 DRG neurons induced by preclustered NiG-Δ20-AP, Nogo-66-AP, or Sema3A. After the indicated time periods, the cultures were fixed and doubly labeled by anti-tubulin antibody and tetramethylrhodamine B isothiocyanate-phalloidin. *B*, Dose-dependent growth cone collapse of chicken E13–E15 DRG explants treated with preclustered NiG-Δ20-AP, Nogo-66-AP, and AP-Sema3A. All three proteins induce growth cone collapse, but Nogo-66-AP is more potent than NiG-Δ20-AP. Both Nogo-AP fragments have a much weaker collapse-inducing activity than AP-Sema3A.

range similar to what has been described previously with an apparent EC$_{50}$ of ~2 nM (Fig. 4B) (GrandPré et al., 2000). Growth cone collapse could also be elicited by the Nogo-A-specific, soluble, and dimeric fragment aa 544–725 (NiG-Δ20-AP), with an apparent EC$_{50}$ of 200–400 nM (Fig. 4B). Bacterially expressed recombinant monomeric NiG (aa 174–979) or NiG-Δ20 (aa 544–725) had no collapse-inducing activities, nor had NiR-G (aa 1–979). Time-lapse studies on dissociated rat P6 DRG neurons revealed that growth cone collapse induced by Nogo-66-AP and NiG-Δ20-AP occurred with a slower time course than collapse elicited by hSema3A (Fig. 4A). In addition, although AP-Sema3A induced collapse of virtually all growth cones at low nanomolar concentration, both Nogo-66-AP and NiG-Δ20-AP did not lead to collapse of >60% of the rat or chicken growth cones (Fig. 4A,B).
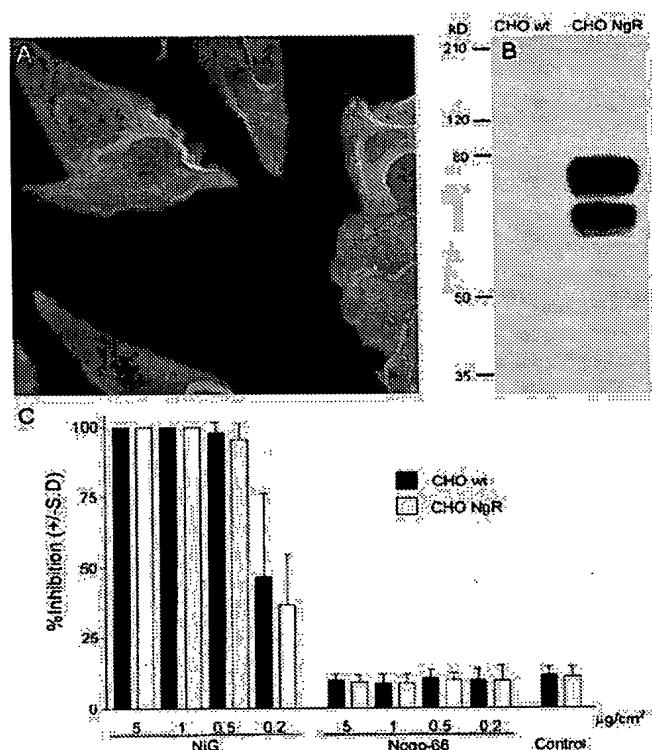
Figure 5. Activity of NgR-expressing CHO cells versus wild-type cells on Nogo fragments. *A*, An mAb against the V5-epitope stains the surface of a CHO cell line stably transfected with rat NgR. *B*, On Western blot, no NgR protein is detectable in lysates of wild-type CHO cells, whereas high amounts of NgR are detectable in lysates of the CHO–NgR cell line. *C*, Both wild-type and NgR-transfected CHO cells are strongly inhibited in spreading by the Nogo-A-specific region NiG, whereas they are unresponsive to Nogo-66.

The Nogo-66 receptor NgR is not required for inhibition of cell spreading

We isolated a cDNA encoding the rat NgR protein (GenBank accession number AF462390) and generated antisera against specific peptides of the protein. To study the role of NgR for inhibition of cell spreading, we generated a CHO cell line stably expressing rat NgR at high levels on its cell surface (Fig. 5*A*,*B*). Wild-type CHO cells (CHO-wt) do not express detectable amounts of NgR as determined by RT-PCR (40 cycles; data not shown) and Western blotting (Fig. 5*B*). Spreading of both CHO-wt and CHO-NgR was dose-dependently inhibited by Nogo-A aa 174–979 (NiG). Independent of NgR expression, neither cell line responded to coated Nogo-66 (Fig. 5*C*).

These results show that the inhibition of fibroblast-like cells by the Nogo-A-specific active region can occur in the absence of NgR and that the presence of NgR does not change the responsiveness of the cells to Nogo-66 or Nogo-A.

Presence of binding site(s) for active Nogo-A-specific fragments on 3T3 fibroblasts and rat brain cortical membranes

Because the Nogo-A fragments aa 1–172 and aa 544–725 (NiR-Δ2 and NiG-Δ20) were inhibitory for cell spreading and neurite outgrowth despite the absence of Nogo-66 and independently of NgR, the presence of a separate, Nogo-A-specific receptor has to be postulated. We therefore performed binding studies of multimerized, myc-tagged, and IMAC-purified Nogo-A aa
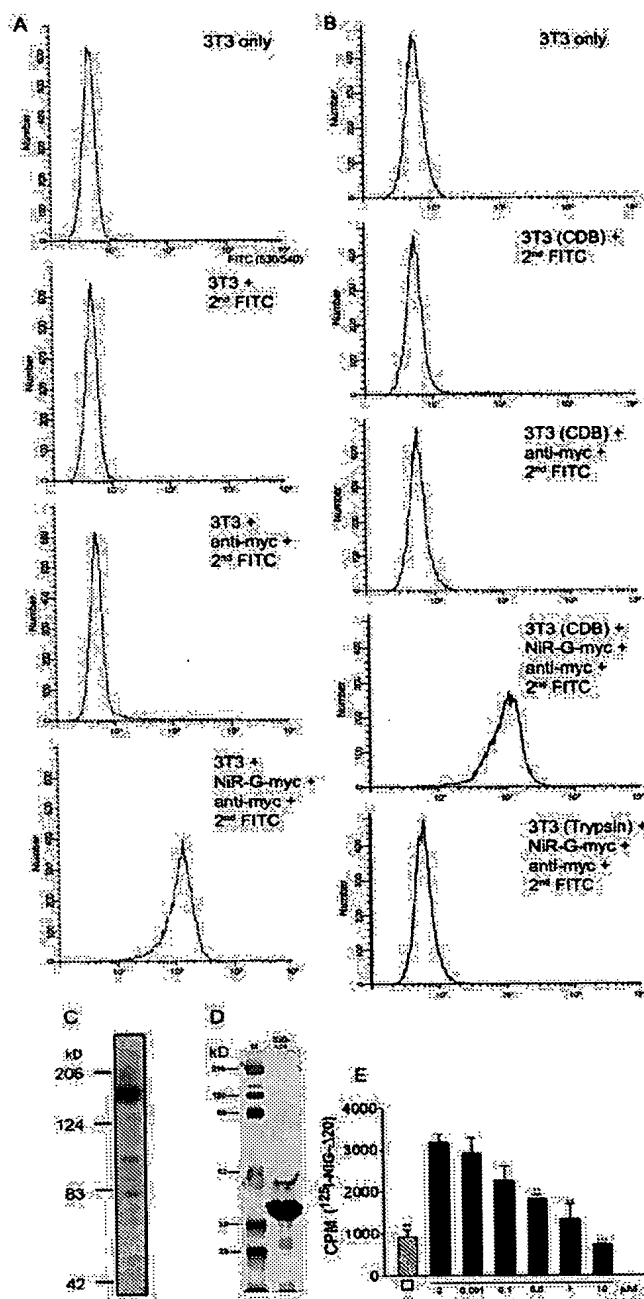
Figure 6. Binding of amino terminal Nogo fragments to 3T3 cells and cortical membranes. *A*, Binding of NiR-G (aa 1–979) to 3T3 cells. 3T3 fibroblasts were incubated with a preformed complex consisting of α-myc antibody (9E10), FITC-conjugated F(ab)₂ goat α-mouse IgG fragments, and myc-tagged amino-terminal fragment of Nogo-A (NiR-G). Binding of the complex to 3T3 fibroblasts was analyzed by flow cytometry. Unstained 3T3 fibroblasts were used as negative control. Further negative controls include 3T3 cells incubated with a complex consisting of the α-myc antibody and the FITC-conjugated α-mouse Ab or with the FITC-conjugated α-mouse Ab alone. *B*, Binding of NiR-G to 3T3 cells is protease sensitive: trypsinization of 3T3 fibroblasts before incubation with Nogo completely abolishes Nogo-binding to their surface. *C*, Western blot of purified, myc-epitope-tagged NiR-G. *D*, Silver-stained gel of IMAC-purified NiG-Δ20. M, Molecular weight standard. *E*, Binding of 1.3 nм [¹²⁵I]-NiG-Δ20 to rat brain cortical membranes and competition by increasing concentration of unlabeled NiG-Δ20. □ indicates the values obtained after incubation of 1.3 nм [¹²⁵I]-NiG-Δ20 in the absence of cortical membranes, i.e., nonspecific binding to the tubes. Values are represented as mean ± SE (**p < 0.01; ***p < 0.001; Student's *t* test for competition; *n* = 3).

1–979 (Fig. 6C) to living 3T3 fibroblasts. The cells were labeled in suspension at 4°C and subsequently analyzed by flow cytometry. Anti-myc monoclonal antibody-complexed myc-tagged Nogo-A fragment (NiR-G) bound efficiently to 3T3 cells as seen by a shift in fluorescence of >90% of the 3T3 cells (Fig. 6A). In contrast, 3T3 cells were not labeled after incubation with the primary mouse anti-myc mAb complexed with an FITC-conjugated secondary F(ab)₂ goat anti-mouse IgG in the absence of Nogo-A or with the secondary Ab alone. The binding of the amino terminal Nogo-A fragment to the surface of fibroblasts is protease sensitive, because 3T3 cells that were dissociated with trypsin before Nogo-A incubation do not bind Nogo-A (Fig. 6B).

To test binding of Nogo-A aa 544–725 (NiG-Δ20) to rat cortical membranes, we used [^{125}I]-labeled NiG-Δ20 in a radioligand binding assay (Fig. 6D). [^{125}I]-labeled Nogo fragment bound to these brain plasma membranes. The specificity of binding was shown by a concentration-dependent competition of [^{125}I]-NiG-Δ20 binding at a concentration of 1.3 nM by increasing amounts of unlabeled Nogo-A aa 544–725 (Fig. 6E).

These results show that defined, bioactive fragments of Nogo-A can bind to the surface of 3T3 cells and rat cortical membranes, demonstrating the presence of membrane-bound, Nogo-A-specific binding sites or receptor(s) different from the Nogo-66 receptor NgR.
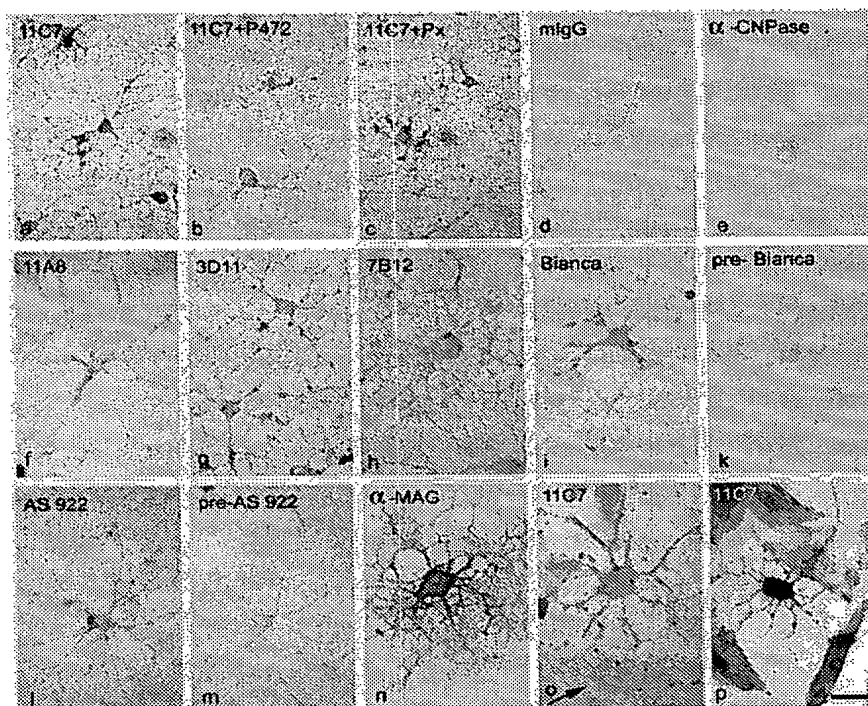

Figure 7. Nogo-A is present at the cell surface of cultured oligodendrocytes. Live, unpermeabilized oligodendrocytes (3 d in culture) were incubated with anti-Nogo-A antibodies, fixed, and visualized with secondary antibodies conjugated with alkaline phosphatase. All antibodies against the N-terminus of Nogo-A stain the cell surface of oligodendrocytes (mAb 11C7, mAb 11A8, mAb 3D11, mAb 7B12, AS Bianca), although more weakly than an antibody against the surface glycoprotein MAG (shorter development; see Materials and Methods). The control mouse IgG (d) and an antibody against the intracellular oligodendrocyte protein CNPase (e) do not stain oligodendrocytes. Preincubation of 11C7 with the immunogen, peptide P472, reduced the staining to background levels (b), whereas preincubation with an unspecific peptide (Px) did not result in a reduction in staining intensity (c). Furthermore, AS 922 against the C-terminal Nogo-66-region stains the cell surface of living oligodendrocytes (l), whereas the corresponding preimmune serum (pre-922) gives only background staining (m). Staining of co-cultures of oligodendrocytes with CHO cells expressing rat Nogo-A with mAb 11C7 shows that although intact oligodendrocytes are stained, Nogo-A produced by CHO cells (arrow) is not detectable at the cell surface (o). Both cell types are stained with 11C7 after permeabilization (p). Scale bar, 25 μm.

Antibodies against Nogo-A

Antisera and monoclonal antibodies were raised against Nogo-A peptides or recombinant protein fragments (Fig. 1). The monoclonal antibody 11C7 was raised against Nogo-A aa 623–640, i.e., the same Nogo-A specific peptide as the rabbit AS 472 (Chen et al., 2000). Three other mAbs raised against Nogo-A aa 1–979 (NiR-G) reacted with different epitopes as determined by ELISA on the Nogo protein fragment library: 11A8 recognizes the most N-terminal part of the Nogo-A-specific region (~aa 209–233), and 7B12 (~aa 763–820) and 3D11 (~aa 910–920) recognize the C-terminal part of the Nogo-A-specific region of the molecule. Two antisera (AS Bianca and AS Rosa) recognize the N-terminal region aa 1–172 (NiR), common to both Nogo-A and Nogo-B. Finally, antisera were raised against the Nogo-66 region (AS 922) and the C terminus of Nogo including the ER retention signal (AS 294), respectively.

Antibodies against all epitopes identified the 190 kDa Nogo-A band on a Western blot of oligodendrocyte cell culture homogenate (Fig. 1B). AS Bianca, AS 922, and AS 294 also recognize the 55 kDa band of Nogo-B. mAb 3D11 and AS 922 recognized an additional band at ~80 kDa, which could be a breakdown product of Nogo-A. At longer exposure times, AS 922 and AS 294 both stained additional bands even after affinity purification.

Domains of Nogo-A present at the cell surface of cultured oligodendrocytes

Cultures of unpermeabilized living oligodendrocytes were incubated with different anti-Nogo-A antibodies. The Nogo-A-specific mAbs 11C7, 11A8, 7B12, and 3D11 (Figs. 1, 7a,f,g,h) as well as AS 472 (data not shown) stained the surface of the differentiated oligodendrocyte cell bodies and their process network. Compared with stainings for GalC or sulfatide (data not shown) or an mAb against the oligodendrocyte surface protein MAG (Fig. 7n), the Nogo staining was relatively weak. The specificity of the cell surface staining is suggested by the following results. (1) The control mouse IgG and the antibodies against the intracellular protein CNPase did not stain intact living cells (Fig. 7d,e). (2) Preincubation of mAb 11C7 (or AS 472; data not shown) with the corresponding immunogenic peptide P472 reduced staining to background levels (Fig. 7b). Preincubation of mAb 11C7 or AS 472 with an unspecific peptide (Px) before their addition to the cells did not reduce the staining (Fig. 7c). (3) Co-cultures of oligodendrocytes with transfected Nogo-A-expressing CHO cells were stained with mAb 11C7. Although intracellular Nogo-A was detectable in both cell types after permeabilization (Fig. 7p), surface Nogo-A could be detected only on oligodendrocytes but not on the transfected CHO cells (Fig. 7o). This observation suggests that transport of Nogo-A to the cell surface could be cell-type
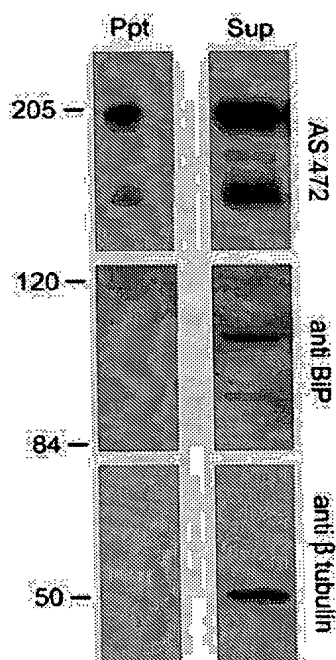
Figure 8. Precipitation of Nogo-A from cell-surface biotinylated oligodendrocytes. Living cultures of oligodendrocytes were incubated with a cell-impermeable NHS-biotin analog. The biotinylated proteins were precipitated with streptavidin-coated beads, and the precipitate (Ppt) and supernatant (Sup) were analyzed by Western blot. All of the pellet and 1/10 of the supernatant were loaded. AS 472 showed the presence of Nogo-A in the precipitated sample, whereas the intracellular proteins β-tubulin and BiP were not present in the precipitated material. Intracellular Nogo-A, β—tubulin, and BiP were found in the supernatant.

specific. AS Bianca recognizing the N-terminus of Nogo-A, but not the corresponding preimmune serum, also stained the cell surface of living oligodendrocytes (Fig. 7i,k). Staining with AS 922 showed that also the Nogo-66 region is exposed on the surface of oligodendrocytes, confirming previous reports (GrandPré et al., 2000). Because AS 922 stains additional bands on Western blot (Fig. 1B), however, we cannot exclude the possibility that the antiserum also recognizes proteins other than Nogo on the cell surface of oligodendrocytes. Cell surface staining was present on all major and small processes and on the cell body.

These results suggest that the Nogo-A-specific part and the N-terminus of the molecule as well as the Nogo-66 loop are exposed to the extracellular space on the plasma membrane of oligodendrocytes.

Cell surface biotinylation of Nogo-A

To confirm the presence of Nogo-A on the cell surface of oligodendrocytes, living, unpermeabilized cultures of new-born rat brain oligodendrocytes were exposed to a membrane-impermeable biotinylating reagent. Biotinylated proteins were precipitated with streptavidin-coated beads. The precipitated proteins and the supernatants of the precipitates were analyzed by Western blot. In the precipitate, Nogo-A was recognized by the Nogo-A-specific AS 472 with the expected molecular weight of 190 kDa (Fig. 8). This band was also recognized by another anti-Nogo-A antiserum, AS Bruna (data not shown) and was not detected when biotin was omitted in control experiments (data not shown). The abundant intracellular proteins β-tubulin and
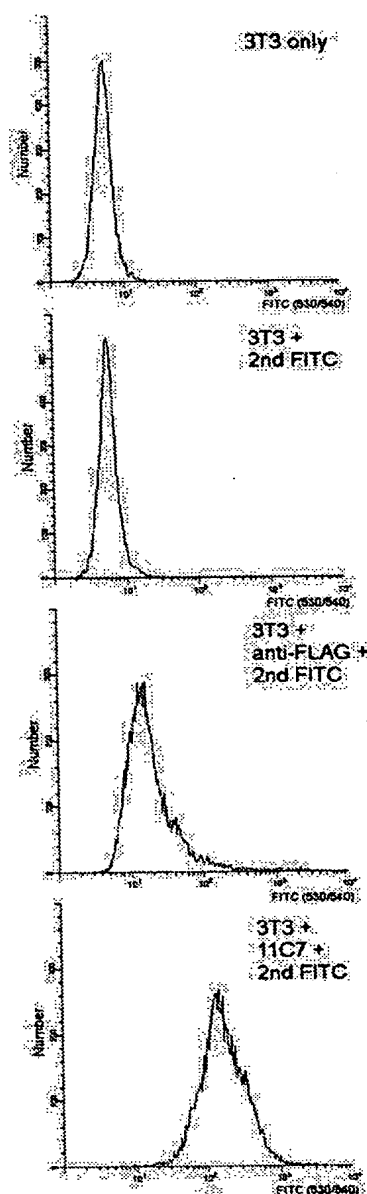

Figure 9. Nogo-A-specific epitopes are detected at the cell surface of 3T3 fibroblasts. 3T3 fibroblasts were detached with Cell Dissociating Buffer (Invitrogen) and incubated with 11C7 (α-Nogo-A) at a concentration of 0.1 μM for 1 hr. As an isotype control, the α-FLAG-M2 antibody is used at a concentration of 0.1 μM. After washing twice with PBS, the cells were incubated with a goat α-mouse FITC-labeled antibody (1:100) and analyzed by flow cytometry. Additional negative controls include unstained 3T3 fibroblasts and the secondary antibody alone. In all experiments dead cells were detected by Via-Probe (BD-PharMingen) and are excluded from the analysis. Note that the 11C7 antibody detects the Nogo-A-specific region on intact, unpermeabilized 3T3 fibroblasts.

BiP were not present in the precipitated material but were detected in the supernatant (Fig. 8). In line with the data shown below (see Fig. 10), large amounts of Nogo-A were also present intracellularly. Densitometric analysis of blots of three separate experiments revealed that ~1% of total cellular Nogo-A could be precipitated by biotinylation from the cell surface of the cultured oligodendrocytes.

Tx-100   DIG

11C7

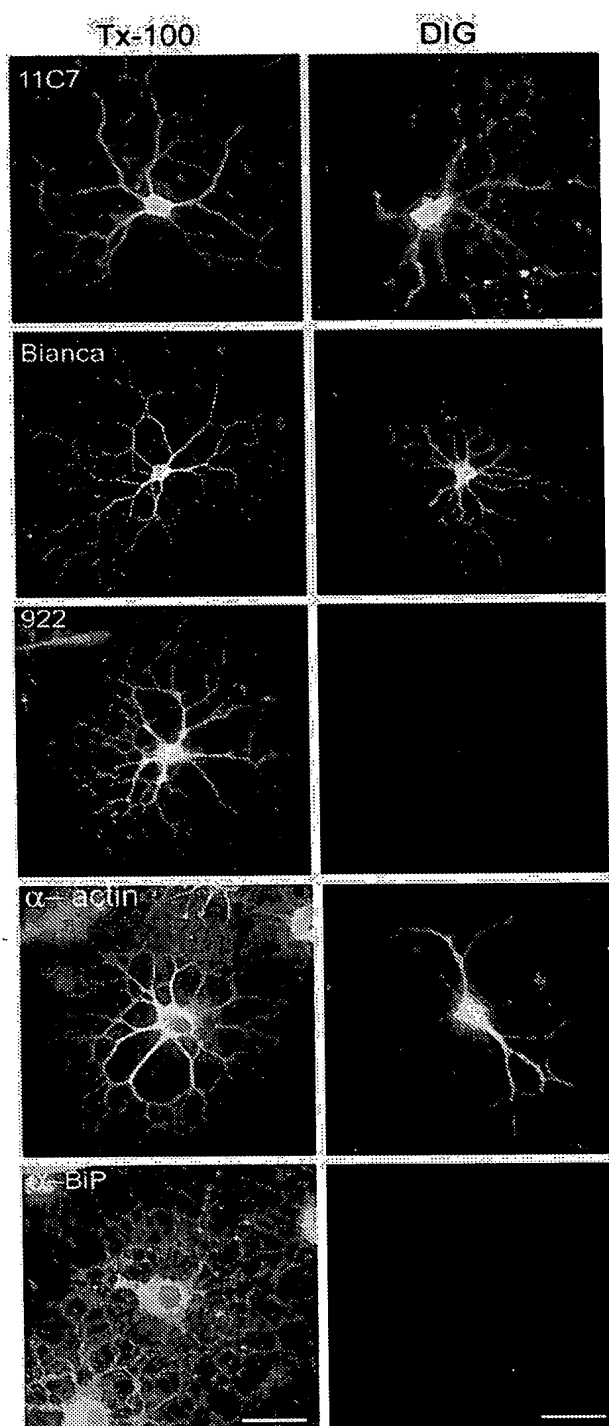Bianca

922

α-actin

α-BiP

Figure 10. Topology of Nogo-A in cultured oligodendrocytes. Oligodendrocytes (3–5 d in culture) were either fixed and completely permeabilized with Triton X-100 (Tx-100) or only plasma membrane permeabilized with digitonin (DIG). Cells were incubated with different α-Nogo-A antibodies. All α-Nogo-A Abs, mAb 11C7, AS Bianca, and AS 922 specifically recognize oligodendrocytes in dissociated rat optic nerve cultures (left row). After selective permeabilization with DIG, mAb 11C7, AS Bianca, and α-actin IgM mAb stain Nogo in the cytoplasm of oligodendrocytes (right row), whereas AS 922 does not. Antibodies against the luminal ER protein BiP were used as a control for the selective permeabilization. In DIG-permeabilized cells, no α-BiP staining could be detected, whereas all cells were strongly stained in the Tx-100-permeabilized cultures. Scale bar, 30 μm.

Nogo-A is present at the surface of 3T3 fibroblasts with Nogo-A-specific regions facing the extracellular space

Nogo-A is expressed endogenously in various cultured cell lines including the Nogo-A-responsive 3T3 fibroblasts (as shown by RT-PCR and Western blot) (Oertle et al., 2003b). To analyze whether Nogo-A-specific regions are also present on the surface of these cells, 3T3 fibroblasts were detached from the culture flask with Cell Dissociation Solution and incubated in suspension with 0.1 μM Nogo-A-specific mAb 11C7, followed by FITC-conjugated secondary Ab. Cells that bound the Nogo-A antibody were separated from unlabeled cells by fluorescence-activated cell sorting. mAb 11C7, but not a mouse IgG control Ab or the secondary Ab alone, labeled the 3T3 cells as seen by a large shift of the fluorescence intensity of the 3T3 cell population (Fig. 9).

This result indicates that the mAb 11C7 epitope, aa 623–640, which lies within the Nogo-A-specific region with highest inhibitory activity, is present on the surface of living 3T3 fibroblasts.

Intracellular localization and topology of Nogo-A

Fixed and permeabilized oligodendrocytes in cultures derived from P7–P10 optic nerve were stained with AS 472, AS 922, AS Bianca, and the mAbs 11C7, 11A8, and 3D11 (Fig. 10). The bulk of the staining was reticular, present in both the cell body and the large processes of the oligodendrocytes. Note the difference in staining between Nogo-A (Fig. 10, 11C7 Tx-100), an ER membrane protein, and BiP (Fig. 10, α-BiP Tx-100), which is a soluble protein present in the ER lumen. (The same reticular staining patterns were obtained with calnexin, also an ER membrane protein) (Fig. 11A–C). Nogo-A was not detectable on the membrane sheaths formed between the fine processes at longer culture times (data not shown). To elucidate the orientation of the intracellular protein, we selectively permeabilized oligodendrocytes with digitonin (DIG), an agent that at low concentrations permeabilizes solely the plasma membrane and leaves intracellular membranes intact (De Strooper et al., 1997). In cultures permeabilized with DIG, all antibodies and antisera except for AS 922 stained Nogo-A in the cytoplasm of oligodendrocytes (Fig. 10, right row). Staining with an antibody against a lumenal ER protein, BiP, was negative (Fig. 10), whereas staining against actin was positive (Fig. 10), showing the selectivity of the plasma membrane, but not ER, permeabilization.

These results demonstrate that the Nogo-A-specific region and the N-terminus of Nogo-A are exposed to the cytoplasmic side of intracellular membranes, at least for a large part of the Nogo-A residing in the ER.

We then examined in which intracellular compartment Nogo-A was present by colocalization studies using confocal microscopy. Double labeling with antibodies against Nogo-A and the ER marker calnexin (Fig. 11A–C) revealed that most but not all Nogo-A colocalized with calnexin. The colocalization was most marked in the oligodendrocyte processes. In the cell body, an area could often be observed to one side of the nucleus where only Nogo-A was present but the ER marker was absent (Fig. 11C, arrowhead). In this perinuclear region, Nogo-A colocalized with the Golgi marker MG160 (Gonatas et al., 1989; Croul et al., 1990; Gonatas et al., 1995) (Fig. 11D–F). Thus, Nogo-A is present intracellularly in both the ER and the Golgi complex.
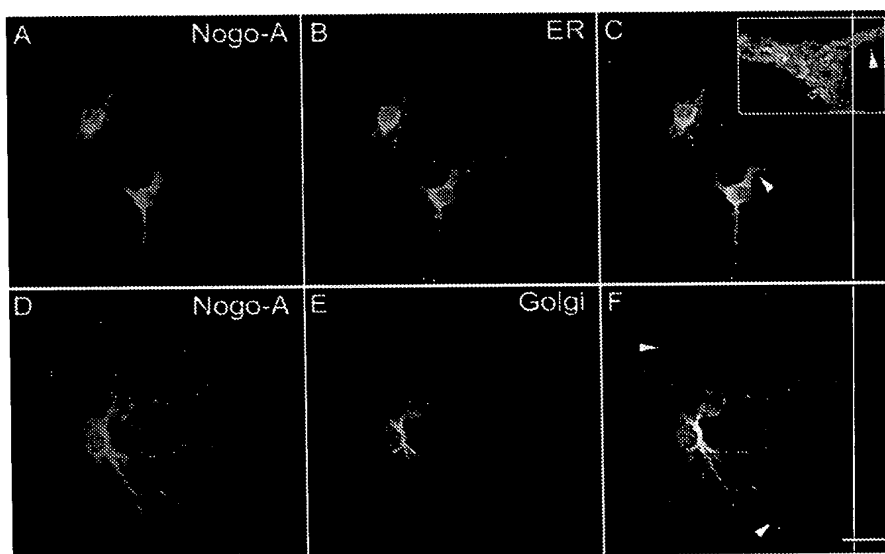
Figure 11. Intracellular localization of Nogo-A in cultured oligodendrocytes. Fixed oligodendrocytes permeabilized with Triton X-100 were double stained with mAb 11C7 (A, red) and the ER marker α-calnexin (B, green) or AS 472 (D, red) and α-MG160 outlining the Golgi complex (E, green) and analyzed by confocal microscopy in single optical sections. Nogo-A colocalizes with calnexin (C, yellow) as well as with the Golgi-marker (F, yellow). The magnification in C is taken from a different cell. The planes of the optical sections were chosen for optimal visualization of the colocalization of Nogo with the marker proteins in the cell body and the main processes. Both mAb 11C7 and AS 472 stain the entire cell with all the processes. Note the regions in which the Nogo-A immunoreactivity does not completely overlap with the ER-marker (C, arrowheads) or Golgi-marker (F, arrowheads). Scale bar: (in F) A–C, 20 μm; D–F, 15 μm.

Discussion

Three domains of Nogo-A are differentially involved in the inhibition of cell spreading, neurite outgrowth, and growth cone collapse

More than 50 Nogo protein fragments were expressed in *E. coli* or eukaryotic cells and coated as culture substrates or added as soluble proteins to cultured cells. Three active regions of Nogo could be defined. (1) On the basis of our semiquantitative analysis, the N-terminus of Nogo-A/-B inhibits 3T3 cell spreading as a substrate but has only a minor effect on neurons. (2) The Nogo-A-specific region and its central 181 amino acids are an inhibitory substrate for primary neurons, PC12 cells, and fibroblasts, and the same regions induce growth cone collapse when added as dimers in solution. (3) Dimeric Nogo-66 (loop region between the two C-terminal hydrophobic regions) induces growth cone collapse, but Nogo-66 or Nogo-C coated as substrate are inhibitory for neither E7–E9 chick retina or PC12 cell neurite outgrowth nor fibroblast spreading. Thus, Nogo-66 peptide seems to be *prime facie* more potent than the Nogo-A-specific region in inducing DRG growth cone collapse, whereas the Nogo-A-specific region has a stronger neurite outgrowth inhibitory activity. This might indicate that the interaction of Nogo-66 with its receptor NgR could be involved primarily in axonal guidance, whereas the Nogo-A-specific region could be involved in limiting plasticity and regeneration. It is known from other proteins that multiple distinct regions might contribute to their inhibitory activity (Ughrin et al., 2003).

The potent inhibitory activity of the Nogo-A regions has been recognized previously (Chen et al., 1999, 2000; Oertle et al., 2000; Prinjha et al., 2000; Fournier et al., 2001). The physiological importance of this region is emphasized by the fact that an antiserum (AS 472) against aa 623–640 in the Nogo-A-specific region neutralizes the inhibitory activity of CNS myelin *in vitro* (Chen et

al., 2000) and induces sprouting of adult rat Purkinje axons *in vivo* (Buffo et al., 2000). A contribution of the aa 763–865 region (NiG-Δ19) to the inhibitory activity *in vivo* is emphasized by recent findings showing that pump-infused mAb 7B12, which binds to an epitope within NiG-Δ19, leads to compensatory axonal sprouting along with improved functional recovery after experimental stroke in adult rats (Wiessner et al., 2003). On the other hand, the role of Nogo-B and Nogo-C (both containing Nogo-66), which have a broad expression pattern in peripheral tissues as shown by Northern and Western blots (Morris et al., 1999; Tagami et al., 2000; Huber et al., 2002), is still unclear.

The Nogo-A-specific region has an inhibitory effect on a range of cells including neurons, 3T3 fibroblasts, and CHO cells. Nogo-A, which is predominantly present in oligodendrocytes and myelin in the adult CNS, may therefore not only restrict neurite growth, plasticity, and axonal regeneration, but also limit the invasion and migration of cells and tumors in the CNS (Amberger et al., 1998; Belien et al., 1999). The presence of Nogo-A in various cell lines *in vitro* (Oertle et al., 2003b), and on the surface of 3T3 fibroblast cells in particular, may suggest an additional role, e.g., in the context of cell contact-mediated growth control.

All of these results suggest that the Nogo-A molecule possesses several binding sites (at least two for fibroblasts and neurons, respectively) and that the Nogo receptor is possibly a complex composed of several different subunits. One such subunit, NgR, serves as receptor component for the Nogo-66 peptide (Fournier et al., 2001), OMgp (Wang et al., 2002a), and MAG (Domeniconi et al., 2002; Liu et al., 2002). Being a GPI-anchored protein, it requires additional subunits for signal transduction. The bioactive Nogo-A-specific regions bind efficiently to the surface of 3T3 fibroblasts and to rat brain membranes, hence strongly suggesting the presence of Nogo-A-specific receptor(s). Our data demonstrate that the Nogo-A-mediated inhibition of cell spreading can occur in the absence of NgR and that the presence of NgR does not change the responsiveness of CHO cells to Nogo-66 or Nogo-A.

Activation of the small GTPase RhoA has been shown to be a crucial step in the signal transduction of inhibitory cues in various neurons (Li et al., 2002; Winton et al., 2002). The Nogo-66 peptide can activate Rho-A (Niederost et al., 2002), probably via activation of the NgR coreceptor p75^{NTR} (Wang et al., 2002b). Interestingly, the Nogo-A fragments aa 174–979 (NiG) and aa 544–725 (NiG-Δ20) have been shown to also activate RhoA and inhibit Rac in cerebellar granule cells and 3T3 fibroblasts (Niederost et al., 2002), and this still occurs after removal of NgR by phosphoinositide-specific phospholipase C treatment. These results suggest that RhoA activation is a key downstream component for both NgR and the putative Nogo-A-specific receptor.

Heteromeric receptor complexes interacting with different binding sites of a given ligand are well known for axonal guidance molecules [e.g., plexins and neuropilins for semaphorins (Tama-

gnone et al., 1999)] as well as for neurotrophic factors [e.g., tropomyosin related kinases and p75 neurotrophin receptor (p75^{NTR}) for neurotrophins (Lee et al., 2001)] and inhibitory proteins [e.g., p75, NgR and gangliosides for MAG (Domeniconi et al., 2002; Liu et al., 2002; Vyas et al., 2002; Yamashita et al., 2002]. Whether the specificity of the response to Nogo (growth inhibition vs growth cone collapse; cell type specificities) is linked to specific binding sites and receptor subunits remains to be investigated.

Inhibitory regions of Nogo-A are exposed at the cell surface of oligodendrocytes

Several lines of evidence suggest the presence of large parts of Nogo-A, including the inhibitory regions at the cell surface facing the extracellular space. These include cell surface biotinylation, immunocytochemistry on living cultured oligodendrocytes with three antisera and four monoclonal antibodies, all against different parts of Nogo-A, and cell sorting of surface-labeled 3T3 fibroblasts. The presence of Nogo-A at the cell surface of oligodendrocytes *in vitro* is consistent with results obtained *in vivo*: sprouting of axons can be elicited in intact regions of the adult rat CNS by application of AS 472 or mAb 7B12 (Buffo et al., 2000; Wiessner et al., 2003).

Nevertheless, a high proportion of Nogo-A protein was found intracellularly, associated with ER and Golgi membranes. In transfected cell lines such as COS or CHO cells, ectopically expressed Nogo is also localized in the ER and Golgi and was not detected on the cell surface (data not shown). Interestingly, Nogo-A was detected on the cell surface only in differentiated oligodendrocytes, but intracellular Nogo-A was present also in oligodendrocyte precursors (Wang et al., 2002c) (our unpublished observations). This is in agreement with the observation that the contact-mediated inhibition exerted by cultured oligodendrocytes was not detectable in precursor cells (Schwab and Caroni, 1988; Bandtlow et al., 1990). In addition, intracellular Nogo-A released to the extracellular matrix after oligodendrocyte and myelin damage might contribute to the inhibition of axonal regeneration as has been proposed previously (Goldberg and Barres, 2000).

Permeabilization of only the plasma membrane of oligodendrocytes before addition of antibodies revealed that the Nogo-A-specific sequences that face the extracellular space at the plasma membrane can also be exposed at the cytoplasmic side of intracellular Nogo. This would support the hypothesis that Nogo-A exists in at least two different membrane topologies in oligodendrocytes. The topogenic contribution of the unusually long hydrophobic domains (35 and 36 aa) is thought to be important for this uncommon membrane orientation of the Nogo proteins. It is unclear whether Nogo-A that is present at the cell surface of oligodendrocytes is translocated in the ER in two different orientations or whether it changes its topology at a later stage, e.g., in the Golgi or at the plasma membrane, analogous to certain viral envelope glycoproteins of hepatitis B and C virus (Ostapchuk et al., 1994; Cocquerel et al., 2002).

Nogo-A has no signal sequence. As an alternative, many unconventional membrane proteins can use internal hydrophobic sequences as signal anchor (Goder and Spiess, 2001); for Nogo-A this could be one of the C-terminal transmembrane domains. The N-terminal domain would then be translocated only after synthesis has been completed, as has been described for other proteins (Lu et al., 1998; Monne et al., 1999; Nilsson et al., 2000; Goder and Spiess, 2001; Cocquerel et al., 2002). It is also possible that Nogo-A reaches the cell surface by a nonconventional path-

way, for example by inserting directly into the plasma membrane. For several proteins that have been shown to exhibit more than one topological orientation, such as P-glycoprotein, ductin, cytochrome P450, microsomal epoxide hydrolase, or prion protein, the different topological forms can result in protein targeting to different cellular compartments or correlate with multiple biological functions (for review, see Levy, 1996; Hegde et al., 1998).

Cell-surface Nogo-A comprises ~1% of the total cellular Nogo-A. The large intracellular pool of Nogo-A present in oligodendrocytes may represent an unprocessed precursor form [as for cystic fibrosis transmembrane regulator (CFTR)] (Lu et al., 1998) and/or may have an intracellular, additional function as for, e.g., members of the S100 protein family (for review, see Donato, 1999), CFTR (Bradbury, 1999), and the inositol 1,4,5-trisphosphate receptor (Cunningham et al., 1993; Bush et al., 1994; Mayrleitner et al., 1995; Quinton and Dean, 1996; Tanimura et al., 2000).

Additional studies are required to unequivocally demonstrate the herein proposed surface exposure of Nogo-A-specific and Nogo-66 epitopes. Moreover, the identification of the exact topology of the two large C-terminal hydrophobic regions, e.g., by TROSY-based nuclear magnetic resonance (Fernandez et al., 2001), could further clarify our model of two different membrane orientations of Nogo-A.

In summary, our data demonstrate that the Nogo-A-specific part of the molecule has neurite growth inhibitory properties *in vitro*, and we propose that it is present at the cell surface of certain cells. Different stretches of Nogo-A contribute to this inhibitory activity. The Nogo-A-specific stretches are shown to bind to the surface of responsive cells and brain cortical membranes, suggesting the presence of new, so far unknown, Nogo-A-specific receptor(s) functioning independently of or in a complex with the Nogo-66 receptor NgR. Results from several experiments indicate that Nogo-A can have at least two different membrane topologies, pointing to the possibility of multiple functions both at the cell surface and intracellularly. The data presented here contribute to the understanding of the mechanisms underlying Nogo-mediated neurite growth inhibition and provide important information for the identification of new interacting molecules (receptors, intracellular binding partners) involved in Nogo processing and signaling.

References

Amberger VR, Hensel T, Ogata N, Schwab ME (1998) Spreading and migration of human glioma and rat C6 cells on central nervous system myelin in vitro is correlated with tumor malignancy and involves a metalloproteolytic activity. Cancer Res 58:149–158.

Bandtlow CE, Löschinger J (1997) Developmental changes in neuronal responsiveness to the CNS myelin-associated neurite growth inhibitor NI-35/250. Eur J Neurosci 9:2743–2752.

Bandtlow CE, Zachleder T, Schwab ME (1990) Oligodendrocytes arrest neurite growth by contact inhibition. J Neurosci 10:3837–3848.

Bandtlow CE, Schmidt MF, Hassinger TD, Schwab ME, Kater SB (1993) Role of intracellular calcium in NI-35-evoked collapse of neuronal growth cones. Science 259:80–83.

Behar O, Mizuno K, Neumann S, Woolf CJ (2000) Putting the spinal cord together again. Neuron 26:291–293.

Belien ATJ, Paganetti PA, Schwab ME (1999) Membrane-type 1 matrix metalloprotease (MT1-MMP) enables invasive migration of glioma cells in central nervous system white matter. J Cell Biol 144:373–383.

Bradbury NA (1999) Intracellular CFTR: localization and function. Physiol Rev 79:175–191.

Buffo A, Zagrebelsky M, Huber AB, Skerra A, Schwab ME, Strata P, Rossi F (2000) Application of neutralizing antibodies against NI-35/250 myelin-associated neurite growth inhibitory proteins to the adult rat cerebellum

induces sprouting of uninjured Purkinje cell axons. J Neurosci 20:2275–2286.

Bush KT, Stuart RO, Li SH, Moura LA, Sharp AH, Ross CA, Nigam SK (1994) Epithelial inositol 1,4,5-trisphosphate receptors. Multiplicity of localization, solubility, and isoforms. J Biol Chem 269:23694–23699.

Caroni P, Schwab ME (1988) Two membrane protein fractions from rat central myelin with inhibitory properties for neurite growth and fibroblast spreading. J Cell Biol 106:1281–1288.

Chen MS, Schnell L, van der Haar ME, Oertle T, Schwab ME (1999) Inhibitory activity and domain(s) of the myelin protein Nogo-A. Soc Neurosci Abstr 25:2030.

Chen MS, Huber AB, van der Haar ME, Frank M, Schnell L, Spillmann AA, Christ F, Schwab ME (2000) Nogo-A is a myelin-associated neurite outgrowth inhibitor and an antigen for monoclonal antibody IN-1. Nature 403:434–439.

Cocquerel L, Op dB, Lambot M, Roussel J, Delgrange D, Pillez A, Wychowski C, Penin F, Dubuisson J (2002) Topological changes in the transmembrane domains of hepatitis C virus envelope glycoproteins. EMBO J 21:2893–2902.

Croul S, Mezitis SG, Stieber A, Chen YJ, Gonatas JO, Goud B, Gonatas NK (1990) Immunocytochemical visualization of the Golgi apparatus in several species, including human, and tissues with an antiserum against MG-160, a sialoglycoprotein of rat Golgi apparatus. J Histochem Cytochem 38:957–963.

Cunningham AM, Ryugo DK, Sharp AH, Reed RR, Snyder SH, Ronnett GV (1993) Neuronal inositol 1,4,5-trisphosphate receptor localized to the plasma membrane of olfactory cilia. Neuroscience 57:339–352.

De Strooper B, Beullens M, Contreras B, Levesque L, Craessaerts K, Cordell B, Moechars D, Bollen M, Fraser P, George-Hyslop PS, Van Leuven F (1997) Phosphorylation, subcellular localization, and membrane orientation of the Alzheimer's disease-associated presenilins. J Biol Chem 272:3590–3598.

Domeniconi M, Cao Z, Spencer T, Sivasankaran R, Wang KC, Nikulina E, Kimura N, Cai H, Deng K, Gao Y, He Z, Filbin MT (2002) Myelin-associated glycoprotein interacts with the Nogo66 receptor to inhibit neurite outgrowth. Neuron 35:283–290.

Donato R (1999) Functional roles of S100 proteins, calcium-binding proteins of the EF-hand type. Biochim Biophys Acta 1450:191–231.

Fernandez C, Adeishvili K, Wuthrich K (2001) Transverse relaxation-optimized NMR spectroscopy with the outer membrane protein OmpX in dihexanoyl phosphatidylcholine micelles. Proc Natl Acad Sci USA 98:2358–2363.

Flanagan JG, Leder P (1990) The kit ligand: a cell surface molecule altered in steel mutant fibroblasts. Cell 63:185–194.

Fournier AE, GrandPre T, Strittmatter SM (2001) Identification of a receptor mediating Nogo-66 inhibition of axonal regeneration. Nature 409:341–346.

Fritsche J, Reber BFX, Schindelholz B, Bandtlow CE (1999) Differential cytoskeletal changes during growth cone collapse in response to hSemaIII and thrombin. Mol Cell Neurosci 14:398–418.

Goder V, Spiess M (2001) Topogenesis of membrane proteins: determinants and dynamics. FEBS Lett 504:87–93.

Goldberg JL, Barres BA (2000) Nogo in nerve regeneration. Nature 403:369–370.

Gonatas JO, Mezitis SG, Stieber A, Fleischer B, Gonatas NK (1989) MG-160. A novel sialoglycoprotein of the medial cisternae of the Golgi apparatus. J Biol Chem 264:646–653.

Gonatas JO, Mourelatos Z, Stieber A, Lane WS, Brosius J, Gonatas NK (1995) MG-160, a membrane sialoglycoprotein of the medial cisternae of the rat Golgi apparatus, binds basic fibroblast growth factor and exhibits a high level of sequence identity to a chicken fibroblast growth factor receptor. J Cell Sci 108:457–467.

GrandPré T, Nakamura F, Vartanian T, Strittmatter SM (2000) Identification of the Nogo inhibitor of axon regeneration as a reticulon protein. Nature 403:439–444.

Hegde RS, Mastrianni JA, Scott MR, DeFea KA, Tremblay P, Torchia M, DeArmond SJ, Prusiner SB, Lingappa VR (1998) A transmembrane form of the prion protein in neurodegenerative disease. Science 279:827–834.

Huber AB, Weinmann O, Brosamle C, Oertle T, Schwab ME (2002) Patterns of nogo mRNA and protein expression in the developing and adult rat and after CNS lesions. J Neurosci 22:3553–3567.

Kaupmann K, Huggel K, Heid J, Flor PJ, Bischoff S, Mickel SJ, McMaster G, Angst C, Bittiger H, Froestl W, Bettler B (1997) Expression cloning of GABA(B) receptors uncovers similarity to metabotropic glutamate receptors. Nature 386:239–246.

Kelleher DJ, Kreibich G, Gilmore R (1992) Oligosaccharyltransferase activity is associated with a protein complex composed of ribophorins I and II and a 48 kd protein. Cell 69:55–65.

Lee FS, Kim AH, Khursigara G, Chao MV (2001) The uniqueness of being a neurotrophin receptor. Curr Opin Neurobiol 11:281–286.

Levy D (1996) Membrane proteins which exhibit multiple topological orientations. Essays Biochem 31:49–60.

Li X, Saint CP, Aktories K, Lamarche-Vane N (2002) Rac1 and Cdc42 but not RhoA or Rho kinase activities are required for neurite outgrowth induced by the Netrin-1 receptor DCC (deleted in colorectal cancer) in N1E-115 neuroblastoma cells. J Biol Chem 277:15207–15214.

Liu BP, Fournier A, GrandPre T, Strittmatter SM (2002) Myelin-associated glycoprotein as a functional ligand for the nogo-66 receptor. Science 297:1190–1193.

Loschinger J, Bandtlow CE, Jung J, Klostermann S, Schwab ME, Bonhoeffer F, Kater SB (1997) Retinal axon growth cone responses to different environmental cues are mediated by different second-messenger systems. J Neurobiol 33:825–834.

Lu Y, Xiong X, Helm A, Kimani K, Bragin A, Skach WR (1998) Co- and posttranslational translocation mechanisms direct cystic fibrosis transmembrane conductance regulator N terminus transmembrane assembly. J Biol Chem 273:568–576.

Mayrleitner M, Schafer R, Fleischer S (1995) IP3 receptor purified from liver plasma membrane is an (1,4,5)IP3 activated and (1,3,4,5)IP4 inhibited calcium permeable ion channel. Cell Calcium 17:141–153.

Merril CR, Dunau ML, Goldman D (1981) A rapid sensitive silver stain for polypeptides in polyacrylamide gels. Anal Biochem 110:201–207.

Monne M, Gafvelin G, Nilsson R, von Heijne G (1999) N-tail translocation in a eukaryotic polytopic membrane protein: synergy between neighboring transmembrane segments. Eur J Biochem 263:264–269.

Moreira EF, Jaworski CJ, Rodriguez IR (1999) Cloning of a novel member of the reticulon gene family (RTN3): gene structure and chromosomal localization to 11q13. Genomics 58:73–81.

Morris NJ, Ross SA, Neveu JM, Lane WS, Lienhard GE (1999) Cloning and characterization of a 22 kDa protein from rat adipocytes: a new member of the reticulon family. Biochim Biophys Acta 1450:68–76.

Niederöst B, Zimmermann DR, Schwab ME, Bandtlow CE (1999) Bovine CNS myelin contains neurite growth-inhibitory activity associated with chondroitin sulfate proteoglycan. J Neurosci 19:8979–8989.

Niederost B, Oertle T, Fritsche J, McKinney RA, Bandtlow CE (2002) Nogo-A and myelin-associated glycoprotein mediate neurite growth inhibition by antagonistic regulation of RhoA and Rac1. J Neurosci 22:10368–10376.

Nilsson I, Witt S, Kiefer H, Mingarro I, von Heijne G (2000) Distant downstream sequence determinants can control N-tail translocation during protein insertion into the endoplasmic reticulum membrane. J Biol Chem 275:6207–6213.

Oertle T, Bandtlow CE, Schwab ME (2000) Characterization of the gene structure and the inhibitory regions of Nogo-RTN4. Soc Neurosci Abstr 26:573.

Oertle T, Merkler D, Schwab ME (2003a) Do cancer cells die because of Nogo-B? Oncogene 22:1390–1399.

Oertle T, Huber C, van der Putten H, Schwab ME (2003b) Genomic structure and functional characterisation of the promoters of human and mouse Nogo/Rtn-4. J Mol Biol 325:299–323.

Oertle T, Klinger M, Stuermer CAO, Schwab ME (2003c) A reticular rhapsody: phylogenic evolution and nomenclature of the RTN/Nogo gene family. FASEB J, in press.

Olpe HR, Karlsson G, Pozza MF, Brugger F, Steinmann M, Van Riezen H, Fagg G, Hall RG, Froestl W, Bittiger H (1990) CGP 35348: a centrally active blocker of GABAB receptors. Eur J Pharmacol 187:27–38.

Ostapchuk P, Hearing P, Ganem D (1994) A dramatic shift in the transmembrane topology of a viral envelope glycoprotein accompanies hepatitis B viral morphogenesis. EMBO J 13:1048–1057.

Prinjha R, Moore SE, Vinson M, Blake S, Morrow R, Christie G, Michalovich D, Simmons DL, Walsh FS (2000) Inhibitor of neurite outgrowth in humans. Nature 403:383–384.

Quinton TM, Dean WL (1996) Multiple inositol 1,4,5-trisphosphate recep-

tor isoforms are present in platelets. Biochem Biophys Res Commun 224:740–746.

Roebroek AJM, van de Velde HJK, Van Bokhoven A, Broers JLV, Ramaekers FCS, Van de Ven WJM (1994) Cloning and expression of alternative transcripts of a novel neuroendocrine-specific gene and identification of its 135-kDa translational product. J Biol Chem 268:13439–13447.

Roebroek AJ, Contreras B, Pauli IG, Van de Ven WJ (1998) cDNA cloning, genomic organization, and expression of the human RTN2 gene, a member of a gene family encoding reticulons. Genomics 51:98–106.

Rubin BP, Spillmann AA, Bandtlow CE, Keller F, Schwab ME (1995) Inhibition of PC12 cell attachment and neurite outgrowth by detergent solubilized CNS myelin proteins. Eur J Neurosci 7:2524–2529.

Schmalfeldt M, Bandtlow CE, Dours-Zimmermann MT, Winterhalter KH, Zimmermann DR (2000) Brain derived versican V2 is a potent inhibitor of axonal growth. J Cell Sci 113:807–816.

Schwab ME, Bartholdi D (1996) Degeneration and regeneration of axons in the lesioned spinal cord. Physiol Rev 76:319–370.

Schwab ME, Caroni P (1988) Oligodendrocytes and CNS myelin are nonpermissive substrates for neurite growth and fibroblast spreading *in vitro*. J Neurosci 8:2381–2393.

Spillmann AA, Bandtlow CE, Lottspeich F, Keller F, Schwab ME (1998) Identification and characterization of a bovine neurite growth inhibitor (bNI-220). J Biol Chem 273:19283–19293.

Tagami S, Eguchi Y, Kinoshita M, Takeda M, Tsujimoto Y (2000) A novel protein, RTN-XS, interacts with both Bcl-XL and Bcl-2 on endoplasmic reticulum and reduces their anti-apoptotic activity. Oncogene 19:5736–5746.

Tamagnone L, Artigiani S, Chen H, He Z, Ming G, Song H, Chedotal A, Winberg ML, Goodman CS, Poo M-M, Tessier-Lavigne M, Comoglio PM (1999) Plexins are a large family of receptors for transmembrane, secreted, and GPI-anchored semaphorins in vertebrates. Cell 99:71–80.

Tanimura A, Tojyo Y, Turner RJ (2000) Evidence that type I, II, and III inositol 1,4,5-trisphosphate receptors can occur as integral plasma membrane proteins. J Biol Chem 275:27488–27493.

Ughrin YM, Chen ZJ, Levine JM (2003) Multiple regions of the NG2 proteoglycan inhibit neurite growth and induce growth cone collapse. J Neurosci 23:175–186.

van de Velde HJK, Roebroek AJ, Senden NH, Ramaekers FC, Van de Ven WJ (1994) NSP-encoded reticulons, neuroendocrine proteins of a novel gene family associated with membranes of the endoplasmic reticulum. J Cell Sci 107:2403–2416.

van der Haar ME, Visser HW, de Vries H, Hoekstra D (1998) Transport of proteolipid protein to the plasma membrane does not depend on glycosphingolipid cotransport in oligodendrocyte cultures. J Neurosci Res 51:371–381.

Vielmetter J, Stolze B, Bonhoeffer F, Stuermer CA (1990) In vitro assay to test differential substrate affinities of growing axons and migratory cells. Exp Brain Res 81:283–287.

Vyas AA, Patel HV, Fromholt SE, Heffer-Lauc M, Vyas KA, Dang J, Schachner M, Schnaar RL (2002) Gangliosides are functional nerve cell ligands for myelin-associated glycoprotein (MAG), an inhibitor of nerve regeneration. Proc Natl Acad Sci USA 99:8412–8417.

Wang KC, Koprivica V, Kim JA, Sivasankaran R, Guo Y, Neve RL, He Z (2002a) Oligodendrocyte-myelin glycoprotein is a Nogo receptor ligand that inhibits neurite outgrowth. Nature 417:941–944.

Wang KC, Kim JA, Sivasankaran R, Segal R, He Z (2002b) p75 interacts with the Nogo receptor as a co-receptor for Nogo, MAG and OMgp. Nature 420:74–78.

Wang X, Chun SJ, Treloar H, Vartanian T, Greer CA, Strittmatter SM (2002c) Localization of nogo-a and nogo-66 receptor proteins at sites of axon-myelin and synaptic contact. J Neurosci 22:5505–5515.

Wiessner C, Bareyre FM, Allegrini PR, Mir AK, Frentzel S, Zurini M, Schnell L, Oertle T, Schwab ME (2003) Anti Nogo-A antibody infusion 24 hours after experimental stroke improved behavioral outcome and corticospinal plasticity in normotensive and spontaneously hypertensive rats. J Cereb Blood Flow Metab 23:154–165.

Winton MJ, Dubreuil CI, Lasko D, Leclerc N, McKerracher L (2002) Characterization of new cell permeable C3-like proteins that inactivate Rho and stimulate neurite outgrowth on inhibitory substrates. J Biol Chem 277:32820–32829.

Yamashita T, Higuchi H, Tohyama M (2002) The p75 receptor transduces the signal from myelin-associated glycoprotein to Rho. J Cell Biol 157:565–570.

Reference 4

HUGO Gene Nomenclature Committee

| About HGNC | Gene Search | Guidelines | Gene Submission | Downloads | Home |

Giving unique and meaningful names to every human gene

HGNC Activities

Useful Links

HCOP Search Tool

Public Engagement of Science

FAQs

International Advisory Committee

Gene Families/Groupings

Current committee:

- Prof Sue Povey (Chair)
- Dr Elspeth Bruford
- Dr Ruth Lovering
- Dr Matt Wright
- Dr Varsha Khodiyar
- Dr Tam Sneddon
- Dr Kate Sneddon
- Mr Connie Talbot Jr.

Bioinformatics support:

- Dr Michael Lush
- Mr Fabrice Ducluzeau

Powered by FreeBSD

Powered by APACHE

FEEDBACK - we welcome your feedback, please click here to leave your comments and/or suggestions.

[   ] Quick Gene Search

Advanced Gene Search
We have approved over 24,000 human gene symbols and names. Each symbol is unique and we ensure that each gene is only given one approved gene symbol. Search the HGNC database for your gene.

Request a Gene Symbol - NEW online request form
Obtaining a gene symbol before publication will avoid any possible conflicts with existing symbols and will ensure that your gene is promptly recorded in our database and others. Any information that you provide will be treated in the strictest confidence. For bulk data submissions please email us at nome@galton.ucl.ac.uk prior to submission.

Hot Topic
We would like to hear your opinion on the latest issues in the world of human gene nomenclature.

Gene Families and Groupings
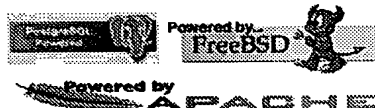We strongly encourage the use of a stem (or root) symbol as a basis for a hierarchical series that allows the easy identification of other related members in both database searches and the literature. Please contact us as soon as possible with new members of gene families, as some symbols may be reserved in our database.

Google [   ] Google Search

Search gene.ucl.ac.uk/nomenclature

Reference 5

Tumor necrosis factor receptor superfamily

HG NC   HUGO

About HGNC   Gene Search   Guidelines   Gene Submission   Downloads   Home

Giving unique and meaningful names to every human gene

Return to Advanced Search   [   ]   Quick Gene Search

This online database does not include our confidential data. If you would like to create a new gene symbol and name, the only way to confirm it as unique is by contacting us.

Click on the Approved Gene Symbol to retrieve the complete gene record

Approved Symbol	Approved Name	Previous Symbols	Aliases	Chromosome	Accession Numbers	RefSeq IDs
CD27	CD27 molecule	TNFRSF7	S152, Tp55	12p13	M63928	
CD40	CD40 molecule, TNF receptor superfamily member 5	TNFRSF5	p50, Bp50	20q12-q13.2	X60592	
FAS	Fas (TNF receptor superfamily, member 6)	FAS1, APT1, TNFRSF6	CD95, APO-1	10q24.1	M67454	
LTBR	lymphotoxin beta receptor (TNFR superfamily, member 3)	D12S370	TNFCR, TNFR-RP, TNFR2-RP, TNF-R-III, TNFRSF3	12p13	L04270	
NGFR	nerve growth factor receptor (TNFR superfamily, member 16)		TNFRSF16, CD271	17q21-q22	M14764	
TNFRSF1A	tumor necrosis factor receptor superfamily, member 1A	TNFR1	TNF-R, TNFAR, TNFR60, TNF-R-I, CD120a, TNF-R55	12p13.2	M75866	
TNFRSF1B	tumor necrosis factor receptor superfamily, member 1B	TNFR2	TNFBR, TNFR80, TNF-R75, TNF-R-II, p75, CD120b	1p36.22	M32315	NM_001066
TNFRSF4	tumor necrosis factor receptor superfamily, member 4	TXGP1L	ACT35, OX40, CD134	1p36	X75962	
TNFRSF6B	tumor necrosis factor receptor superfamily, member 6b, decoy		DcR3, DCR3, TR6, M68	20q13.3	AF104419	
TNFRSF8	tumor necrosis factor receptor superfamily, member 8	CD30, D1S166E	KI-1	1p36	M83554	
TNFRSF9	tumor necrosis factor receptor superfamily, member 9	ILA	CD137, 4-1BB	1p36	L12964	
TNFRSF10A	tumor necrosis factor receptor superfamily, member 10a		DR4, Apo2, TRAILR-1, CD261	8p21	U90875	NM_003844
			DR5, KILLER,			

TNFRSF10B	tumor necrosis factor receptor superfamily, member 10b		TRICK2A, TRAIL-R2, TRICKB, CD262	8p22-p21	AF012628	NM_147187
TNFRSF10C	tumor necrosis factor receptor superfamily, member 10c, decoy without an intracellular domain		DcR1, TRAILR3, LIT, TRID, CD263	8p22-p21	AF012536	
TNFRSF10D	tumor necrosis factor receptor superfamily, member 10d, decoy with truncated death domain		DcR2, TRUNDD, TRAILR4, CD264	8p21	AF029761	
TNFRSF11A	tumor necrosis factor receptor superfamily, member 11a, NFKB activator		RANK, CD265	18q22.1	AF018253	
TNFRSF11B	tumor necrosis factor receptor superfamily, member 11b (osteoprotegerin)	OPG	OCIF, TR1	8q24	U94332	
TNFRSF12A	tumor necrosis factor receptor superfamily, member 12A		FN14, TweakR, CD266	16p13.3	AB035480	
TNFRSF13B	tumor necrosis factor receptor superfamily, member 13B		TACI, CD267	17p11.2	AF023614	
TNFRSF13C	tumor necrosis factor receptor superfamily, member 13C		BAFFR, CD268	22q13.1-q13.3	AF373846	
TNFRSF14	tumor necrosis factor receptor superfamily, member 14 (herpesvirus entry mediator)		HVEM, ATAR, TR2, LIGHTR, HVEA	1p36.22-36.3	U70321	
TNFRSF17	tumor necrosis factor receptor superfamily, member 17	BCMA	BCM, CD269	16p13.1	Z29574	
TNFRSF18	tumor necrosis factor receptor superfamily, member 18		AITR, GITR	1p36.3	AF125304	NM_004195
TNFRSF19	tumor necrosis factor receptor superfamily, member 19		TAJ-alpha, TROY, TAJ, TRADE	13q12.11-q12.3	AB040434	
TNFRSF19L	tumor necrosis factor receptor superfamily, member 19-like		FLJ14993, RELT	11q13.2	AF319553	
TNFRSF21	tumor necrosis factor receptor superfamily, member 21		DR6	6p21.1	AF068868	NM_014452
TNFRSF25	tumor necrosis factor receptor superfamily, member 25	TNFRSF12	DR3, TRAMP, WSL-1, LARD, WSL-LR, DDR3, TR3, APO-3	1p36.2	U72763	NM_148965

MRC Medical Research Council

wellcometrust

Contact us: nome@galton.ucl.ac.uk   Back to top   This page last updated: October 6, 2006

Reference 6

Tumor necrosis factor receptor superfamily member TROY is a novel melanoma biomarker and potential therapeutic target

Remco A. Spanjaard[1,2*], Kara M. Whren[3], Carole Graves[1] and Jag Bhawan[3]

[1]*Department of Otolaryngology, Cancer Research Center, Boston University School of Medicine, Boston, MA*
[2]*Department of Biochemistry, Cancer Research Center, Boston University School of Medicine, Boston, MA*
[3]*Department of Dermatology, Skin Pathology Laboratory, Boston University School of Medicine, Boston, MA*

Incidence of melanoma continues to rise, and a better understanding of its genetics will be critical to improve diagnosis and develop new treatments. Here, we search for novel melanoma-specific genes that may serve as biomarkers and therapeutic targets by using an *in vitro* genetic screen. One identified cDNA encoded TROY, a member of the tumor necrosis factor receptor superfamily (TNFRSF). TROY is widely expressed during embryogenesis, but in adults expression is restricted to hair follicles and brain. However, TROY had never been associated with melanoma, and it was selected for further study. First we show that expression in melanoma is specific by semiquantitative RT-PCR analysis of a large panel of established tumor cell lines. Next, specificity of expression was evaluated by immunohistochemistry analysis of primary cell cultures and patient tissues. TROY is expressed in 2/2 primary melanoma cells and 45/45 melanoma tissue samples ($p < 0.0001$). With the exception of sebaceous glands, TROY is not expressed in normal skin biopsies ($p < 0.0001$) or primary skin cell cultures that contain keratinocytes and epidermal melanocytes, nor is it expressed in other skin tumor cells ($p < 0.0001$). Finally, we show that TROY regulates melanoma growth, because replication of melanoma cells with reduced TROY levels through treatment with short-interfering RNA was significantly decreased relative to control cells ($p < 0.004$). In summary, TROY is the first TNFRSF member that is a biomarker for melanoma. TROY also presents a potentially novel cell surface signaling target for inhibitors, cell and/or antibody-based immunotherapies.
© 2006 Wiley-Liss, Inc.

While incidence of most cancers is declining, melanoma is an exception, because there is about a 3% rise in cases per year. According to statistics compiled by the American Cancer Society, there was an estimated 59,000 new cases in 2005, of which over 7,800 patients were expected to have died. Even worse, in the past 3 decades, no therapeutic advances have been made that would increase survival rates of patients with late stage disease, which currently hovers around 3–9%. Metastatic melanoma, the usual cause of death, is notoriously resistant to conventional therapy. Only improved understanding of the genetics of this disease can be expected to lead to new therapeutic breakthroughs, and much progress has been made in the identification of important genes such as *B-RAF, N-RAS,*[1,2] *TP53, RB,*[3] *bFGF,*[4] *c-Kit/SCF,*[5] *EGFR*[6] and CDK inhibitor *p16[INK4a]*, which was identified as a susceptibility gene in familial melanoma, and p19[ARF], an alternative product of the murine *INK4a/ARF* locus, equivalent to *p14[ARF]* in humans.[7] Lately, much attention has been devoted to MITF and BRAF as new molecular targets,[8] and a new BRAF inhibitor is currently evaluated in clinical trials.[9] Moreover, gene expression profiling techniques have provided information on whole classes of genes that predispose or direct tumors to acquire different physiological properties.[1,10–12] Based on these findings, several new mouse melanoma models have been developed that mimic human disease.[13] However, despite all these efforts, few significant new drugs or therapies have come to the clinic and immuno and biochemotherapy remain the most promising strategies.[14–17] Although some candidates have been identified,[15,18,19] the scarcity of tumor-specific cell surface proteins has largely prevented the development of therapeutic antibodies that have proven relatively success-

ful in other solid tumors.[20] Thus, more targets, ideally signaling molecules present on the cell surface, are urgently needed to develop new intervention therapies.

We have been using murine S91 melanoma cells as a valuable *in vitro* model of melanoma and for the cloning of melanoma-associated genes and pathways that mediate growth, differentiation and apoptosis in response to treatment with retinoids.[21,22] Using this model, we identified a Type I transmembrane receptor member of the tumor necrosis receptor superfamily (TNFRSF) called TROY,[23] TAJ[24] or TNFRSF19.[25] In addition, some hTROY C-terminal splice variants have been reported[25] as well as a putative decoy receptor that misses the cytoplasmic tail, named dTROY,[23] which was recently shown to act as a dominant negative TROY.[26]

During mouse embryogenesis, TROY RNA is detected in many developing tissues, such as limb buds, eyelids, whiskers, mammary glands, epidermis, bronchial, tongue, dental and gastric epithelium, conjunctiva and cochlea, while some expression is also seen in mesenchymal tissues. However, in adult animals, this pattern changes dramatically and TROY expression becomes restricted to hair follicles and neuron-like cells in the cerebrum, cerebral cortex, cerebellum and developing olfactory system, as well as dorsal root and retinal ganglion neurons.[25–30] In humans, TROY RNA was also found highly expressed in brain and also in prostate, while low or undetectable levels were seen in heart, lung, liver, thymus, uterus, skeletal muscle, spleen, colon, testis, kidney and peripheral blood lymphocytes.[24] The reason or mechanism for this striking off-switch after birth is unknown, but its strict control indicates that aberrant expression may be detrimental.

TROY is also a member of the ectodysplasin (EDA) receptor (EDAR) subfamily that includes EDAR and X-linked EDAR (XEDAR). Hypohidrotic ectodermal dysplasia (HED) is a congenital disease that presents with sparse scalp hair, lack of sweat glands, and abnormal or missing teeth. HED is caused by mutations in EDA, EDAR or XEDAR, and it is suspected that TROY also plays a role in this disease.[31,32] It was recently established that TROY is a Nogo-66 receptor coreceptor that mediates inhibition of axonal regeneration by myelin inhibitors,[26,30] and so TROY has never been associated with melanoma.

In this report, we show that TROY is expressed in all primary and metastatic melanoma cells and tissue samples, but not in melanocytes found in normal skin biopsies and primary skin cell cultures, nor is TROY detectable in other (skin) tumor cells. We also

provide evidence that TROY signaling is functional and contributes to DNA replication in melanoma cells. Together, these results identify TROY as the first TNFRSF that can serve as a biomarker for melanoma. Moreover, TROY presents a novel and potentially unique cell surface-based signaling target for inhibitors, cell and/or antibody-based immunotherapies.

Material and methods

Cell cultures

Primary melanocytes were obtained from Cambrex Bio Science (Rockland, ME) and maintained in manufacturer's melanocyte growth media. Primary melanoma cells (Fig. 3b) were derived by Dr. Byers et al.[33] and maintained in Dulbecco's modified Eagle's medium with 8% (vol/vol) calf serum and 2% fetal calf serum (FCS). Established cell lines (Fig. 2) were obtained from the American Type Culture Collection (Manassas, VA) and grown in Dulbecco's modified Eagle's medium, with 10% (vol/vol) FCS at 37°C, in 5% CO_2 in humidified air.

Northern and Western blot analysis

RNA was extracted using Trizol reagent (Invitrogen, Carlsbad, CA) and subjected to electrophoresis through a denaturing formaldehyde–agarose gel (1.6%). Other procedures, including generation of [^{32}P]-labeled cDNA probes, were done as described.[21,22] Relative TROY induction was calculated by scanning densitometry. For Western blot analysis, 10^5 SK-Mel-2 cells were lysed in protein loading buffer and immunoblotted as described.[21,22] TROY/TAJ expression was determined using anti-TROY/TAJ antibody (1:100) and β-actin by anti-actin antibody (1:2,000), followed by visualization with HRP-coupled secondary antibody (1:2,500) (Santa Cruz, Santa Cruz, CA) and ECL-plus reagent (GE Healthcare Bio-Sciences, Piscataway, NJ) as described.[21,22]

RT-PCR assay

One microgram of RNA was used for reverse transcriptase (RT) reactions according to the manufacturer's protocol (Superscript First-Strand Synthesis System, Invitrogen). PCR conditions for amplification of TROY/TAJ and β-actin were as follows: 2 min at 94°C, and then 40 and 35 cycles, respectively, of 1 min at 94°C, 1 min at 56°C and 2 min at 72°C. Primer sequences are TROY/TAJ, forward: 5'-GCAAGAATTCAGGGATCGGTCTGG, reverse: 5'-AGCGCTGCAGATAACGGCAGCCAG. β-Actin primers have been described.[21]

Short-interfering RNA, transfections and [³H]-thymidine incorporation assay

SK-Mel-2 (2.5 × 10^5) cells plated in 6-well plates were transfected using Lipofectamine Plus, according to the manufacturer's protocol (Invitrogen), with 30 nM scrambled control short-interfering RNA (siRNA) or siRNA (Ambion, Austin, CA) targeting hTROY/TAJ exon 3 (Genbank: NM_148957)/exon 2 (Genbank: NM_018647) After 6 hr, cells received complete media and were allowed to recover for 24 hr. Cells were then serum-starved for 16 hr, after which they received complete media containing 1 µCi [³H]-thymidine for 10 hr. Next, cells were fixed in 5% TCA, lysed in 0.5 M NaOH/0.5% SDS and radioactive nucleotide incorporation was determined in a scintillation counter, or they were prepared for Western blot analysis to determine TROY expression levels.

Antibodies, tissues and immunohistochemical analysis

IRB approval was obtained prior to all studies involving patient materials. Only specimens that were ≥1 mm³ with ≥10% tumor cells and ≤30% necrosis were included.

Paraffin-embedded sections. Eleven paraffin-embedded melanomas taken from cases at Skin Pathology Laboratory, Department of Dermatology, Boston University were cut at 4 µM and incubated overnight at room temperature with anti-TROY anti-

body (1:20; Santa Cruz). Next, an IgG-AP polymer-labeled secondary antibody was applied and incubated for 2 hr, followed by staining with liquid permanent red (Dakocytomation, Carpinteria, CA). Samples were also stained with anti-HMB-45 antibody (1:100, Dakocytomation) for 32 min on a Ventana Benchmark LT with enhanced v-red detection kit (Ventana Medical Systems, Tucson, AZ). MART-1 staining was done after microwave antigen retrieval with anti-MART-1 antibody (Santa Cruz) using a Mach 4 Polymer Detection system with diaminobenzidine as chromogen according to the manufacturer's instructions (Biocare, Concord, CA).

Frozen sections. Thirty-four fresh frozen melanomas were obtained from the Cooperative Breast Cancer Tissue Resource (NCI). Other investigators may have received the same tumors. In addition, 6 basal cell carcinomas (BCC) and 10 histologically and clinically normal appearing skin samples adjacent to BCC, taken from Moh's surgery at the Department of Dermatology, Boston University Medical Center, were embedded in OCT (Sakura Finetek, Torrance, CA), cut at 5 µM and fixed in acetone. Slides were then immunostained with our own anti-TROY antibody for 32 min at 1:10 on the Ventana Benchmark LT using the enhanced v-red detection kit (Ventana Medical Systems). This antibody was raised by immunization of rabbits with a TROY-peptide located in its N-terminus (Qbiogene, Carlsbad, CA). Serum was affinity-purified against peptide (Arista Biologicals, Allentown, PA) and verified by ELISA (not shown). In addition, 10 melanoma samples were costained with anti-TRAF6 antibody (Santa Cruz) at 1:20 for 32 min, using the same techniques.

Cell lines. Two cell lines representing a primary and a metastatic melanoma[32] were grown on glass slides, fixed in acetone and immunostained with anti-TROY antibody (1:20, Santa Cruz) as described earlier.

Skin cell culture. Keratinocyte cultures that contain some melanocytes were obtained by cutting foreskin into 1-mm squares and incubating for 45 min at 37°C and then overnight in 0.25% trypsin at 4°C. Next, epidermis was separated from the dermis, and primary cultures were obtained by placing keratinocytes in primary keratinocyte media.[34]

Statistical analysis

Statistical significance of TROY expression in melanoma and absence of TROY expression in skin biopsies and BCC was determined by 2-tailed Fisher's exact test. Statistical significance of reduced DNA proliferation in cells with suppressed TROY levels was determined by Student's t-test analysis. A difference of $p < 0.05$ was considered statistically significant.
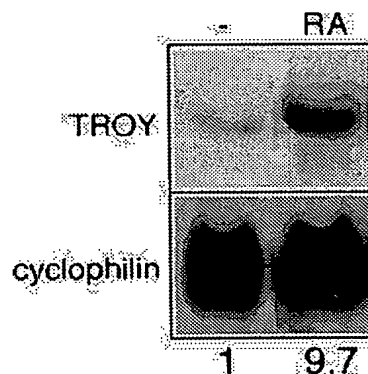

FIGURE 1 – Northern blot assay (20 µg RNA/lane) showing that TROY is a novel RA-induced gene in S91 murine melanoma cells. Cells were treated for 16 hr with 1 µM RA or 0.1% DMSO vehicle control. Fold induction is shown later. Cyclophilin serves as loading control.
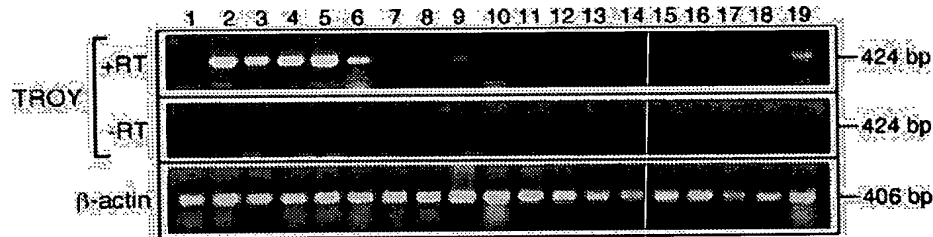
FIGURE 2 – Semiquantitative RT-PCR assay readily detects TROY mRNA in all human melanoma cell lines, but no or very low levels in normal primary melanocytes, or nonrelated tumor cell lines. Embryonic 293 cells serve as positive control. –, no detectable expression; ±, very low expression; +, low expression; ++, moderately high expression; +++, high expression. RT-panel shows lack of product in control reaction without added RT. β-Actin serves as loading and quality control. SCC, squamous cell carcinoma.

Lane	Cells	Tissue type	TROY expression	Notes
1	Melanocytes	Normal cells	–	Melanotic
2	SK-Mel-2	Melanoma	+++	Melanotic
3	SK-Mel-3	Melanoma	+++	Melanotic
4	Hs695t	Melanoma	+++	Amelanotic
5	C32	Melanoma	+++	Amelanotic
6	A375	Melanoma	++	Amelanotic
7	MCF-7	Breast carcinoma	–	
8	MDA-MB-231	Breast carcinoma	±	
9	MDA-MB-435s	Breast carcinoma	±	
10	Hela	Cervical carcinoma	–	
11	OV4	Ovarian carcinoma	–	
12	OV7	Ovarian carcinoma	–	
13	SCC-9	Head and neck SCC	–	
14	SCC-15	Head and neck SCC	–	
15	SCC25	Head and neck SCC	–	
16	Fadu	Head and neck SCC	–	
17	Hep 3B	Hepatocellular carcinoma	–	
18	P3HR-1	Burkitt lymphoma	–	
19	293	Embryonal kidney	+	

Results

TROY is a novel retinoic acid-regulated gene in S91 melanoma cells

S91 murine melanoma cells, which differentiate in response to retinoic acid (RA), serve as a valuable *in vitro* model of this disease. During a genetic screen for melanoma-associated genes that may be important for growth and differentiation in murine S91 cells,[21,22] we identified TROY as a RA-regulated gene, as shown in a Northern blot analysis in Figure 1, where TROY expression is strongly induced (9.7-fold) after 16-hr treatment with RA. While it has been shown that TNFα-receptors are induced by RA in neuroblastoma cells,[35] this is the first example of TROY or any other TNFSFR member that is induced in melanoma cells. Very few established cell lines express TROY RNA, although melanoma cells have never been tested.[25]

TROY RNA is specifically detected in melanoma cell lines

TNFRSF members make up a very large gene family that control signaling pathways for cell proliferation, differentiation and apoptosis. These are processes that shape development and the immune system, but which also play a role in carcinogenesis.[36,37] Thus, our finding that TROY is expressed in this cell line is potentially interesting for melanoma biology. To assess its relevance for human disease, we first wanted to verify that TROY is expressed in human melanoma in a RA-independent manner. We also wanted to know whether TROY is expressed in melanocytes or other malignant cells. To address these issues, we used semiquantitative RT-PCR to determine relative TROY RNA expression levels in a panel of cell lines representing a selection of widely used melanoma and epithelial cancer cells and one lymphoma that were all cultured in the absence of RA. Figure 2 shows that primary melanocytes do not express detectable TROY RNA, nor do any of

the other established cancer cells, although 2 breast cancer cell lines (MDA-MB-231 and 435s) expressed very low levels. In contrast, 5/5 melanoma cell lines expressed moderate (A375) or more typically high (SK-Mel-2 and 3, Hs695t and C32) levels of TROY RNA, independent of their pigmentation status. The magnitude of TROY expression is substantial because 293 cells, one of the very few nonmelanoma cell lines that are known to express TROY, in accordance with its embryonic lineage,[25] have lower levels than do the melanoma cells. These results suggest that TROY is not normally expressed in melanocytes; however, it is aberrantly reexpressed at high levels in melanoma.

Immunohistochemical analysis of TROY expression in epidermal skin melanocytes compared to primary and metastatic melanoma

Next, we wanted to validate and expand upon our previous experiments by performing an immunohistochemical analysis of TROY expression in normal skin biopsies and primary skin cell cultures that contain epidermal melanocytes, and comparing that with expression in primary melanoma cells and primary and metastatic melanoma tissue samples. Representative examples of our staining procedures are illustrated in Figure 3, and our complete results are summarized in Table I. Consistent with our *in vitro* studies, 0/10 (0%) of normal skin biopsies (Fig. 3a, panel 1), cultured skin keratinocytes mixed with epidermal melanocytes (Fig. 3a, panel 2) showed any detectable TROY expression. A benign nevus also stained negative (not shown). In addition, 0/6 (0%) of BCC as a representative, nonmelanoma skin cancer did not show TROY expression (Fig. 3a, panel 3). Interestingly, we found moderately strong TROY-staining of germinative cells in sebaceous glands (Fig. 3a, panel 4), an observation that had not been reported from mouse studies. However, sebaceous glands develop as an appendix from the developing hair follicle,[36] a site of known TROY expression in adult mice,[23] and thus this finding was not
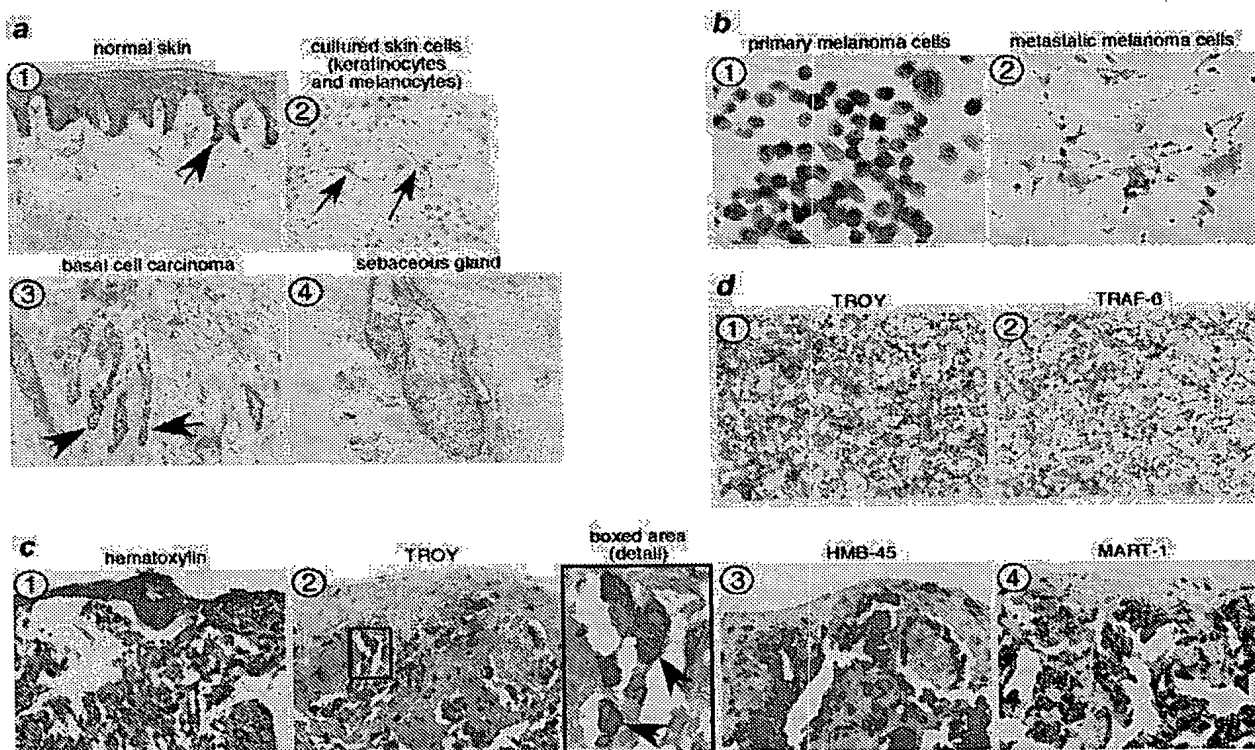
FIGURE 3 — Immunohistochemical analysis showing that TROY is specifically reexpressed at high levels in melanoma. TROY-signaling is likely functional in these tumors because TROY and TRAF-6 are coexpressed. Representative samples of various tissues and cells stained with various antibodies or hematoxylin. Original magnification, ×20. See Table I for overview of complete staining results. (a) Negative TROY-staining is found in normal skin biopsies that include epidermal melanocytes (panel 1, arrow), and also cultured normal primary skin that consist of keratinocytes mixed with melanocytes (panel 2, arrows). BCC (panel 3, arrows) samples are also negative although moderately strong TROY staining is observed in sebaceous glands (panel 4). (b) In contrast to normal skin constituents, strong TROY staining is detected in primary cells derived from a primary (panel 1) and metastatic (panel 2) melanoma. (c) Melanoma (paraffin-embedded) tissue samples are also strongly positive for TROY as illustrated by staining of a serial section of this tumor (panel 1, hematoxylin-stained for reference; panel 2, TROY-staining). The area in the indicated box is enlarged to provide more detail and intense cytoplasmic staining of individual tumor cells (indicated by arrows) can be appreciated (panel 2). Additional sections were also found to be positive for widely used melanoma biomarkers HMB-45 (panel 3) and MART-1 (panel 4). (d) Finally, another serial (fresh frozen) section from a different tumor shows coexpression of TROY (panel 1) and adapter molecule TRAF-6 (panel 2). Note that infiltrating lymphocytes remain unstained (blue color in panels 1 and 2).

unexpected. In contrast, 2/2 primary cell lines derived from a primary and a metastatic tumor stained strongly positive for TROY (Fig. 3b, panels 1 and 2, respectively). Moreover, analysis of all known primary (3) and metastatic (38, with 4 unclassified) melanoma patient samples showed that 45/45 (100%) samples were TROY-positive with typically high levels of cytoplasmic expression in individual tumor cells, as illustrated by a metastatic tumor in Fig. 3c, panels 1 and 2. For comparison, a serial section of this tumor was also stained for 2 widely used melanoma biomarkers. The HMB-45 antigen is thought to be a sialylated glycoprotein (gp100) that is also present on normal melanocytes. MART-1 is a melanocyte differentiation antigen that is recognized by cytotoxic T cells in a MHC class I-restricted fashion. Like HMB-45, not only is MART-1 expressed in most, but not all, melanomas, it is also expressed in normal melanocytes and benign nevi.[38,39] Antibodies against HMB-45 and MART-1 stain this tumor with about the same intensity as TROY (Fig. 3c, panels 3 and 4, respectively) but, given the large number of studies on HMB-45 and MART-1 expression in melanoma, these markers were not further assessed here.

These results are in agreement with our RT-PCR analysis, and show that TROY is a novel, melanoma-associated gene that is not expressed in benign melanocytes or other skin cells, nor is it expressed in nonmelanoma skin cancer.

TNFR-associated factor-6 is coexpressed with TROY

Next, we wanted to establish whether TROY is functionally important for melanoma. There is no known ligand for TROY. TNF ligands 4-1BBL, APRIL, BAFF/THANK, CD27L, CD30L, CD40L, EDA1, EDA2, FasL, GITRL, LIGHT, lymphotoxin α, lymphotoxin αβ, OX40L, RANKL, TL1A, TL6, TNF, TRAIL and TWEAK were all excluded, and indeed, it cannot be certain that a ligand exists at this point.[25,40] Therefore, we addressed this issue in the following manner. TNFR-associated factors (TRAFs) are important adapter molecules for various TNFRs. Overexpressed TROY-signaling was previously found to be inhibited by dnTRAF-2, 5 and 6,[23] and in agreement with these studies, TROY was shown to directly associate with all tested TRAFs-1, 2, 3 and 5.[24] Although these results suggest a rather redundant signaling cascade, we were particularly interested in TRAF-6, because TRAF-6-deficient mice display HED[29] and abnormalities in tooth development,[41] a known site of TROY-expression during mouse embryogenesis.[27,41] Moreover, TRAF-6 plays an important role in JNK activation by related XEDAR, and JNK is also activated by forced expression of TROY.[24,31,32] Thus, we focused on TRAF-6 as a major, representative indicator of functional TROY-signaling, and serial sections of metastatic melanoma tissues were stained with anti-TROY and anti-TRAF-6 antibodies, as shown in Fig. 3d, panels 1 and 2,

TABLE I – SUMMARY OF IMMUNOHISTOCHEMICAL ANALYSIS OF TROY AND TRAF-6 EXPRESSION

Tissue/cells	TROY	TROY + TRAF-6
Melanoma[1]	45/45 (100)[2]*	10/10 (100)
Primary cultured melanoma cells[3]	2/2 (100)	ND
Primary cultured keratinocytes + melanocytes	0/1 (0)	ND
Normal skin	0/10 (0)*	ND
Sebaceous glands[4]	2/2 (100)	ND
Basal cell carcinoma	0/6 (0)*	ND

[1]Three primary, 38 metastatic, and 4 unclassified melanomas.–[2]Values in parentheses indicate percentage of samples with TROY-positive cells.–[3]Primary cells derived from one primary and one metastatic melanoma.–[4]Germinative cells. $*p < 0.0001$ (by 2-tailed Fisher's exact test). ND, not determined.

respectively. TROY and TRAF-6 are coexpressed in 10/10 (100%) cases, suggesting that the TROY-TRAF-6-signaling axis is likely functional in melanoma cells.

TROY contributes to melanoma proliferation

Earlier reports showed that transiently overexpressed TROY resulted in a form of caspase-independent programmed cell death called paraptosis[42] in some, but not all cell types. This mechanism may involve different TRAFs and is possibly mediated through activation of JNK,[24,31,32] but not NFκB.[24] However, high levels of TROY expression during embryonic development and its reexpression in melanoma argue against this activity. A more conceivable effect may be stimulation of tumor growth, as some TNFRSF members are known to do.[36,37] Indeed, it was already suggested that TROY controls precursor cell proliferation or maintenance of the undifferentiated state during development of neuroepithelial cells,[29] which would be consistent with its reexpression in melanoma. This hypothesis was addressed in the following manner. TROY-positive SK-Mel-2 cells were transfected with a control siRNA, or a siRNA that effectively suppressed endogenous TROY expression (Fig. 4, top). Next, proliferation of cells with normal (high) and low levels of TROY were determined by [3H]-thymidine incorporation assay. As shown in Figure 4 (bottom), DNA replication is strongly reduced by about 50% in TROY-depleted cells compared with control cells, a significant effect considering that these cells are transfected with 40–50% efficiency (not shown). This result suggests that TROY performs an important growth-promoting role in melanoma.

Discussion

Melanoma is extremely dangerous when it penetrates the dermis because of its propensity to metastasize, and correct diagnosis and early detection of micrometastases are of critical importance. A variety of techniques are available for this purpose, such as morphometry, DNA ploidy evaluation, chromosome analysis and nuclear organizing region analysis,[38] but immunohistochemistry is generally favored. In turn, this technique depends on the reliability, specificity and sensitivity of the reagents used to detect melanoma markers. A large number of serum, molecular and immunohistochemical factors have been analyzed for their clinical usefulness as diagnostic and/or prognostic melanoma biomarkers, but many, if not all suffer from various problems in a clinical setting. For instance, widely used MART-1, HMB-45 and similar S100b cannot distinguish between benign melanocytic lesions and melanoma.[38,39] Moreover, MART-1 is not fully melanoma-specific, because it is also expressed in certain steroid-producing tumors,[43] and although the HMB-45 antibody, which was raised against an extract of melanoma cells, is thought to react against a sialylated glycoprotein (gp100), it may also react against other proteins.[44] Thus, a more specific melanoma biomarker would be a valuable addition to the pathologist's arsenal. Our combined studies show that TROY is expressed in 7/7 established and primary cells, and 45/45 primary
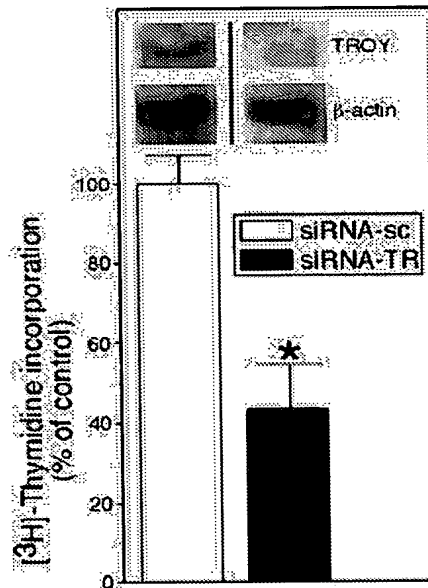
FIGURE 4 – Suppression of TROY expression reduces DNA replication in melanoma cell line SK-Mel-2. Cells transfected with an siRNA targeting TROY (siRNA-TR) but not a scrambled control siRNA (siRNA-sc) have reduced TROY expression as shown in immunoblot (top; β-actin serves as loading and specificity control). DNA replication was determined by [3H]-thymidine incorporation assay, and results are shown at the bottom panel. Proliferation was significantly reduced to about 50% in cells with low TROY expression relative to control cells. Shown is a representative experiment done in triplicate and repeated 3 times with similar results. Data are expressed as the mean ± SD. $*p \leq 0.004$ (by Student's *t*-test analysis).

and metastatic melanoma tissues, while normal melanocytes, either cultured or in skin biopsies representing both dividing and resting cells, remained unstained. Normally, TROY is widely expressed only during embryonic development, but then its expression gets largely switched off after birth, except for expression in hair follicles, certain brain areas, perhaps prostate, and as we showed here, sebaceous glands. We hypothesize that TROY is an embryonic gene/antigen that is aberrantly reexpressed in melanoma, thereby providing a growth advantage to the tumor through an as-yet unidentified pathway which may involve binding with an unknown ligand and signaling through TRAFs like TRAF-6. As such, TROY deserves attention as a novel biomarker for this disease.

TROY is a member of the large TNFRSF. These receptors play critical roles in organizing lymphoid tissues, hair follicles, sweat glands and bone, as well as in organizing transient structures such as the lactating mammary gland[36] and wound healing.[45] TNFRSF members are directly coupled to signaling pathways for cell proliferation and differentiation, and are well studied with respect to their function in immune responses. The other major activity is induction of apoptosis which is mediated by a subgroup of TNFRs called the death receptors, several of which have been linked to cancer.[37] TROY does not have a death domain but it was reported that forced expression of TROY induced paraptosis in some, but not all cell types examined.[24,31,32] The physiologal relevance of this phenomenon remains uncertain, however, considering its high expression in proliferating tissues. Indeed, during mouse embryogenesis, TROY shows particularly high levels of expression in neuroepithelial cells, where it may function to regulate cell proliferation or maintenance of the undifferentiated state.[29] This would also provide a rationale for its reexpression in melanoma, and it would be consistent with our *in vitro* data that suggest TROY con-

tributes to DNA replication in these tumors. These combined findings suggest that TROY functions as growth-promoting signaling molecule and provide more insight into the genetic network that controls proliferation of melanoma.

At the same time, our findings establish TROY as a novel potential target with unique properties. TROY antigen-expressing melanoma cells may be targeted by both tumor-specific cytotoxic T cell as well as therapeutic antibodies, of which only extremely few candidates exist. For instance, cell surface protein CD74 is also expressed in melanoma but not melanocytes; however, this antigen is also present on normal dendrocytes and B cells, making it much less suitable target for this therapy than does TROY.[12,43] Transmembrane glycoprotein NMB may show more promise, but its function is unknown, it is not expressed on all melanomas, and those that do are only sensitive to drug-conjugated antibodies.[18] Second, ligand-therapy is a potential option, because inhibitors or

modulators of TROY signaling or expression may reduce tumor growth.[46–49] Finally, it may be possible to detect circulating TROY-expressing melanoma cells in serum using RT-PCR-based techniques. MITF in particular has already showed some promise as a single marker in this regard[39,50] but with TROY, specific immunological detection of melanoma cells rather than their less-specific secreted antigens[51] may also be feasible. These questions are currently being addressed in our laboratory and will hopefully result in new treatment options for melanoma patients.

Acknowledgements

References

1. Curtin JA, Fridlyand J, Kageshita T, Patel HN, Busam KJ, Kutzner H, Cho KH, Aiba S, Brocker EB, LeBoit PE, Pinkel D, Bastian BC. Distinct sets of genetic alterations in melanoma. N Engl J Med 2005;353: 2135–47.
2. Pollock PM, Harper UL, Hansen KS, Yudt LM, Stark M, Robbins CM, Moses TY, Hostetter G, Wagner U, Kakareka J, Salem G, Pohida T, et al. High frequency of BRAF mutations in nevi. Nat Genet 2003; 33:19–20.
3. Bardeesy N, Bastian BC, Hezel A, Pinkel D, DePinho RA, Chin L. Dual inactivation of RB and p53 pathways in RAS-induced melanomas. Mol Cell Biol 2001;21:2144–53.
4. Wang Y, Becker D. Antisense targeting of basic fibroblast growth factor and fibroblast growth factor receptor-1 in human melanomas blocks intratumoral angiogenesis and tumor growth. Nat Med 1997;3: 887–93.
5. Gutman M, Singh RK, Radinsky R, Bar-Eli M. Intertumoral heterogeneity of receptor-tyrosine kinases expression in human melanoma cell lines with different metastatic capabilities. Anticancer Res 1994;14: 1759–65.
6. Ellis DL, King LE, Jr, Nanney LB. Increased epidermal growth factor receptors in melanocytic lesions. J Am Acad Dermatol 1992;27:539–46.
7. Haluska FG, Hodi FS. Molecular genetics of familial cutaneous melanoma. J Clin Oncol 1998;16:670–82.
8. Garraway LA, Widlund HR, Rubin MA, Getz G, Berger AJ, Ramaswamy S, Beroukhim R, Milner DA, Granter SR, Du J, Lee C, Wagner SN, et al. Integrative genomic analyses identify MITF as a lineage survival oncogene amplified in malignant melanoma. Nature 2005;436:117–22.
9. Thomas NE. BRAF somatic mutations in malignant melanoma and melanocytic nevi. Melanoma Res 2006;16:97–104.
10. Suyama E, Wadhwa R, Kaur K, Miyagishi M, Kaul SC, Kawasaki H, Taira K. Identification of metastasis-related genes in a mouse model using a library of randomized ribozymes. J Biol Chem 2004;279: 38083–6.
11. Carr KM, Bittner M, Trent JM. Gene-expression profiling in human cutaneous melanoma. Oncogene 2003;22:3076–80.
12. Weeraratna AT, Becker D, Carr KM, Duray PH, Rosenblatt KP, Yang S, Chen Y, Bittner M, Strausberg RL, Riggins GJ, Wagner U, Kallioniemi OP, et al. Generation and analysis of melanoma SAGE libraries: SAGE advice on the melanoma transcriptome. Oncogene 2004;23:2264–74.
13. Kabbarah O, Chin L. Advances in malignant melanoma: genetic insights from mouse and man. Front Biosci 2006;11:928–42.
14. Atallah E, Flaherty L. Treatment of metastatic malignant melanoma. Curr Treat Options Oncol 2005;6:185–93.
15. Komenaka I, Hoerig H, Kaufman HL. Immunotherapy for melanoma. Clin Dermatol 2004;22:251–65.
16. Luftner D, Pollmann D, Schildhauer S, Sehouli J, Possinger K. Perspectives of immunotherapy in metastatic breast cancer. Anticancer Res 2005;25:4599–604.
17. Parmiani G, Castelli C, Rivoltini L, Casati C, Tully GA, Novellino L, Patuzzo A, Tosi D, Anichini A, Santinami M. Immunotherapy of melanoma. Semin Cancer Biol 2003;13:391–400.
18. Tse KF, Jeffers M, Pollack VA, McCabe DA, Shadish ML, Khramtsov NV, Hackett CS, Shenoy SG, Kuang B, Boldog FL, MacDougall JR, Rastelli L, et al. CR011, a fully human monoclonal antibody-auristatin E conjugate, for the treatment of melanoma. Clin Cancer Res 2006; 12:1373–82.
19. Luo W, Ko E, Hsu JC, Wang X, Ferrone S. Targeting melanoma cells with human high molecular weight-melanoma associated antigen-specific antibodies elicited by a peptide mimotope: functional effects. J Immunol 2006;176:6046–54.
20. Nahta R, Esteva FJ. Herceptin: mechanisms of action and resistance. Cancer Lett 2006;232:123–38.
21. Spanjaard RA, Lee PJ, Sarkar S, Goedegebuure PS, Eberlein TJ. Clone 10d/BM28 (CDCL1), an early S-phase protein, is an important growth regulator of melanoma. Cancer Res 1997;57:5122–8.
22. Zhao X, Demary K, Wong L, Vaziri C, McKenzie AB, Eberlein TJ, Spanjaard RA. Retinoic acid receptor-independent mechanism of apoptosis of melanoma cells by the retinoid CD437 (AHPN). Cell Death Differ 2001;8:878–86.
23. Kojima T, Morikawa Y, Copeland NG, Gilbert DJ, Jenkins NA, Senba E, Kitamura T. TROY, a newly identified member of the tumor necrosis factor receptor superfamily, exhibits a homology with Edar and is expressed in embryonic skin and hair follicles. J Biol Chem 2000;275: 20742–7.
24. Eby MT, Jasmin A, Kumar A, Sharma K, Chaudhary PM. TAJ, a novel member of the tumor necrosis factor receptor family, activates the c-Jun N-terminal kinase pathway and mediates caspase-independent cell death. J Biol Chem 2000;275:15336–42.
25. Hu S, Tamada K, Ni J, Vincenz C, Chen L. Characterization of TNFRSF19, a novel member of the tumor necrosis factor receptor superfamily. Genomics 1999;62:103–7.
26. Park JB, Yiu G, Kaneko S, Wang J, Chang J, He XL, Garcia KC, He Z. A TNF receptor family member, TROY, is a coreceptor with Nogo receptor in mediating the inhibitory activity of myelin inhibitors. Neuron 2005;45:345–51.
27. Pispa J, Mikkola ML, Mustonen T, Thesleff I. Ectodysplasin, Edar and TNFRSF19 are expressed in complementary and overlapping patterns during mouse embryogenesis. Gene Expr Patterns 2003;3:675–9.
28. Hisaoka T, Morikawa Y, Kitamura T, Senba E. Expression of a member of tumor necrosis factor receptor superfamily, TROY, in the developing olfactory system. Glia 2004;45:313–24.
29. Hisaoka T, Morikawa Y, Kitamura T, Senba E. Expression of a member of tumor necrosis factor receptor superfamily, TROY, in the developing mouse brain. Brain Res Dev Brain Res 2003;143:105–9.
30. Shao Z, Browning JL, Lee X, Scott ML, Shulga-Morskaya S, Allaire N, Thill G, Levesque M, Sah D, McCoy JM, Murray B, Jung V, et al. TAJ/TROY, an orphan TNF receptor family member, binds Nogo-66 receptor 1 and regulates axonal regeneration. Neuron 2005; 45:353–9.
31. Naito A, Yoshida H, Nishioka E, Satoh M, Azuma S, Yamamoto T, Nishikawa S, Inoue J. TRAF6-deficient mice display hypohidrotic ectodermal dysplasia. Proc Natl Acad Sci USA 2002;99:8766–71.
32. Sinha SK, Zachariah S, Quinones HI, Shindo M, Chaudhary PM. Role of TRAF3 and -6 in the activation of the NF-κ B and JNK pathways by X-linked ectodermal dysplasia receptor. J Biol Chem 2002;277: 44953–61.
33. Byers HR, Etoh T, Doherty JR, Sober AJ, Mihm MC, Jr. Cell migration and actin organization in cultured human primary, recurrent cutaneous and metastatic melanoma. Time-lapse and image analysis. Am J Pathol 1991;139:423–35.
34. Gilchrest BA. Relationship between actinic damage and chronologic aging in keratinocyte cultures of human skin. J Invest Dermatol 1979;72:219–23.
35. Chambaut-Guerin AM, Martinez MC, Hamimi C, Gauthereau X, Nunez J. Tumor necrosis factor receptors in neuroblastoma SKNBE cells and their regulation by retinoic acid. J Neurochem 1995;65:537–44.
36. Locksley RM, Killeen N, Lenardo MJ. The TNF and TNF receptor superfamilies: integrating mammalian biology. Cell 2001;104:487–501.
37. de Thonel A, Eriksson JE. Regulation of death receptors-Relevance in cancer therapies. Toxicol Appl Pharmacol 2005;207 (2 Suppl):123–32.

38. Mangini J, Li N, Bhawan J. Immunohistochemical markers of mela-
    nocytic lesions: a review of their diagnostic usefulness. Am J Derma-
    topathol 2002;24:270–81.
39. Li N, Mangini J, Bhawan J. New prognostic factors of cutaneous
    melanoma: a review of the literature. J Cutan Pathol 2002;29:
    324–40.
40. Bossen C, Ingold K, Tardivel A, Bodmer JL, Gaide O, Hertig S,
    Ambrose C, Tschopp J, Schneider P. Interactions of tumor necrosis
    factor (TNF) and TNF receptor family members in the mouse and
    human. J Biol Chem 2006;281:13964–71.
41. Ohazama A, Courtney JM, Tucker AS, Naito A, Tanaka S, Inoue J,
    Sharpe PT. Traf6 is essential for murine tooth cusp morphogenesis.
    Dev Dyn 2004;229:131–5.
42. Wang Y, Li X, Wang L, Zhang Y, Han W, Ma D. An alternative form
    of paraptosis-like cell death, triggered by TAJ/TROY and enhanced
    by PDCD5 overexpression. J Cell Sci 2004;117:1525–32.
43. Busam KJ, Iversen K, Coplan KA, Old LJ, Stockert E, Chen YT,
    McGregor D, Jungbluth A. Immunoreactivity for A103, an antibody
    to melan-A (Mart-1), in adrenocortical and other steroid tumors. Am J
    Surg Pathol 1998;22:57–63.
44. Matsumoto Y, Horiba K, Usuki J, Chu SC, Ferrans VJ, Moss J.
    Markers of cell proliferation and expression of melanosomal antigen
    in lymphangioleiomyomatosis. Am J Respir Cell Mol Biol 1999;21:
    327–36.

45. Ong GL, Goldenberg DM, Hansen HJ, Mattes MJ. Cell surface ex-
    pression and metabolism of major histocompatibility complex class II
    invariant chain (CD74) by diverse cell lines. Immunology 1999;
    98:296–302.
46. van Horssen R, Ten Hagen TL, Eggermont AM. TNF-α in cancer
    treatment: molecular insights, antitumor effects, and clinical utility.
    Oncologist 2006;11:397–408.
47. Trent JT, Kerdel FA. Tumor necrosis factor α inhibitors for the treat-
    ment of dermatologic diseases. Dermatol Nurs 2005;17:97–107.
48. Nash PT, Florin TH. Tumour necrosis factor inhibitors. Med J Aust
    2005;83:205–8.
49. Carter PH, Scherle PA, Muckelbauer JK, Voss ME, Liu RQ, Thompson LA,
    Tebben AJ, Solomon KA, Lo YC, Li Z, Strzemienski P, Yang G, et al.
    Photochemically enhanced binding of small molecules to the tumor ne-
    crosis factor receptor-1 inhibits the binding of TNF-α. Proc Natl Acad
    Sci USA 2001;98:11879–84.
50. Koyanagi K, O'Day SJ, Gonzalez R, Lewis K, Robinson WA,
    Amatruda TT, Kuo C, Wang HJ, Milford R, Morton DL, Hoon DS.
    Microphthalmia transcription factor as a molecular marker for circu-
    lating tumor cell detection in blood of melanoma patients. Clin Can-
    cer Res 2006;12:1137–43.
51. Reynolds SR, Vergilis IJ, Szarek M, Ferrone S, Bystryn JC. Cytoplas-
    mic melanoma-associated antigen (CYT-MAA) serum level in patients
    with melanoma: a potential marker of response to immunotherapy? Int
    J Cancer 2006;119:157–61.

TAJ, a Novel Member of the Tumor Necrosis Factor Receptor Family, Activates the c-Jun N-terminal Kinase Pathway and Mediates Caspase-independent Cell Death*

Michael T. Eby‡, Alan Jasmin‡, Arvind Kumar‡, Kiran Sharma§, and Preet M. Chaudhary‡¶

From the ‡Hamon Center for Therapeutic Oncology Research, University of Texas Southwestern Medical Center, Dallas, Texas 75390-8593 and the §University of Washington, Seattle, Washington 98195

We have isolated a novel member of the TNFR family, designated TAJ, that is highly expressed during embryonic development. TAJ possesses a unique cytoplasmic domain with no sequence homology to the previously characterized members of the TNFR family. TAJ interacts with the TRAF family members and activates the JNK pathway when overexpressed in mammalian cells. Although it lacks a death domain, TAJ is capable of inducing apoptosis by a caspase-independent mechanism. Based on its unique expression profile and signaling properties, TAJ may play an essential role in embryonic development.

Members of the TNFR[1] superfamily play an important role in regulating diverse biological activities, such as cell proliferation, differentiation, and programmed cell death or apoptosis. The majority of TNFR family members are type I membrane proteins that share significant sequence homology in their extracellular domains (1). This homology is due to the presence of highly conserved cysteine residues in so-called cysteine-rich pseudo-repeats, a hallmark of this family. The cytoplasmic domains of the various TNFR family members, on the other hand, differ greatly not only in their sequence but also in their length. Some of the apoptosis-inducing members of this family, such as TNFR1, CD95/Fas/APO-1, DR3/TRAMP/APO-3, DR4/TRAIL/APO-2, and DR5/TRAIL-R2, contain a conserved domain of approximately 80 amino acids, called a death domain, which is essential for mediation of cell death (2–4). Although death domains are absent in other members of the TNFR family, some of these non-death domain-containing receptors, such as TNFR2, CD30, and LT-βR, are nevertheless capable of inducing cell death under certain circumstances (5–7).

In the present report, we describe the isolation and characterization of a novel member of the TNFR family, designated TAJ (for Toxicity And JNK inducer). We present evidence that, based on its unique expression profile and signaling activities, TAJ may be a key regulator of cell activation and death during embryonic development.

EXPERIMENTAL PROCEDURES

Cell Lines and Reagents—293T cells were obtained from Dr. David Han (University of Washington, Seattle). 293EBNA cells were obtained from Invitrogen. Rabbit polyclonal antibodies against FLAG and HA tags were obtained from Santa Cruz Laboratories. FLAG beads were obtained from Sigma. The pull-down kinase assay kit for JNK was obtained from New England Biolabs, and the constructs for the Pathdetect luciferase reporter assay were purchased from Stratagene. YO-PRO-1 was obtained from Molecular Probes.

Cloning of TAJ cDNA—Two murine EST clones (IMAGE consortium clones 650744 and 664665) encoding the extracellular domain of a new member of the TNFR superfamily were identified by searching the data base of expressed sequence tags (dbEST) for sequences sharing homology to the extracellular domain of human DR3. The sequence corresponding to the cytoplasmic domain of this receptor was obtained by using 3′-rapid amplification of cDNA ends (RACE) on murine spleen Marathon Ready cDNA (CLONTECH) using the Marathon cDNA amplification kit (CLONTECH) and following the manufacturer's instructions. A repeat search of the EST data base for sequences with homology to the cytoplasmic tail of murine TAJ revealed the presence of a human EST clone (IMAGE consortium clone 340844). The sequence corresponding to the 5′ end of human TAJ (hTAJ) was obtained by performing 5′-RACE on human fetal spleen Marathon-ready cDNA (CLONTECH).

Northern Blot Analysis—Northern blot analysis was performed using mouse embryo and human multiple tissue Northern blots (CLONTECH). Blots were hybridized under high stringency conditions with ^{32}P-labeled probes corresponding to the protein-coding regions of mTAJ and hTAJ and following the instructions of the manufacturer.

Expression Vectors—To construct FLAG or Myc epitope-tagged receptors, the amino acids 23–424 of hTAJ were amplified using *Pfu* polymerase (Stratagene) with a primer containing a *Bgl*II site at the 5′ end and a *Sal*I site at the 3′ end and then were ligated to a modified pSectag A vector (Invitrogen) containing a FLAG or a Myc epitope downstream of a murine Ig κ chain signal peptide. Expression constructs for dominant-negative FADD, caspase 8 C360S, CrmA, p35, MRIT, Orf-K13, and TRAFs have been described previously (8–10).

Reporter Assays—For the c-Jun transcriptional activation assay, 293 EBNA cells (1.2×10^5) were transfected in duplicate with various expression constructs (500 ng) along with a fusion transactivator plasmid containing the yeast GAL4 DNA-binding domain fused to transcription factor c-Jun (pFA-cJun) (50 ng), a reporter plasmid encoding the luciferase gene downstream of the GAL4 upstream activating sequence (pFR-luc) (500 ng), as well as a RSV/LacZ (β-galactosidase) reporter construct (75 ng). Transfection was performed using calcium phosphate coprecipitation method. Forty hours later cell extracts were prepared using the Luciferase Cell Culture Lysis Reagent (Promega, Madison, WI), and luciferase assays were performed using 20 μl of cell extract. The cell lysate was diluted 1:20 with phosphate-buffered saline, pH 7.4, and used for the measurement of β-galactosidase activity. Luciferase activity was normalized relative to the β-galactosidase activity to control for the difference in the transfection efficiency. Western

[1] The abbreviations used are: TNFR, tumor necrosis factor receptor; DR3, death receptor 3; EST, expressed sequence tag; MRIT, Mach-related inducer of toxicity; TRAF, tumor necrosis factor-associated factor; JNK, c-Jun N-terminal kinase; NF-κB, nuclear factor kappa B; JIP1, JNK interacting protein 1; JBD, JNK binding domain; GFP, green fluorescent protein;; ASK1, apoptosis signal-regulating kinase 1; HA, hemagglutinin; CHAPS, 3-[(3-cholamidopropyl)dimethylammonio]-1-propanesulfonic acid; PBS, phosphate-buffered saline; RACE, rapid amplification of cDNA ends; hTAJ, human TAJ; pNA, p-nitroanilide; GST, glutathione S-transferase; FADD, Fas-associated death domain.

A

```
1 mTAJ-αL MALKVLPLERTVLFA AILFLLHLACKVSCE TGDCRQQEFKDRSGN CVLCKQCGPGMELSK ECGFGYGEDAQCVPC RPHRFKEDWGFQKCK
2 mTAJ-β  MALKVLPLERTVLFA AILFLLHLACKVSCE TGDCRQQEFKDRSGN CVLCKQCGPGMELSK ECGFGYGEDAQCVPC RPHRFKEDWGFQKCK
3 mTAJ-αS MALKVLPLERTVLFA AILFLLHLACKVSCE TGDCRQQEFKDRSGN CVLCKQCGPGMELSK ECGFGYGEDAQCVPC RPHRFKEDWGFQKCK
4 hTAJ    MALKVLLRQERTFFT LLVLLGYLSCKVTCE SGDCRQQEFRDRSGN CVPCNQCGPGMELSK ECGFGYGEDAQCVAC RLHRFKEDWGFQKCK
           91          105 106          120 121          135 136          150 151          165 166          180
1 mTAJ-αL PCADCALVNRFQRAN CSHTSDAVCGDCLPG FYRKTKLVGFQDMEC VPCGDPPPPYEPHCT SKVNLVKISSTVSSP RDTALAAVICSALAT
2 mTAJ-β  PCADCALVNRFQRAN CSHTSDAVCGDCLPG FYRKTKLVGFQDMEC VPCGDPPPPYEPHC- --------------- RDTALAAVICSALAT
3 mTAJ-αS PCADCALVNRFQRAN CSHTSDAVCGDCLPG FYRKTKLVGFQDMEC VPCGDPPPPYEPHCT SKVNLVKISSTVSSP RDTALAAVICSALAT
4 hTAJ    PCLDCAVVNREQRAN CSATSDAICGDCLPG FYRKTKLVGFQDMEC VPCGDPPPPYEPHCA SKVNLVKIASTASSR RDTALAAVICSALAT
           181         195 196          210 211          225 226          240 241          255 256          270
1 mTAJ-αL VLLALLILCVIYCKR QFMEKKPSWSLRSQD IQYNGSELSCFDQPR LRHCAHRACCQYRRD SAPMYGPVHLIPSLC CEEARGSARAVLGCG
2 mTAJ-β  --------------- --------------- --------------- --------------- --------------- ---------------
3 mTAJ-αS VLLALLILCVIYCKR QFMEKKPSCKLPSLC LTVK----------- --------------- --------------- ---------------
4 hTAJ    VLLALLILCVIYCKR QFMEKKPSWSLRSQD IQYNETELSCFDRPQ LHEYAHRACCQCRRD SVQTCGPVRLLPSMC CEEACSPNPATLGCG
           271         285 286          300 301          315 316          330 331          345 346          360
1 mTAJ-αL LRSPTTLQERNPASV GNTMPAFFGSVGRSI CAEFSDAWPLMQNPL GGD-SSLCDSYPELT GEDTNSLNFENESTA SLDSSGGQDLAGTAA
2 mTAJ-β  --------------- --------------- --------------- --------------- --------------- ---------------
3 mTAJ-αS --------------- --------------- --------------- --------------- --------------- ---------------
4 hTAJ    VHSAASLQARNAGPA GEMVPTFFGSLTQSI CGEFSDAWPLMQNPH GGDNISFCDSYPELT GEDIHSLNPELESST SLDSNSSQDLVGGAV
           361         375 376          390 391          405 406          420 421          435 436          450
1 mTAJ-αL -LES-SGNVSESTDS PRHGDTGTVWEQTLA QDAQRTPSQCGWEDR ENLHLAMPTAFQDA- ------    416
2 mTAJ-β  --------------- --------------- --------------- ---------------  ------   149
3 mTAJ-αS --------------- --------------- --------------- --------------- ------    214
4 hTAJ    PVQSHSERFTAATDL SRYNN--TLVESAST QDALTMRSQLDQESG AVIRPATQTSLQVRQ RLGSL     423
```

B

```
hTAJ   1
DR3    1
Fas    1
TNFR1  1
OPG    1

hTAJ   70
DR3    68
Fas    60
TNFR1  79
OPG    60

hTAJ   139
DR3    145
Fas    150
TNFR1  150
OPG    125
```

FIG. 1. *A*, amino acid sequence of murine and human TAJ isoforms. The signal peptides and transmembrane domains are shown in *bold* and *italics*, respectively. *B*, sequence alignment of the extracellular domains of TNFR family members. Identical amino acids are *shaded dark* and homologous residues *shaded gray*.

blot analysis on cell extracts prepared from similarly transfected cells was used to confirm that the various expression constructs lead to the production of the desired proteins. The NF-κB reporter assay was performed essentially as described above using a luciferase reporter plasmid containing four copies of a consensus NF-κB binding site (11).

Caspase Activation Assay—293T cells (2 × 10^5) were transfected with 2 μg of an empty vector or expression vectors encoding TNFR1 or hTAJ along with a GFP-encoding plasmid. Cells were examined under a fluorescent microscope 32 hours later to ensure equal transfection efficiency. Cells were subsequently lysed in 100 μl of lysis buffer (0.1% Triton X-100, 20 mM sodium phosphate, pH 7.4, 150 mM NaCl). For assaying caspase 3 activation, 10 μl of cell extract was mixed with 80 μl of assay buffer (50 mM Hepes, pH 7.4, 100 mM NaCl, 0.1% CHAPS, 10 mM dithiothreitol, 1 mM EDTA, 10% glycerol) in a 96-well microtiter plate in triplicate, and the was reaction started by the addition of 10 μl of Ac-DEVD-pNA substrate. Caspase 3-mediated cleavage of Ac-DEVD-pNA into p-nitroanilide was measured using a plate reader at 405 nm.

DNA Content Analysis—293T cells (2 × 10^6) were transfected with the various test plasmids along with a GFP-encoding plasmid. Approximately 32 h post-transfection, cells were examined under a fluorescent microscope to ensure equal transfection efficiency. Cells were subsequently trypsinized, washed once with PBS, and fixed in 50% ethanol at 4 °C. After washing with PBS, cells were treated with 500 μg of RNase A (Sigma) in 100 μl of PBS for 30 min at 37 °C and resuspended in 0.5 ml of PBS containing 50 μg/ml propidium iodide. After further incubation at 4 °C for 15 min, cells were analyzed by flow cytometry.

Coimmunoprecipitation Assays—For studying *in vivo* interaction, 2 × 10^6 293T cells were plated in a 100-mm plate and cotransfected 18–24 h later with 5 μg/plate of each epitope-tagged construct along with 1 μg of a hemagglutinin-tagged GFP-encoding plasmid (HA-GFP) by calcium phosphate coprecipitation. Eighteen to thirty-six hours post-
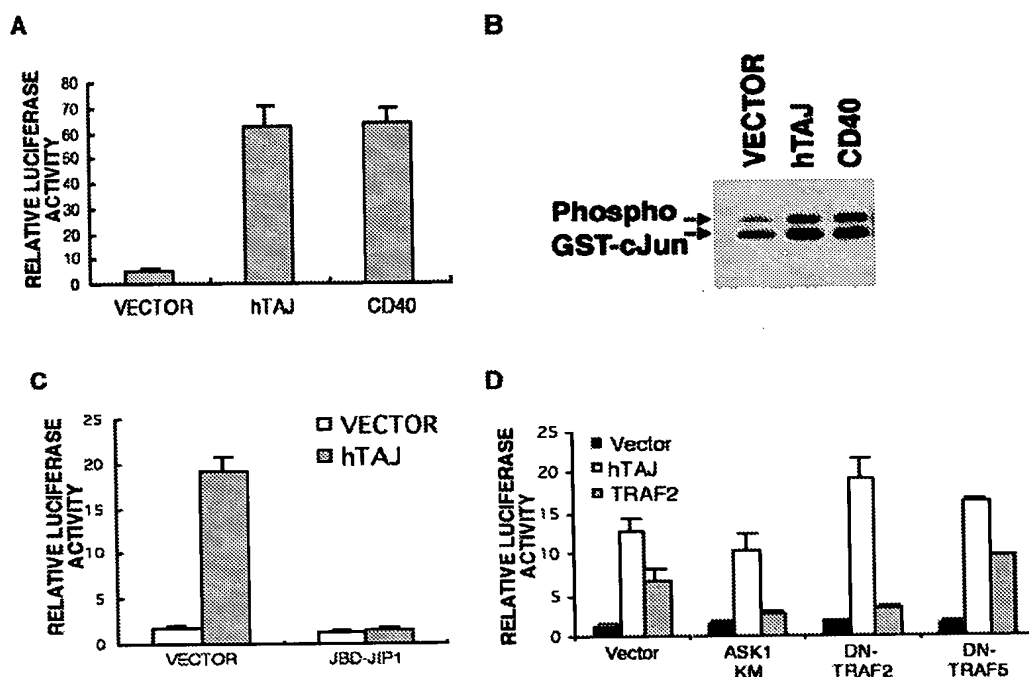

Mouse Embryos   Adult Human Tissues

FIG. 2. **Northern blot analysis of TAJ expression during murine embryonic development and human adult tissues.** *kb*, kilobase pairs; *PBL*, peripheral blood leukocytes.

A

B

C

D
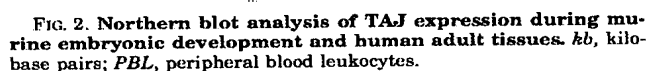
FIG. 3. *A*, TAJ mediates c-Jun transcriptional activation. 293 EBNA cells were transfected with an empty vector or expression vectors encoding human TAJ or CD40 receptors along with pFA-cJun, pFR-luc, and RSV/LacZ encoding plasmids in duplicate. The experiment was performed as described under "Experimental Procedures." Values shown are mean ± S.E. of a representative of two independent experiments performed in duplicate. *B*, TAJ activates JNK pathway. 293EBNA cells (3 × 10⁶) were transfected with the indicated plasmid and JNK activation measured by a "pull-down" JNK assay kit (New England Biolabs). GST-c-Jun coupled to agarose beads was used to both pulling down the endogenously expressed JNK and as a substrate for activated JNK-induced phosphorylation. A representative of two independent experiments. *C*, JBD-JIP1 blocks TAJ-induced JNK activation. 293EBNA cells (1.2 × 10⁶) were transfected with an empty vector or an hTAJ expression vector (250 ng/well) with and without JBD-JIP1 (500 ng/well) in each well of a 24-well plate in duplicate. The total amount of transfected DNA was kept constant by adding empty vector. The experiment was performed as described for *A*. Values shown are mean ± S.E. of a representative of two independent experiments performed in duplicate. *D*, dominant-negative mutants of TRAF2 and ASK1 fail to block TAJ-induced JNK activation. The experiment was performed essentially as described for *C*. Values shown are mean ± S.E. of a representative of two independent experiments performed in duplicate.

transfection, cells were lysed in 1 ml of lysis buffer containing 0.1% Triton X-100, 20 mM sodium phosphate, pH 7.4, 150 mM NaCl, and 1 EDTA-free mini-protease inhibitor tablet per 10 ml (Roche Molecular Biochemicals). For immunoprecipitation, cell lysates (500 μl) were incubated for 1 h at 4 °C with 10 μl of FLAG or control mouse Ig beads precoated with 2% bovine serum albumin. Beads were washed twice with lysis buffer, twice with a wash buffer containing 0.1% Triton X-100, 20 mM sodium phosphate, pH 7.4, 500 mM NaCl, and again with lysis buffer. Bound proteins were eluted by boiling, separated by SDS-polyacrylamide gel electrophoresis, transferred to a nitrocellulose membrane, and analyzed by Western blot.

RESULTS

Cloning of Murine and Human TAJ cDNAs—In order to identify new members of the TNFR family, we searched the EST data base (dbEST) for sequences with homology to the extracellular domain of Death Receptor 3 (DR3) and identified two mouse cDNA clones. Both clones originated from cDNA libraries made from 13.5- to 14.5-day mouse embryos and, upon sequencing, were found to represent the alternatively spliced forms of the same gene. One of the clones, named mTAJ-αS, was found to encode an open reading frame of 214 amino acids (Fig. 1*A*). Sequence analysis of this clone revealed the presence of an N-terminal signal peptide (amino acids 1–23), cysteine-rich pseudo-repeats with significant sequence homology to the extracellular domain of other members of the TNFR family (20–25% sequence identity and 35–46% sequence similarity), a hydrophobic stretch of amino acids representing the trans-membrane region (amino acids 171–193), and a short cytoplasmic tail (Fig. 1*A*). Based on the presence of the short cytoplas-

mic tail, this clone may encode for a decoy receptor. The sequence of the second murine clone, named mTAJ-β, was identical to mTAJ-αS in the N-terminal 149 amino acids. This region contains its signal peptide, and the cysteine-rich pseudo-repeats representing the majority of the ligand-binding domain (Fig. 1*A*). However, mTAJ-β has a stop codon after amino acid 150 and, therefore, may represent a soluble receptor lacking a transmembrane domain (Fig. 1*A*). Based on the sequence of mTAJ-αS, primers were designed and used in 3'-RACE to clone the sequence representing the cytoplasmic tail of TAJ. The full-length cDNA clone, named mTAJ-αL, was found to contain an open reading frame of 416 amino acids with a unique cytoplasmic domain having no significant homology to any other member of the TNFR family (Fig. 1*A*).

A repeat search of the EST data base for clones homologous to the cytoplasmic tail of mTAJ led to the identification of a human EST clone derived from an embryonic heart library constructed from a 19-week-old embryo. Based on the sequence of this clone, primers were designed, and 5'-RACE was used to clone the full-length human TAJ (hTAJ) clone. The full-length hTAJ clone encoded a protein of 423 amino acids having 68.4% amino acid identity and 79.2% amino acid similarity with mTAJ-αL (Fig. 1*A*). In addition, hTAJ was found to have significant sequence similarity to other members of the TNFR family in its extracellular ligand-binding domain (Fig. 1*B*).

Expression of TAJ—As discussed above, almost all the EST clones encoding TAJ are derived from cDNA libraries originating from embryonic tissues. To test further the expression of
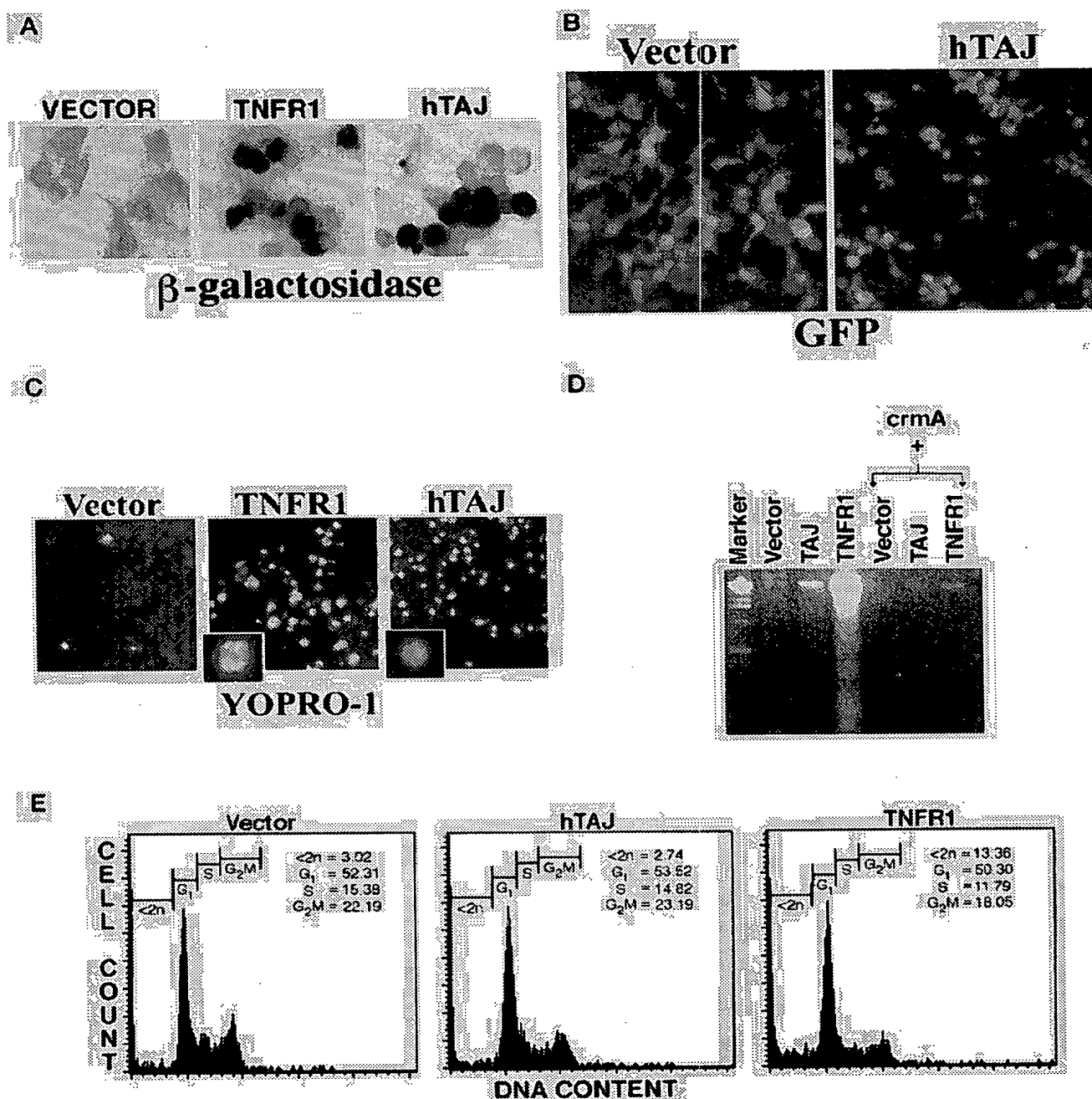
FIG. 4. *A*, TAJ induces cell death. 293T cells (2×10^6) were transfected with the indicated plasmids (5 µg) along with a β-galactosidase-encoding plasmid (2 µg). Cells were fixed and stained with 5-bromo-4-chloro-3-indolyl-β-D-galactopyranoside 36 h post-transfection as described previously (8). Dying cells have a dark rounded appearance and are becoming detached from the plate. *B*, 293T cells (2×10^6) were transfected with a control vector or a TAJ expression vector along with a GFP-encoding vector. Thirty six hours after transfection, cells were examined under a fluorescent microscope and photographed. TAJ-transfected cells have a rounded appearance and are becoming detached from the plate. *C*, absence of nuclear fragmentation during TAJ-induced cell death. 293T cells were transfected with an empty vector or vectors encoding TNFR1 or TAJ. Approximately 40 h later cells were stained with YOPRO-1, which stains only those cells that have lost membrane integrity. Fragmented nuclei of TNFR1-transfected cells are shown with *arrowheads*. *Insets* show nuclear morphology of TNFR1- and TAJ-transfected cells under higher magnification. *D*, cell death induced by TAJ is not accompanied by oligonucleosomal DNA fragmentation. 293T cells (2×10^6) were transfected with the indicated plasmids (5 µg), and DNA fragmentation assay was performed after 38 h essentially as described (48). *E*, DNA content frequency distribution. Cell death induced by TNFR1 is accompanied by an increase in the hypodiploid cell population ($<2n$) that is absent in the TAJ-transfected cells. The percentage of cells in various stages of cell cycle is also shown. DNA content analysis was performed using flow cytometry on ethanol-permeabilized cells stained with propidium iodide. The transfection efficiency of the tested plasmids, as determined by the expression of cotransfected GFP, ranged from 40 to 50%.
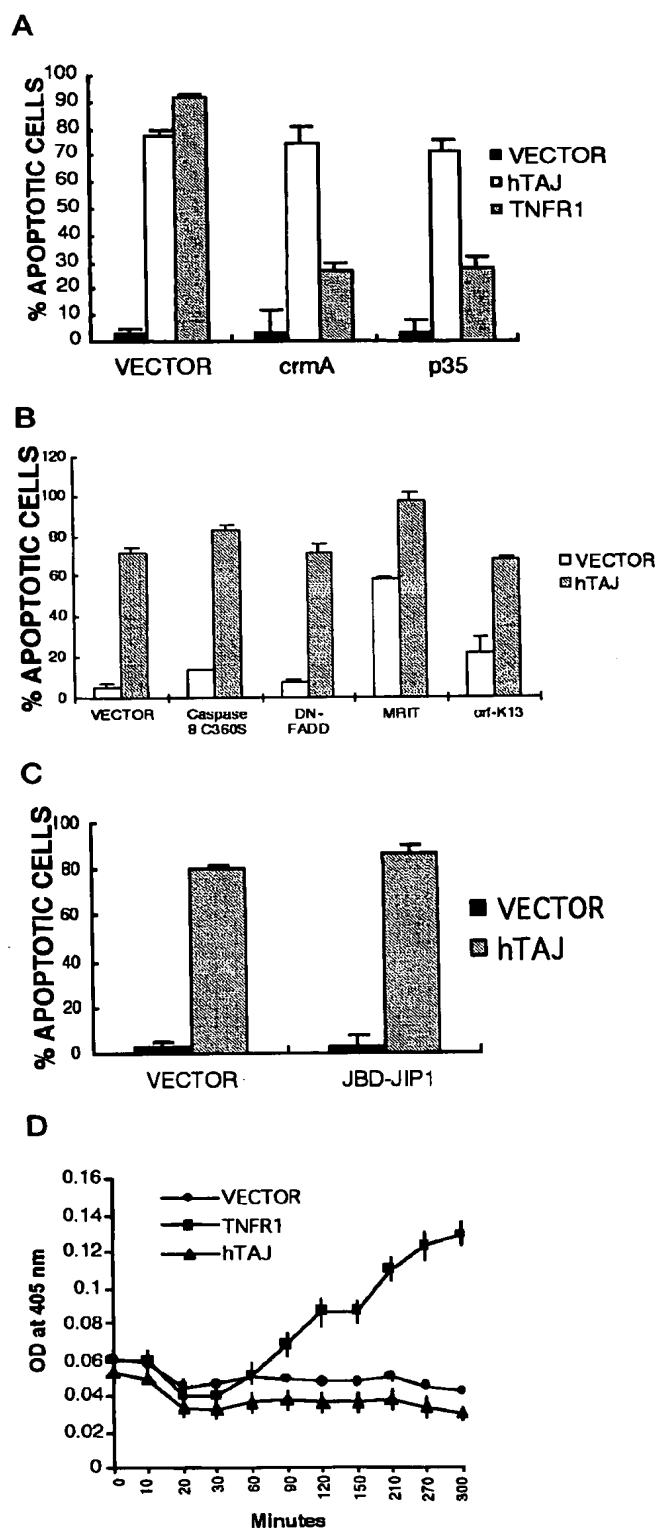
A

B

C

D

FIG. 5. *A*, caspase inhibitors fail to block TAJ-induced cell death. 293T cells (2 × 10⁶) were transfected with an empty vector or the indicated receptor plasmids along with a β-galactosidase reporter plasmid in duplicate in each well of a 24-well plate. The amount of inhibitor plasmids (CrmA and p35) was three times the amount of receptor plasmids, and the total amount of transfected DNA was kept constant by adding empty vector. Cells were fixed, stained, and percentage of apoptotic cells determined based on criteria described in Fig. 4*A*. Values shown are mean ± S.E. of a representative of two independent experiments performed in duplicate. *B*, lack of inhibitory effect of dominant-negative FADD, caspase 8 C360S, MRIT/cFLIP, and Orf-K13 on TAJ-induced cell death. The experiment was performed essentially as described for *A*. *C*, JBD-JIP1 fails to block TAJ-induced cell death. The experiment was performed essentially as described for *A*. Values shown are mean ± S.E. of a representative of two independent experiments performed in duplicate. *D*, TAJ fails to activate caspase 3. 293T (2 × 10⁶) cells were transfected with the indicated plasmids (5 μg each). Cells were lysed 36 h post-transfection and 10 μl of cellular extracts used for the measurement of caspase 3 activation as described under "Experimental Procedures." Values shown are mean ± S.E. of a representative of two independent experiments performed in duplicate or triplicate.

TAJ during embryonic development, Northern analysis was performed on a multiple tissue Northern blot containing poly(A) RNA from 7-, 11-, 15-, and 17-day mouse embryos. The protein-coding region of mTAJ-αL cDNA was used as a probe. A strong signal of 4.4 kilobase pairs was detected in lanes containing RNA from day 11, 15, and 17 embryos indicating the expression of TAJ during embryonic development (Fig. 2).

Expression of TAJ in adult human tissues was studied by Northern analysis using the protein-coding region of hTAJ cDNA as a probe. Major expression was seen only in the prostate gland with only very low expression seen in other tissues such as spleen, thymus, testis, uterus, small intestine, colon, and peripheral blood leukocytes (Fig. 2). Expression of TAJ was also detected in 293 (human embryonic kidney) and LNCaP (prostate cancer) cell lines (data not shown).

TAJ Activates the JNK Pathway—Activation of the JNK and the NF-κB pathways is a common feature of the TNFR family members. Previous studies have also shown that members of this family can be activated in a ligand-independent fashion upon transient transfection-based overexpression (8, 12–14). Therefore, the ability of TAJ to activate the JNK pathway upon transient overexpression in 293EBNA cells was tested using a luciferase-based c-Jun transcriptional assay. In this assay, luciferase expression is driven by JNK-mediated phosphorylation of the activation domain of the transcription factor c-Jun that is fused to the GAL4 DNA-binding domain. TAJ could strongly activate the JNK pathway in these cells which was comparable in magnitude to that observed with CD40 (Fig. 3*A*). The ability of TAJ to activate the JNK pathway was also confirmed by a "pull-down" kinase assay based on *in vitro* phosphorylation of GST-cJun (Fig. 3*B*).

TAJ-induced JNK activation was successfully blocked by the JNK-binding domain of JIP1 (15), a recently isolated specific inhibitor of the JNK pathway (Fig. 3*C*). TRAF2 and its homologs have been shown to play an essential role in the JNK activation by TNFR family members by activating the protein kinase ASK1 (16). However, as shown in Fig. 3*D*, dominant-negative mutants of TRAF2 and ASK1 failed to block JNK activation via TAJ, while successfully blocking TRAF2-induced JNK activation.

We also investigated the ability of TAJ to activate the NF-κB pathway. However, transient transfection of TAJ led to only a weak activation of NF-κB in 293EBNA cells and completely failed to activate this pathway in 293T or MCF7 cells (not shown).

TAJ Induces Caspase-independent Cell Death—During the course of investigating the above signaling functions of TAJ, we noticed that it could also induce cell death. This result was somewhat unexpected since TAJ does not possess a death domain. To characterize further the death inducing property of TAJ, 293T cells were transfected with a control plasmid, or plasmids containing TNFR1 or TAJ, along with a reporter
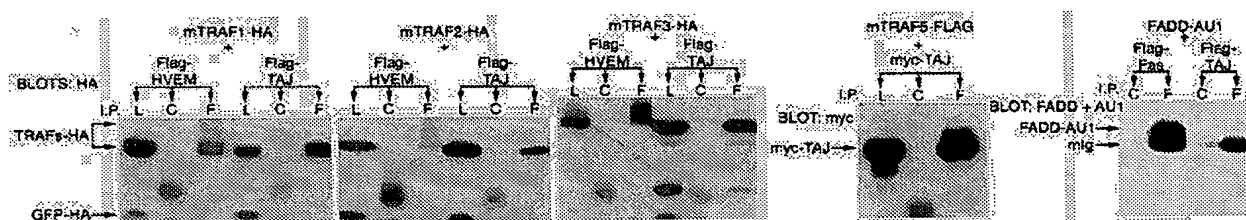
FIG. 6. **TAJ coimmunoprecipitates TRAFs but fails to coimmunoprecipitate FADD.** 293T cells were transfected with the indicated plasmids and cell lysates (L) immunoprecipitated with FLAG (F) beads or control beads (C). Coimmunoprecipitated proteins were detected by Western analysis with the indicated antibodies. Lack of immunoprecipitation of cotransfected GFP-HA demonstrates the specificity of the interactions. The *lower band* in the *right-most panel* corresponds to the mouse Ig light chain.

plasmid encoding β-galactosidase or the green fluorescent protein (GFP). Approximately 32 h post-transfection, TAJ-transfected cells became rounded and started to detach from the plate (Fig. 4, *A* and *B*). In addition to 293T cells, TAJ also induced cell death in 293EBNA cells. However, we have so far failed to observe significant TAJ-induced apoptosis in COS cells, which might reflect the tissue or species specificity of this response.

A comparison with TNFR1-transfected cells revealed several unique features of TAJ-induced apoptosis. First, cell death induced by TAJ was slightly delayed as compared with that induced by TNFR1 (32 *versus* 24 h). Second, whereas TAJ-transfected cells showed cytoplasmic swelling and nuclear condensation, they demonstrated relatively little membrane budding as compared with the TNFR1-transfected cells (Fig. 4A). Third, based on nuclear staining with YOPRO-1, a cell-impermeant DNA-intercalating dye, we have recognized differences in the nuclear morphology of cells undergoing apoptosis in response to TAJ or TNFR1. As shown in Fig. 4C, whereas the majority of the vector-transfected cells did not stain with YO-PRO-1, a large number of TAJ or TNFR1-transfected cells showed nuclear staining with this dye reflecting the loss of membrane integrity. However, unlike the TNFR1-transfected cells, those dying in response to TAJ did not demonstrate nuclear fragmentation, a key feature of caspase-induced cell death (Fig. 4C). Finally, as compared with TNFR1-transfected cells, TAJ-transfected cells demonstrated a complete absence of oligonucleosomal DNA fragmentation, one of the essential features of caspase-induced apoptosis (Fig. 4D).

Absence of nuclear fragmentation in the TAJ transfected cells was confirmed by DNA content analysis using flow cytometry. As shown in Fig. 4E, transfection of TNFR1 in 293T cells is accompanied by the appearance of a hypodiploid population of cells, which is absent in cells transfected with an empty vector or TAJ. Furthermore, there was no significant difference in the cell cycle distribution of cells transfected with TAJ or control vector, making it unlikely that TAJ induces cell death via a block in cell cycle transition.

To characterize further TAJ-induced cell death, we tested the ability of several known inhibitors of apoptosis to block cell death induced by it. TAJ-induced cell death was not blocked by two virally encoded caspase inhibitors, CrmA and p35, and a synthetic caspase inhibitor, benzyloxycarbonyl-VAD-fmk, all of which successfully blocked TNFR1-induced apoptosis (Fig. 5A and data not shown). Similarly, MRIT/cFLIP, Orf-K13, and dominant-negative inhibitors of FADD and caspase 8 (caspase 8 C360S) had no effect on TAJ-induced cell death (Fig. 5B). Finally, JBD-JIP1 failed to effectively block TAJ-induced cell death, ruling out a major role of the JNK pathway in TAJ-induced cell death (Fig. 5C).

Lack of activation of the caspase cascade during TAJ-induced cell death was further supported by a chromogenic assay based on caspase 3-mediated cleavage of the chromogenic substrate,

*p*NA-DEVD. Caspase 3 is one of the executioner caspases of the caspase cascade and is activated during death receptors-induced apoptosis (17). As shown in Fig. 5D, cell lysates from cells transfected with TNFR1 demonstrated caspase 3 activation, whereas TAJ-transfected cells failed to do so.

TAJ Interacts with TRAF Family Members—TRAF family members have been previously implicated in the signal transduction by various TNFR family members (18). To test the involvement of TRAFs in the signaling via TAJ, we tested their ability to interact with each other using a coimmunoprecipitation assay in 293T cells. As shown in Fig. 6, TAJ successfully coimmunoprecipitated with TRAF1, TRAF2, TRAF3, and TRAF5 in the above assay. However, consistent with the absence of a death domain in its cytoplasmic tail, TAJ failed to interact with FADD (Fig. 6).

DISCUSSION

Programmed cell death or apoptosis plays an important role in the development and morphogenesis of multicellular organisms by controlling cell number and removing mutated or defective cells (19). Despite the recent progress in the identification of downstream effector molecules involved in developmental cell death (20), the cell surface receptors regulating this process remain to be identified. Members of the TNFR family are well known for their role in the mediation of cell death in adult tissues. Based on its unique expression profile during development, TAJ may play a similar role during embryogenesis.

In addition to its full-length isoform, we have isolated two alternative spliced forms of murine TAJ that are likely to act as decoy and soluble receptors, respectively. Such receptors have been previously identified for other members of the TNFR family and shown to block signaling via the full-length receptors (14, 21, 22). It remains to be seen whether the mTAJ-αS and mTAJ-β isoforms play a similar role in regulating signaling via the full-length TAJ receptor.

Despite sharing significant sequence homology with TNFR family members in the extracellular ligand-binding domain, TAJ possesses a unique cytoplasmic domain, which suggests that it utilizes novel signal transduction pathways for the activation of JNK and cell death pathways. Consistent with this hypothesis, TAJ-induced JNK activation was not blocked by dominant-negative inhibitors of TRAF2, TRAF5, or ASK1, which have been previously implicated in JNK activation via TNFR1 and CD40. However, coimmunoprecipitation assays revealed that TAJ is capable of binding a number of different TRAF family members, and it is possible that TAJ-induced JNK activation is mediated by an as yet untested TRAF homolog, such as TRAF6. Similarly, in addition to ASK1, alternative pathways for JNK activation via TNFR family members have been described (23–25), and it remains to be seen whether TAJ utilizes one of these alternative pathways.

A surprising result of this study was the ability of TAJ to induce cell death since it does not possess a death domain. Our

results indicate that TAJ induces cell death by a mechanism independent of the classical death domain receptor-FADD-caspase 8/10 pathway. Although, caspase-mediated cell death is the best characterized form of apoptosis, several caspase-independent forms of death are also known in the literature. For example, FADD, in addition to its role in the activation of caspases, can also induce caspase-independent cell death (26). This death is resistant to caspase inhibitors and is accompanied by cellular swelling without apoptotic bodies or fragmentation of chromatin (26). Similar forms of caspase-independent death have been previously reported for both Fas and TNFR1 as well (27, 28). Several non-death domain-containing members of the TNFR family have been shown to induce cell death under certain conditions (5–7, 29, 30), and it remains to be seen whether TAJ shares a common caspase-independent mechanism of cell death induction with these receptors. Several additional examples of caspase-independent cell death have been recently reported as well (31–37).

There are several potential mediators of caspase-independent cell death via TAJ. First, Bax and Bax-like proteins have been known to kill mammalian cells even in the presence of caspase inhibitors, provoking chromatin condensation and membrane alterations but without caspase activation or DNA degradation (38–40). It has been proposed that Bax and Bax-like proteins might mediate caspase-independent death via their channel forming ability that could promote mitochondrial permeability transition or puncture the outer mitochondrial membrane (41). Second, nitric oxide, like Bax, also induces cell death accompanied by chromatin condensation, nuclear compaction, and mitochondrial swelling but without caspase activation or DNA fragmentation (42). The recent isolation of apoptosis-inducing factor may provide an additional mechanism for caspase-independent cell death induction by TAJ (43, 44). Apoptosis-inducing factor is a flavoprotein of approximately 57 kDa that is normally confined to mitochondrial intermembrane space but translocates to the nucleus when apoptosis is induced. Apoptosis-inducing factor can induce chromatin condensation in isolated nuclei, dissipation of mitochondrial $\Delta\psi_m$, and exposure of phosphatidylserine in the plasma membrane. None of these effects are blocked by treatment with broad-spectrum caspase inhibitor benzyloxycarbonyl-VAD-fluoromethyl ketone (43, 44). We are currently testing the contribution of the above mediators to TAJ-induced cell death.

The ligand for TAJ has not been identified yet. Recently, two novel ligands belonging to the TNF family, designated APRIL (45) and THANK/BlyS (46, 47), respectively, have been identified. Besides Blys/THANK, TAJ could also be a receptor for VEGI, another member of the tumor necrosis factor family for which receptor has not been identified. Studies are in progress to test whether one of these represents the ligand for TAJ.

REFERENCES

1. Gruss, H. J., and Dower, S. K. (1995) *Blood* 85, 3378–3404
2. Tartaglia, L. A., Ayres, T. M., Wong, G. H., and Goeddel, D. V. (1993) *Cell* 74, 845–853
3. Itoh, N., and Nagata, S. (1993) *J. Biol. Chem.* 268, 10932–10937
4. Ashkenazi, A., and Dixit, V. M. (1998) *Science* 281, 1305–1308
5. Force, W. R., Cheung, T. C., and Ware, C. F. (1997) *J. Biol. Chem.* 272, 30835–30840
6. Vandenabeele, P., Declercq, W., Vanhaesebroeck, B., Grooten, J., and Fiers, W. (1995) *J. Immunol.* 154, 2904–2913
7. Lee, S. Y., Park, C. G., and Choi, Y. (1996) *J. Exp. Med.* 183, 669–674
8. Chaudhary, P. M., Eby, M., Jasmin, A., Bookwalter, A., Murray, J., and Hood,

L. (1997) *Immunity* 7, 821–830
9. Chaudhary, P. M., Eby, M. T., Jasmin, A., and Hood, L. (1999) *J. Biol. Chem.* 274, 19211–19219
10. Chaudhary, P. M., Eby, M. T., Jasmin, A., and Hood, L. (1999) *Oncogene* 18, 5738–5746
11. Berberich, I., Shu, G. L., and Clark, E. A. (1994) *J. Immunol.* 153, 4357–4366
12. Chinnaiyan, A. M., O'Rourke, K., Yu, G. L., Lyons, R. H., Garg, M., Duan, D. R., Xing, L., Gentz, R., Ni, J., and Dixit, V. M. (1996) *Science* 274, 990–992
13. Pan, G., O'Rourke, K., Chinnaiyan, A. M., Gentz, R., Ebner, R., Ni, J., and Dixit, V. M. (1997) *Science* 276, 111–113
14. Pan, G., Ni, J., Wei, Y. F., Yu, G., Gentz, R., and Dixit, V. M. (1997) *Science* 277, 815–818
15. Dickens, M., Rogers, J. S., Cavanagh, J., Raitano, A., Xia, Z., Halpern, J. R., Greenberg, M. E., Sawyers, C. L., and Davis, R. J. (1997) *Science* 277, 693–696
16. Nishitoh, H., Saitoh, M., Mochida, Y., Takeda, K., Nakano, H., Rothe, M., Miyazono, K., and Ichijo, H. (1998) *Mol. Cell* 2, 389–395
17. Salvesen, G. S., and Dixit, V. M. (1997) *Cell* 91, 443–446
18. Darnay, B. G., and Aggarwal, B. B. (1997) *J. Leukocyte Biol.* 61, 559–566
19. Vaux, D. L., and Korsmeyer, S. J. (1999) *Cell* 96, 245–254
20. Los, M., Wesselborg, S., and Schulze-Osthoff, K. (1999) *Immunity* 10, 629–639
21. Sheridan, J. P., Marsters, S. A., Pitti, R. M., Gurney, A., Skubatch, M., Baldwin, D., Ramakrishnan, L., Gray, C. L., Baker, K., Wood, W. I., Goddard, A. D., Godowski, P., and Ashkenazi, A. (1997) *Science* 277, 818–821
22. Pitti, R. M., Marsters, S. A., Lawrence, D. A., Roy, M., Kischkel, F. C., Dowd, P., Huang, A., Donahue, C. J., Sherwood, S. W., Baldwin, D. T., Godowski, P. J., Wood, W. I., Gurney, A. L., Hillan, K. J., Cohen, R. L., Goddard, A. D., Botstein, D., and Ashkenazi, A. (1998) *Nature* 396, 699–703
23. Yuasa, T., Ohno, S., Kehrl, J. H., and Kyriakis, J. M. (1998) *J. Biol. Chem.* 273, 22681–22692
24. Liu, Z. G., Hsu, H., Goeddel, D. V., and Karin, M. (1996) *Cell* 87, 565–576
25. Mathias, S., Pena, L. A., and Kolesnick, R. N. (1998) *Biochem. J.* 335, 465–480
26. Kawahara, A., Ohsawa, Y., Matsumura, H., Uchiyama, Y., and Nagata, S. (1998) *J. Cell Biol.* 143, 1353–1360
27. Vercammen, D., Brouckaert, G., Denecker, G., Van de Craen, M., Declercq, W., Fiers, W., and Vandenabeele, P. (1998) *J. Exp. Med.* 188, 919–930
28. Vercammen, D., Beyaert, R., Denecker, G., Goossens, V., Van Loo, G., Declercq, W., Grooten, J., Fiers, W., and Vandenabeele, P. (1998) *J. Exp. Med.* 187, 1477–1485
29. Frade, J. M., Rodriguez-Tebar, A., and Barde, Y. A. (1996) *Nature* 383, 166–168
30. Rabizadeh, S., Oh, J., Zhong, L. T., Yang, J., Bitler, C. M., Butcher, L. L., and Bredesen, D. E. (1993) *Science* 261, 345–348
31. Pettersen, R. D., Gaudernack, G., Olafsen, M. K., Lie, S. O., and Hestdal, K. (1998) *J. Immunol.* 160, 4343–4352
32. Drenou, B., Blancheteau, V., Burgess, D. H., Fauchet, R., Charron, D. J., and Mooney, N. A. (1999) *J. Immunol.* 163, 4115–4124
33. Deas, O., Dumont, C., MacFarlane, M., Rouleau, M., Hebib, C., Harper, F., Hirsch, F., Charpentier, B., Cohen, G. M., and Senik, A. (1998) *J. Immunol.* 161, 3375–3383
34. Maroney, A. C., Finn, J. P., Bozyczko-Coyne, D., TM, O. K., Neff, N. T., Tolkovsky, A. M., Park, D. S., Yan, C. Y., Troy, C. M., and Greene, L. A. (1999) *J. Neurochem.* 73, 1901–1912
35. Stefanis, L., Park, D. S., Friedman, W. J., and Greene, L. A. (1999) *J. Neurosci.* 19, 6235–6247
36. Belaud-Rotureau, M. A., Lacombe, F., Durrieu, F., Vial, J. P., Lacoste, L., Bernard, P., and Belloc, F. (1999) *Cell Death Differ.* 6, 788–795
37. Heibein, J. A., Barry, M., Motyka, B., and Bleackley, R. C. (1999) *J. Immunol.* 163, 4683–4693
38. Xiang, J., Chao, D. T., and Korsmeyer, S. J. (1996) *Proc. Natl. Acad. Sci. U. S. A.* 93, 14559–14563
39. McCarthy, N. J., Whyte, M. K., Gilbert, C. S., and Evan, G. I. (1997) *J. Cell Biol.* 136, 215–227
40. Gross, A., Jockel, J., Wei, M. C., and Korsmeyer, S. J. (1998) *EMBO J.* 17, 3878–3885
41. Adams, J. M., and Cory, S. (1998) *Science* 281, 1322–1326
42. Okuno, S., Shimizu, S., Ito, T., Nomura, M., Hamada, E., Tsujimoto, Y., and Matsuda, H. (1998) *J. Biol. Chem.* 273, 34272–34277
43. Lorenzo, H. K., Susin, S. A., Penninger, J., and Kroemer, G. (1999) *Cell Death Differ.* 6, 516–524
44. Susin, S. A., Lorenzo, H. K., Zamzami, N., Marzo, I., Snow, B. E., Brothers, G. M., Mangion, J., Jacotot, E., Costantini, P., Loeffler, M., Larochette, N., Goodlett, D. R., Aebersold, R., Siderovski, D. P., Penninger, J. M., and Kroemer, G. (1999) *Nature* 397, 441–446
45. Hahne, M., Kataoka, T., Schroter, M., Hofmann, K., Irmler, M., Bodmer, J. L., Schneider, P., Bornand, T., Holler, N., French, L. E., Sordat, B., Rimoldi, D., and Tschopp, J. (1998) *J. Exp. Med.* 188, 1185–1190
46. Mukhopadhyay, A., Ni, J., Zhai, Y., Yu, G. L., and Aggarwal, B. B. (1999) *J. Biol. Chem.* 274, 15978–15981
47. Moore, P. A., Belvedere, O., Orr, A., Pieri, K., LaFleur, D. W., Feng, P., Soppet, D., Charters, M., Gentz, R., Parmelee, D., Li, Y., Galperina, O., Giri, J., Roschke, V., Nardelli, B., Carrell, J., Sosnovtseva, S., Greenfield, W., Ruben, S. M., Olsen, H. S., Fikes, J., and Hilbert, D. M. (1999) *Science* 285, 260–263
48. Hsu, H., Xiong, J., and Goeddel, D. V. (1995) *Cell* 81, 495–504

CLUSTALW Result (gray.ono)
ClustalW Result

CLUSTAL W (1.83) Multiple Sequence Alignments

Reference 10

Sequence format is Pearson
Sequence 1: HUGO_AB040434   423 aa
Sequence 2: OAF065a   423 aa
Sequence 3: TROY_NP_061117   423 aa
Sequence 4: TAJ_AAF71828   423 aa
Start of Pairwise alignments
Aligning...

Sequences (1:2) Aligned. Score: 99.2908
Sequences (1:3) Aligned. Score: 100
Sequences (1:4) Aligned. Score: 99.2908
Sequences (2:2) Aligned. Score: 100
Sequences (2:3) Aligned. Score: 99.2908
Sequences (2:4) Aligned. Score: 98.5816
Sequences (3:2) Aligned. Score: 99.2908
Sequences (3:3) Aligned. Score: 100
Sequences (3:4) Aligned. Score: 99.2908
Sequences (4:2) Aligned. Score: 98.5816
Sequences (4:3) Aligned. Score: 99.2908
Sequences (4:4) Aligned. Score: 100
Guide tree   file created: [/tmp/21306.dnd]
Start of Multiple Alignment
There are 3 groups
Aligning...
Group 1: Sequences: 2   Score:9292
Group 2: Sequences: 2   Score:9300
Group 3: Sequences: 4   Score:9296
Alignment Score 16419
CLUSTAL-Alignment file created   [/tmp/21306.aln]

CLUSTAL W (1.83) multiple sequence alignment


```
HUGO_AB040434      MALKVLLEQEKTFFTLLVLLGYLSCKVTCESGDCRQQEFRDRSGNCVPCNQCGPGMELSK
TAJ_AAF71828       MALKVLLEQEKTFFTLLVLLGYLSCKVTCESGDCRQQEFRDRSGNCVPCNQCGPGMELSK
OAF065a            MALKVLLEQEKTFFTLLVLLGYLSCKVTCETGDCRQQEFRDRSGNCVPCNQCGPGMELSK
TROY_NP_061117     MALKVLLEQEKTFFTLLVLLGYLSCKVTCESGDCRQQEFRDRSGNCVPCNQCGPGMELSK
                   ***************************:*********************************
```

```
HUGO_AB040434      ECGFGYGEDAQCVTCRLHRFKEDWGFQKCKPCLDCAVVNRFQKANCSATSDAICGDCLPG
TAJ_AAF71828       ECGFGYGEDAQCVACRLHRFKEDWGFQKCKPCLDCAVVNRFQKANCSATSDAICGDCLPG
OAF065a            ECGFGYGEDAQCVTCRLHRFKEDWGFQKCKPCLDCAVVNRFQKANCSATSDAICGDCLPG
TROY_NP_061117     ECGFGYGEDAQCVTCRLHRFKEDWGFQKCKPCLDCAVVNRFQKANCSATSDAICGDCLPG
                   *************:**********************************************
```

```
HUGO_AB040434      FYRKTKLVGFQDMECVPCGDPPPPYEPHCASKVNLVKIASTASSPRDTALAAVICSALAT
TAJ_AAF71828       FYRKTKLVGFQDMECVPCGDPPPPYEPHCASKVNLVKIASTASSPRDTALAAVICSALAT
OAF065a            FYRKTKLVGFQDMECVPCGDPPPPYEPHCASKVNLVKIASTASSPRDTALAAVICSALAT
TROY_NP_061117     FYRKTKLVGFQDMECVPCGDPPPPYEPHCASKVNLVKIASTASSPRDTALAAVICSALAT
                   ************************************************************
```

```
HUGO_AB040434      VLLALLILCVIYCKRQFMEKKPSWSLRSQDIQYNGSELSCFDRPQLHEYAHRACCQCRRD
TAJ_AAF71828       VLLALLILCVIYCKRQFMEKKPSWSLRSQDIQYNETELSCFDRPQLHEYAHRACCQCRRD
OAF065a            VLLALLILCVIYCKRQFMEKKPSWSLRSQDIQYNGSELSCLDRPQLHEYAHRACCQCRRD
TROY_NP_061117     VLLALLILCVIYCKRQFMEKKPSWSLRSQDIQYNGSELSCFDRPQLHEYAHRACCQCRRD
                   ********************************** :****:*******************
```

```
HUGO_AB040434      SVQTCGPVRLLPSMCCEEACSPNPATLGCGVHSAASLQARNAGPAGEMVPTFFGSLTQSI
TAJ_AAF71828       SVQTCGPVRLLPSMCCEEACSPNPATLGCGVHSAASLQARNAGPAGEMVPTFFGSLTQSI
```

```
OAFO65a            SVQTCGPVRLLPSMCCEEACSPNPATLGCGVHSAASLQARNAGPAGEMVPTFFGSLTQSI
TROY_NP_061117     SVQTCGPVRLLPSMCCEEACSPNPATLGCGVHSAASLQARNAGPAGEMVPTFFGSLTQSI
                   ************************************************************


HUGO_AB040434      CGEFSDAWPLMQNPMGGDNISFCDSYPELTGEDIHSLNPELESSTSLDSNSSQDLVGGAV
TAJ_AAF71828       CGEFSDAWPLMQNPMGGDNISFCDSYPELTGEDIHSLNPELESSTSLDSNSSQDLVGGAV
OAFO65a            CGEFSDAWPLMQNPMGGDNISFCDSYPELTGEDIHSLNPELESSTSLDSNSSQDLVGGAV
TROY_NP_061117     CGEFSDAWPLMQNPMGGDNISFCDSYPELTGEDIHSLNPELESSTSLDSNSSQDLVGGAV
                   ************************************************************


HUGO_AB040434      PVQSHSENFTAATDLSRYNNTLVESASTQDALTMRSQLDQESGAVIHPATQTSLQVRQRL
TAJ_AAF71828       PVQSHSENFTAATDLSRYNNTLVESASTQDALTMRSQLDQESGAVIHPATQTSLQVRQRL
OAFO65a            PVQSHSENFTAATDLSRYNNTLVESASTQDALTMRSQLDQESGAIIHPATQTSLQVRQRL
TROY_NP_061117     PVQSHSENFTAATDLSRYNNTLVESASTQDALTMRSQLDQESGAVIHPATQTSLQVRQRL
                   *********************************************:**************


HUGO_AB040434      GSL
TAJ_AAF71828       GSL
OAFO65a            GSL
TROY_NP_061117     GSL
                   ***
```

[樹形図（ガイドツリー）のダウンロード]

[系統樹のダウンロード]   （表示用ソフト）

樹形図（ガイドツリー）データ
```
(
HUGO_AB040434:0.00000,
(
OAFO65a:0.00709,
TROY_NP_061117:0.00000)
:0.00000,
TAJ_AAF71828:0.00709);
```

系統樹データ
```
(
HUGO_AB040434:0.00000,
(
TAJ_AAF71828:0.00709,
TROY_NP_061117:0.00000)
:0.00000,
OAFO65a:0.00709);
```

配列データ：

```
>HUGO_AB040434
MALKVLLEQEKTFFTLLVLLGYLSCKVTCESGDCRQQEFRDRSGNCVPCNQCGPGMELSKE
CGFGYGEDAQCVTCRLHRFKEDWGFQKCKPCLDCAVVNRFQKANCSATSDAICGDCLPGFY
RKTKLVGFQDMECVPCGDPPPPYEPHCASKVNLVKIASTASSPRDTALAAVICSALATVLL
ALLILCVIYCKRQFMEKKPSWSLRSQDIQYNGSELSCFDRPQLHEYAHRACCQCRRDSVQT
CGPVRLLPSMCCEEACSPNPATLGCGVHSAASLQARNAGPAGEMVPTFFGSLTQSICGEFS
DAWPLMQNPMGGDNISFCDSYPELTGEDIHSLNPELESSTSLDSNSSQDLVGGAVPVQSHS
ENFTAATDLSRYNNTLVESASTQDALTMRSQLDQESGAVIHPATQTSLQVRQRLGSL


>OAFO65a
MALKVLLEQEKTFFTLLVLLGYLSCKVTCETGDCRQQEFRDRSGNCVPCNQCGPGMELSKE
CGFGYGEDAQCVTCRLHRFKEDWGFQKCKPCLDCAVVNRFQKANCSATSDAICGDCLPGFY
RKTKLVGFQDMECVPCGDPPPPYEPHCASKVNLVKIASTASSPRDTALAAVICSALATVLL
ALLILCVIYCKRQFMEKKPSWSLRSQDIQYNGSELSCLDRPQLHEYAHRACCQCRRDSVQT
CGPVRLLPSMCCEEACSPNPATLGCGVHSAASLQARNAGPAGEMVPTFFGSLTQSICGEFS
DAWPLMQNPMGGDNISFCDSYPELTGEDIHSLNPELESSTSLDSNSSQDLVGGAVPVQSHS
ENFTAATDLSRYNNTLVESASTQDALTMRSQLDQESGAIIHPATQTSLQVRQRLGSL
```

```
>TROY_NP_061117
1malkvlleqektfftllvllgylsckvtcesgdcrqqefrdrsgncvpcnqcgpgmelsk
61ecgfgygedaqcvtcrlhrfkedwgfqkckpcldcavvnrfqkancsatsdaicgdclpg
121fyrktklvgfqdmecvpcgdppppyephcaskvnlvkiastassprdtalaavicsalat
181vllallilcviyckrqfmekkpswslrsqdiqyngselscfdrpqlheyahraccqcrrd
241svqtcgpvrllpsmcceeacspnpatlgcgvhsaaslqarnagpagemvptffgsltqsi
301cgefsdawplmqnpmggdnisfcdsypeltgedihslnpelesstsldsnssqdlvggav
361pvqshsenftaatdlsrynntlvesastqdaltmrsqldqesgavihpatqtslqvrqrl
421gsl


>TAJ_AAF71828
        1 malkvlleqe ktfftllvll gylsckvtce sgdcrqqefr drsgncvpcn qcgpgmelsk
       61 ecgfgygeda qcvacrlhrf kedwgfqkck pcldcavvnr fqkancsats daicgdclpg
      121 fyrktklvgf qdmecvpcgd ppppyephca skvnlvkias tassprdtal aavicsalat
      181 vllallilcv iyckrqfmek kpswslrsqd iqynetelsc fdrpqlheya hraccqcrrd
      241 svqtcgpvrl lpsmcceeac spnpatlgcg vhsaaslqar nagpagemvp tffgsltqsi
      301 cgefsdawpl mqnpmggdni sfcdsypelt gedihslnpe lesstsldsn ssqdlvggav
      361 pvqshsenft aatdlsrynn tlvesastqd altmrsqldq esgavihpat qtslqvrqrl
      421 gsl
//
```

command : /usr/local/bin/clustalw -INFILE=/tmp/21306.clw -quicktree -
hgapresidues=GPSNDQERK ; /usr/local/bin/clustalw -INFILE=/tmp/21306.aln -tree
ONO in-house server, interpreter version: clustal.pl : in-house ClustalW interface v1.21
Jun MURAI